# ASSESSING TERRAIN MODELLING AND FOREST INVENTORY CAPABILITIES OF DIGITAL AERIAL PHOTOGRAMMETRY FROM AUTONOMOUS AERIAL SYSTEMS

by

Alexander Naoki Vernon Graham

B.A., The University of British Columbia, 2016

A THESIS SUBMITTED IN PARTIAL FULFILLMENT OF

THE REQUIREMENTS FOR THE DEGREE OF

MASTER OF SCIENCE

in

THE FACULTY OF GRADUATE AND POSTDOCTORAL STUDIES

(Forestry)

THE UNIVERSITY OF BRITISH COLUMBIA

(Vancouver)

August 2019

The following individuals certify that they have read, and recommend to the Faculty of Graduate and Postdoctoral Studies for acceptance, a thesis/dissertation entitled:

Assessing terrain modelling and forest inventory capabilities of digital aerial photogrammetry from autonomous aerial systems

submitted by Alexander Graham in partial fulfillment of the requirements for

the degree of Master of Science

in Forestry

**Examining Committee:**

Nicholas C. Coops, Forest Resource Management, Forestry
Supervisor

Allan L. Carroll, Forest and Conservation Sciences, Forestry
Supervisory Committee Member

Mike Wilcox, FYBR Solutions Inc.
Supervisory Committee Member

Naomi B. Schwartz, Geography, Arts
Additional Examiner

**Additional Supervisory Committee Members:**

Supervisory Committee Member

Supervisory Committee Member

**Abstract**

Autonomous aerial systems-based digital aerial photogrammetry (AAS-DAP) is an emerging technology that has the capacity to generate dense three-dimensional (3D) point clouds similar to airborne laser scanning (ALS). Over forested stands, these point-clouds can be used to model forest attributes using an area-based approach however, model accuracy is dependent on digital elevation model quality used to gather vegetation heights above ground. It is known that canopy occlusion contributes to larger gaps in terrain registration from AAS-DAP compared to ALS point clouds. Due to the recent emergence of AAS-DAP as a cost-effective remote sensing platform, few studies have investigated the terrain modelling and forest inventory capacity of AAS-DAP over complex conifer forests. In Chapter 3, through the use of a sensitivity analysis, I established a set of optimal ground points from AAS-DAP by using commercially provided ALS ground points as reference. This optimal set of ground points was then used to test common terrain surface interpolation routines in Chapter 4. Interpolation routines include inverse-distance weighted, natural neighbour, triangulated irregular network, and spline with tension. Using field-measured tree height and stem diameter, allometric relationships were established for dependent variables: mean tree height ($H_{mean}$), Lorey's height ($H_{Lorey}$) and stem volume per hectare ($V_{stem}$). Models were then fit among dependent variables and metrics calculated from the vertical distribution of the AAS-DAP point cloud normalized by the different AAS-DAP terrain surfaces in addition to a reference surface generated from commercially provided ALS ground points. A Kruskal-Wallis with Dunn's posthoc test found no significant difference between predictions derived from different terrain surfaces for all three dependent variables; however, the inverse-distance-weighted method produced a distribution of predictions most similar to those from the

ALS-DEM. The best performing forest attributes models for $H_{mean}$, $H_{Lorey}$ and $V_{stem}$ yielded mean root-mean-square errors (RMSE) of 1.19 m (7.29%), 0.92 m (5.04%) and 54.55 $m^3 \cdot ha^{-1}$ (26.66%) respectively across the four AAS-DAP terrain surfaces generated. Model performance was higher yet comparable when using the ALS-DEM for point cloud height normalization with RMSE of 0.73 m (4.43%), 0.59 m (3.24%) and 37.31 $m^3 \cdot ha^{-1}$ (18.24%).

## Lay Summary

Remote sensing of forest structure can aid decision making towards sustainable forest management goals; however, the complexity of forest ecosystems pose a significant challenge. Prior to the last half century, the predominant method of gathering forest inventory was from field-based sampling techniques. This method is time consuming, costly, and subject to significant error especially when applied over large areas. The recent introduction of airborne light detection and ranging (LiDAR) has given way to a revolution in remotely sensed forest structure analysis of large areas; however; the cost of such acquisitions can be impractical for smaller scale applications or where high temporal resolution is desired. The research presented in this thesis aims to fill this gap though the analysis of autonomous aerial systems (AAS). The results presented in Chapter 3 and 4 show that forest inventory can be conducted from AAS with accuracies similar to LiDAR data.

## Preface

This thesis is the aggregation of two scientific articles written for peer-review of which I am the lead author. I was responsible for research objective definition, methodology development and data analysis, as well as writing and editing both publications. Project supervision, conceptual guidance and editorial assistance was provided by Dr. Nicholas Coops. The project was conducted in partnership with FYBR Solutions Inc. Patrick Crawford, Mike Wilcox and Andrew Plowright, of FYBR Solutions Inc. contributed to the collection and preprocessing of data, as well as technical assistance and a dedicated part-time workspace. Dr. Piotr Tompalski was involved in the second scientific paper and provided methodological and statistical advice in addition to editorial assistance. Max Yancho, Jeremy Arkin, David Fluharty, Lukas Schreiber and Dennis Voss contributed to field data collection. Publications arising from this thesis include:

- Chapter 3: **Graham, A.**, Coops, N., Wilcox, M., & Plowright, A. (2019). Evaluation of ground surface models derived from unmanned aerial systems with digital aerial photogrammetry in a disturbed conifer forest. Remote Sensing, 11(1), 84.

- A version of Chapter 4 is currently in peer review in the International Journal of Remote Sensing as:

  **Graham, A.,** Coops, N. C., Wilcox, M., Plowright, A. (2019). Effect of ground surface interpolation methods on the accuracy of forest attribute modelling using unmanned aerial systems-based digital aerial photogrammetry

**Table of Contents**

**List of Tables**

**List of Figures**

**List of Abbreviations**

AAS - Autonomous aerial system

AAS-DAP - Autonomous aerial systems-based digital aerial photogrammetry

ABA - Area-based approach

AFRF - Alex Fraser Research Forest

ALS - Airborne laser scanning

BC - British Columbia

BEC - Biogeoclimatic ecosystem classification

CHM - Canopy height model

DAP - Digital aerial photogrammetry

DBH - Diameter at breast-height

DEM - Digital elevation model

GIS - Geographic information system

GNSS - Global navigation satellite system

GPS - Global positioning system

DGPS - Differential global navigation system

HRI - Hierarchical robust interpolation

ICH - Interior cedar hemlock

IDW - Inverse distance weighted

IMU - Inertial measurement unit

LiDAR - Light detection and ranging

NATN - Natural neighbour

PTD - Progressive TIN densification

RdNBRr - relative differenced normalized burn ratio

RGB - Red green blue

RMSE - Root-mean-square-error

SBS - Sub-boreal spruce

SMRF - Simple morphological filter

SPLT - Spline with tension

SRTM - Shuttle radar topography mission

TIN - Triangulated irregular network

2D - Two-dimensional

3D - Three-dimensional

**Acknowledgements**

I must first extend my most sincere gratitude to Dr. Nicholas Coops and his incredible guidance throughout my degree. I am thankful to have had the opportunity to join the Integrated Remote Sensing Studio (IRSS) first as an undergraduate student which both prepared and inspired me to pursue a graduate level degree. Nicholas was always able provide prompt constructive feedback on my work which greatly facilitated my progress. Nicholas also has tremendous ability to promote a work-life balance that is both highly productive and enjoyable. I would like to thank my committee members Allan Carroll and Mike Wilcox as they provided invaluable knowledge from external perspectives. Allan is a premier scientist and provided pivotal insight into the key components of my research. Mike provided his time and expert knowledge of the autonomous aerial system used for data acquisition. I am also very appreciative of Dr. Piotr Tompalski and Dr. Tristan Goodbody for their frequent assistance and friendliness throughout my degree and feel very fortunate to have been in the presence of such an elite group of scholars.

I would also like to thank FYBR Solutions Inc. and CEO Patrick Crawford for their sponsorship over the past two years and for providing a dedicated second workspace. I am grateful to have gained this industry experience towards my career. I want to thank Andrew Plowright for his contributions as coauthor, especially his contributions to the formulation of the research objectives. Moreover, I would like to express gratitude to the Natural Sciences and Engineering Research Council of Canada (NSERC) for considering this research worthy of funding.

Thank you to my loving wife and daughter who have continuously supported me in pursing my academic goals. Finally, I would like to thank my fellow IRSS members are an exceptional network of scientists who continuously fostered an enjoyable work environment.

**Dedication**

*Dedicated to my loving wife and daughter*

*Whose sacrificial care and encouragement are my foundation*

# Chapter 1: Introduction

## 1.1 Demand for inventory acquisition of forest structure information

Forest structure refers to the arrangement of vegetative elements across a forested landscape including the vertical distribution of organic matter (e.g. dead and live tree stems, branches, foliage and logs) within the sub-canopy (McElhinny et al. 2005; Frey et al. 2018). Forest attributes informed by measurements of forest structure include ecological diversity (Bengtsson et al. 2000; Culbert et al. 2013), disturbance patterns (Nowacki and Kramer 1998; Alaback and Saunders 2013) and commercial timber supply estimation. It is well established that forest stand structure is driven by continual successional changes due to disturbance, growth and competition. For example, the forests of the Pacific Northwest of North America have recently experienced abnormally severe insect and wildfire disturbances which contributed to widespread changes in forest structure (Kerns and Ager 2007; Wimberly and Liu 2014; Thom and Seidl 2016). Thom & Seidl (2016) provide a global review of the impacts on ecosystem services and biodiversity following fire, wind and bark beetle disturbances between 1981 and 2013. Of the 887 disturbance impacts included in the study, 60% were found in North American forests, while 60% of the North American subset were found in cool temperate forests (Thom and Seidl 2016). The mountain pine beetle epidemic spanning western North America specifically, was the largest contributor to global temperate forest damage between 2003 and 2012 (Van Lierop et al. 2015). In British Columbia (BC), Canada, the outbreak began in the late 1990s and affected 18 million hectares of forested land resulting in a loss of 53% of merchantable pine volume by 2012 (Bleiker 2017), an order of magnitude greater than any previously recorded mountain pine beetle

outbreak (Kurz et al. 2008). More recently, the 2017 and 2018 wildfire seasons respectively burned 1.2 and 1.3 million hectares of forest and were the largest burned areas in BC's recorded history. The significance of forests in BC, along with an increasingly unpredictable climate, warrants a long-term strategy for sustainable forest management by balancing economic goals of timber production and ecological preservation (Hickey and Innes 2008; Wulder et al. 2014).

Commercially, forest structure characterization is fundamental in estimating merchantable timber volume (Means et al. 1999; Lim et al. 2003; McElhinny et al. 2005; Wallace et al. 2016). The commercial forestry industry of Canada is a major component of national and subnational economies (Goodbody et al. 2016). In BC, the forest sector directly employed 65,000 workers, accounted for 36% of total provincial merchandise exports in 2015 (Barnes 2016) and contributed over $10 billion annually to provincial gross domestic product since 2011 (Barnes 2018). A recent reduction in timber supply, caused by aforementioned disturbance impacts, have initiated salvage logging efforts; however, the province's forest products industry is projected to endure a significant mid-term timber supply shortage (Pousette and Hawkins 2006; Patriquin, Wellstead, and White 2007; Burton 2010). Therefore, there is a need to adapt harvesting practices towards efficient methods for both selective and salvage logging to mitigate the shortage (Burton 2010).

Forest inventories quantify the location, condition and composition of forest resources and can be broadly categorized as forest management or operational inventories (Leckie and Gillis 1995). Forest management inventories tend to be conducted at larger spatial scales and are used to inform long-term management decisions whereas operational inventories provide locally specific pre-harvest estimates for supply chain optimization of forest resources. Canadian forest

inventories can be particularly challenging due to the range of growing conditions as a result of climatic subzones influenced by complex topography (Seidel, Ehbrecht, and Puettmann 2016) and these continual and often severe disturbance patterns. Therefore, there is a need for acquiring accurate, timely inventories for informing forest management.

### 1.1.1 Traditional methods of characterizing forest structure

In Canada, forest inventories are conducted at both national and provincial/territorial scales and are re-assessed every five years (M. D. Gillis et al. 2010). Canada's national forest inventory is an aggregation of individual jurisdictions, often further subdivided into management units, responsible for the development of inventory methods based on their respective requirements (Leckie and Gillis 1995). Since the 1950s, remote sensing data were collected for forest inventories in the form of aerial photography (M. Gillis and Leckie 1993); currently a common practice for many operational inventories.

Predating the introduction of geographic information systems (GIS) and automated image classification software, manual interpretation of aerial stereo photography was validated using field data collection campaigns (Wulder et al. 2008). The accuracy of this technique relies heavily on expert photo interpreters, who delineate stands based on their subjective perception of homogenous species, age, height and density compositions. In addition to challenges in validation (Steen Magnussen and Russo 2012), these methods are more time intensive, costly, and prone to error compared to emerging remote sensing techniques (Pozo et al. 2014; Tang and Shao 2015; Herrero-Huerta et al. 2016). Nevertheless, advances in optical remote sensing camera quality and satellite platforms with high-resolution imagery, have significant capacity in quantifying vegetation health and forest composition at large spatial scales.

## 1.2 Advanced 3D remote sensing of forest structure

As a result of recent technological advances, 3D remote sensing techniques such as airborne laser scanning (ALS) and digital aerial photogrammetry (DAP) are now providing additional forest structure information than conventional manual or digital analysis of two-dimensional optical imagery. ALS is an active remote sensing technique, flown using piloted aircraft, and offers significant potential for accurately modelling large forested areas (Means et al., 1999; Dubayah and Drake, 2000; Lim et al., 2003). It is well established that ALS is able to accurately model terrain even in forested areas with high biomass and canopy cover (Reutebuch et al. 2003). Herein, descriptions of ALS refer to small-footprint discrete-return light detection and ranging (LiDAR); however, more complex forms are under continual development, such as full-waveform (Reitberger et al. 2009; Nie et al. 2017) and single-photon LiDAR (Swatantran et al. 2016). Since the 1990s, discrete-return ALS has been rapidly adopted in the forest industry, revolutionizing the monitoring of forest stands (Baltsavias 1999; Næsset 2002). ALS sensors measure the angle of, and time between, sent and returned laser pulses, from which the precise distance to the sensor is calculated. The aggregation of these points is commonly known as a point cloud. Commercial ALS systems are usually acquired in conjunction with a global navigation satellite system (GNSS) and therefore have absolute georeferencing accuracies of 15 and 40 cm respectively in vertical and horizontal directions (Davenport, Holden, and Gurney 2004). A single ALS pulse has the capacity to register multiple points, often facilitating the characterization of sub-canopy elements and terrain.

An additional point cloud generating remote sensing technique is digital aerial photogrammetry (DAP). DAP is the process of acquiring a series of overlapping digital images

and generating 3D information as a result of having multiple perspectives of the same object. The concept of DAP dates back to the 1970's (Woodcock, 1976; Helava, 1978; McGlone et al., 2004) and has only recently become a competitive tool as a result of increases in computing and storage technologies, as well as reductions in their relative cost (Korpela, 2004; Rahlf et al., 2017). Below, I review the application of these two technologies to assess forest structure in more detail.

### 1.2.1 Review of airborne laser scanning for describing forest structure

Forest inventories from ALS are primarily conducted using either an area-based approach (ABA) or individual tree-crown detection (ITCD) (Tompalski et al. 2018). The data requirements for the ABA approach are continuous ALS data, commonly referred to as wall-to-wall coverage, and tree-level measurements from sample field plots (White, Wulder, Varhola, et al. 2013) ideally distributed using stratified random sampling (Corona and Fattorini 2008). Metrics based on the vertical distribution of point-cloud data are summarized at a pre-defined grid cell size and used to develop predictive models of plot-level forest attributes, not limited to tree height, stem volume, stem count, basal area, and biomass (Lim et al. 2003). Using the relationships established between the point-cloud metrics and field measurements at the plot-level, wall-to-wall predictions of forest attributes are made per cell.

Individual-tree level forest inventories rely on the selection and performance of ITCD algorithms and are generally conducted at smaller spatial scales than the ABA. The high density of ALS point-clouds allows for the extraction of tree-top locations, heights and crown edges (Popescu, Wynne, and Nelson 2003). Though highly valuable when performed accurately, the individual-tree-based approach can be problematic where trees beneath the dominant canopy

height fail to be detected (Yu et al. 2011). A summary of studies conducted in the past two decades towards forest inventory acquisition separated into ABA and ITCD techniques is provided below (Table 1.2-1).

**Table 1.2-1. Summary of publications concerning forest inventory from ALS data broken down by ABA and ITCD.**

| Publication | Year | Location | Forest Type | ABA | ITCD |
|---|---|---|---|---|---|
| Bouvier, Durrieu, Fournier, & Renaud, 2015 | 2015 | Southwestern France | Mixed | √ | |
| Scrinzi, Clementel, & Floris, 2015 | 2015 | Bolzano, Italian central Alps | Coniferous | √ | |
| (Tompalski et al. 2015) | 2015 | Vancouver Island, BC, Canada | Coniferous | √ | |
| (Vastaranta et al. 2013) | 2013 | Eastern Finland | Coniferous | √ | |
| (Q. Chen et al. 2013) | 2013 | Ione, California, USA | Deciduous / open savannah | | √ |
| (Koch, Heyder, and Weinacker 2013) | 2013 | Freiburg, southwest Germany | Mixed | | √ |
| (Steen Magnussen et al. 2012) | 2012 | Southeastern Norway | Coniferous | √ | |
| (Vastaranta et al. 2012) | 2012 | Evo, southern Finland | Coniferous | √ | √ |
| (Yu et al. 2011) | 2011 | Evo, southern Finland | Coniferous | | √ |
| (Corona and Fattorini 2008) | 2008 | Bosco della Fontana, northern Italy | Deciduous | √ | |
| (Takahashi et al. 2005) | 2005 | Aichi Prefecture, central Japan | Coniferous | | √ |
| (Popescu, Wynne, and Nelson 2003) | 2003 | Buckingham State Forest, Virginia, USA | Mixed | | √ |

## 1.3 Emerging technologies and remote sensing platforms

### 1.3.1 Review of autonomous aerial systems

Autonomous aerial systems (AAS) originate from military operations (Clarke, 2014), yet recent public and commercial expansion is indicative of the rapidly diversifying AAS market. From 2016 to 2017 global commercial drone revenue increased from $2.8 billion to $3.7 billion (Gartner, 2017). As a result of decreasing size, weight and cost of standard high-resolution consumer-grade cameras paired with increasing power, flight duration and payload capacities of modern AAS (Clarke, 2014; Peasgood and Valentin, 2015), there has been a rapid increase in AAS image acquisition around the world. By flying at lower altitudes than piloted counterparts, drones increase spatial resolution and image quality while reducing dependency on weather conditions (Shi et al., 2016). The low cost of AAS paired with optical imaging systems also allows for frequent acquisitions relative to ALS. Off-the-shelf rotary-wing AAS are capable of acquiring wall-to-wall imagery over areas up to a few hundred hectares per day using multiple flights, provided charged batteries are readily available. An example application for AAS-DAP surveys is the monitoring of crop growth through multi-temporal comparisons of high-resolution crop surface models (Bendig et al., 2013). Similarly, canopy height models (CHM) of tree plantations have been generated to detect small temporal changes in forest height and stem volume, which may be less measurable using ALS (Guerra-Hernandez et al., 2017). AAS-DAP techniques can also be used for comparing efficiencies of different harvesting equipment as well as their impact on service roads and trail networks (Horcher and Visser, 2004).

### 1.3.2 Digital aerial photogrammetry

Photogrammetry, based on principles of stereo-photography, is the process of gathering 3D structure from overlapping portions of adjacent two-dimensional images (Westoby et al. 2012). The extraction of vertical structure relies on the identification of common objects, known as tie-points, in overlapping images. Practical applications for aerial photogrammetry exist (Woodcock 1976; Helava 1978); however, prior to modern digital cameras and advanced computing technology, the creation of photogrammetric products relied on expert photogrammetrists in addition to a pre-existing network of visible tie-points with known coordinates (Lane, James, and Crowell 2000). Automatic tie-point extraction is now possible with the emergence of structure-from-motion algorithms, facilitating a marked increase in image-based 3D data generation (Smith, Carrivick, and Quincey 2015). The processed data product is a point cloud representing a 3D model of the overlapping region with a point density dependent on the pixel resolution. Given that an adequate digital elevation model (DEM) can be extracted from point clouds, derivatives include canopy height models (CHM), ITCD (Wang et al. 2008; Mohan et al. 2017) and ABA estimates of forest attributes such as stand height and timber volume (Tompalski et al. 2015).

The capacity of the initial digital images to provide spectral information is an additional strength of DAP-based approaches. Spectral information has strengths in detecting and classifying vegetation health; however, this often relies on wavelengths beyond the visible spectrum, in particular the near-infrared. Additional challenges with spectral analysis include radiometric calibration techniques to ensure colour consistency throughout captured images

(Markelin et al., 2008; Collings et al., 2011). A summarized comparison of the capabilities and advantages between AAS-DAP and ALS remote sensing techniques is shown in (Table 1.3-1).

**Table 1.3-1. Key differences between ALS and AAS-DAP technologies**

| | Spectral Information | Canopy Penetration | DEM Accuracy | Positional Accuracy | Point Density | Cost | Weather Tolerance |
|---|---|---|---|---|---|---|---|
| ALS | | √ | √ | √ | | | |
| AAS-DAP | √ | | | | √ | √ | √ |

## 1.4 Challenges with new technologies

### 1.4.1 Terrain modelling

Almost any analysis done using 3D point-cloud data is dependent on initial discrimination of terrain from objects and the difficulty of this task increases with surface variability (Meng et al., 2010; Chen et al., 2017). Accuracy of predicted forest metrics such as height and volume are dependent on the generation of an accurate DEM used to normalize vegetation heights. Given BC's expansive forest ranges and their complexity, the identification of forest attributes that allow for an accurate DEM generation at the forest stand level using AAS-DAP is important for reducing reliance on ALS acquisitions. Both DAP and ALS point clouds provide accurate, continuous top-of-crown measurements; however, the ability for DAP to describe forest structure decreases with distance beneath the canopy surface. Furthermore, DAP is prone to producing point-cloud voids where shaded portions of an image appear black, therefore the disparity of terrain coverage between ALS and DAP generally increases with higher tree count per area, crown density and tree height. As a result, ground detection from

DAP has principally been limited to non-forested landscapes, open forests with no understory, or plantations (Table 1.4-1).

**Table 1.4-1. Recent studies utilizing digital aerial photogrammetry divided into forest structure and ground detection.**

| Publication | Year | Aerial Platform | Location | Landcover Type | Forest Structure | Ground Detection |
|---|---|---|---|---|---|---|
| (Tompalski et al. 2018) | 2018 | PA* | Northern Alberta, Canada | Mixedwood, Boreal and Temperate | √ | |
| (Goodbody, Coops, Hermosilla, Tompalski, and Pelletier 2018) | 2018 | AAS | Edmundston, New Brunswick, Canada | Hardwood dominated | | √ |
| (Iizuka et al. 2018) | 2017 | AAS | Otsu City, Shiga Prefecture, Japan | Evergreen coniferous | √ | √ |
| (Guerra-Hernández et al. 2017) | 2017 | AAS | Alcochete, Central Portugal | Pinus pinea plantation | √ | √ |
| (Rahlf et al. 2017) | 2017 | PA | Central Norway | Temperate, coniferous | √ | |
| (Goodbody et al. 2016) | 2016 | AAS | Central BC, Canada | Young coniferous (<15 years since clearcut) | √ | |
| (Clapuyt, Vanacker, and Van Oost 2016) | 2016 | AAS | Central Belgium | Pasture, arable fields without crops | | √ |
| (Jensen and Mathews 2016) | 2016 | AAS | Edwards Plateau, | Savannah, undulating | √ | √ |

| Publication | Year | Aerial Platform | Location | Landcover Type | Forest Structure | Ground Detection |
|---|---|---|---|---|---|---|
| | | | Central Texas, USA | hills, evergreen | | |
| (Ota et al. 2015) | 2015 | PA | Central Cambodia | Evergreen, deciduous, | √ | |
| (Lucieer, Jong, and Turner 2014) | 2014 | AAS | Southern Tasmania, Australia | Landslide zone, exposed soil, short grass | | √ |
| (Fonstad et al. 2013) | 2013 | Helium Blimp | Central Texas, USA | Bedrock | | √ |
| (Harwin and Lucieer 2012) | 2012 | AAS | Southeast Tasmania, Australia | Scattered shrubs, Coastal marsh, erosion scarp | | √ |
| (Niethammer et al. 2012) | 2012 | AAS | Southern Alps, France | Landslide zone, bedrock, exposed soil | | √ |
| (St-Onge et al. 2008) | 2008 | PA | New Brunswick, Canada | Boreal forest | √ | |
| (Korpela and Anttila 2004) | 2004 | PA | Southern Finland | Temperate, coniferous | √ | |

* PA - Piloted Aircraft

### 1.4.2 Area-based forest inventories with AAS-DAP

The majority of studies which examine the forest attribute modelling capacity of AAS-DAP normalize vegetation heights above ground using terrain surfaces generated from ALS or other external data sources (Bohlin, Wallerman, and Fransson 2012). When co-registered with sufficient precision, results show that the photogrammetric CHM can replicate or exceed the accuracies of combining aerial imagery and ALS data (Tuominen et al. 2015). However, there is a lack of research using both ground detection and subsequent forest attribute modelling techniques on AAS-DAP data alone.

## 1.5 Research objectives

The overarching research objective of this thesis is to examine the capacity of AAS-DAP surveys to generate an operational forest inventory in the interior plateau forest region of BC. Remotely sensed forest inventories using 3D point-cloud data are dependent on terrain surface generation to gather above-ground vegetation heights. Therefore, an analysis of terrain classification algorithms as well as the influence of forest characteristics on their errors was required. Following that, the AAS-DAP data were analyzed using an area-based forest inventory approach which has been previously established using ALS data. A visual representation of the data and analysis portions of this thesis are provided below in Figure 1.5-1.

This thesis addresses two main questions each broken into two sub-questions:

1) Chapter 3: To what extent is terrain modeling possible using AAS-DAP in a complex conifer forest?
    a) How do terrain models derived from AAS-DAP compare to those from ALS in a complex conifer forest?
    b) What is the influence of canopy cover and terrain slope on the accuracy of AAS-DAP terrain models?

2) Chapter 4: To what extent are forest height and stem volume predictions possible using AAS-DAP over a complex conifer forest?
    a) How do prediction accuracies compare to those from achieved using ALS with the area-based approach?

b) What is the influence of terrain surface interpolation methods on height and volume predictions?

Chapter 2 presents characteristics of the study area located in the University of BC's Alex Fraser Research Forest Gavin Lake Block. The field-plot data collection scheme and resulting measurements are presented. This is followed by presenting the acquisition parameters of the AAS images, point-cloud processing workflow and georeferencing procedure. Lastly, the acquisition of ALS data is presented.

Chapter 3 addresses research question 1 and sub-questions 1a) and 1b) outlined above. Methods and findings for assessing the terrain modelling capacity of AAS-DAP point-clouds is presented. A sensitivity analysis of point-cloud ground classification algorithms is presented. The influence of canopy cover and terrain slope on classification error is also presented.

Chapter 4 focuses on research question 2 and sub-questions 2a) and 2b). Methodologies and findings for estimating operational forest inventory attributes are presented. Using an optimal ground classification identified in Chapter 3, the effect of terrain surface interpolation methods on the accuracy of forest modelling is presented.

Chapter 5 summarizes the key findings from Chapters 3 and 4 as well as their broader implications for forest management. These findings are then considered from an operational

inventory perspective where some recommendations are made. Lastly, the limitations of this research and opportunities for supplementary research are discussed.

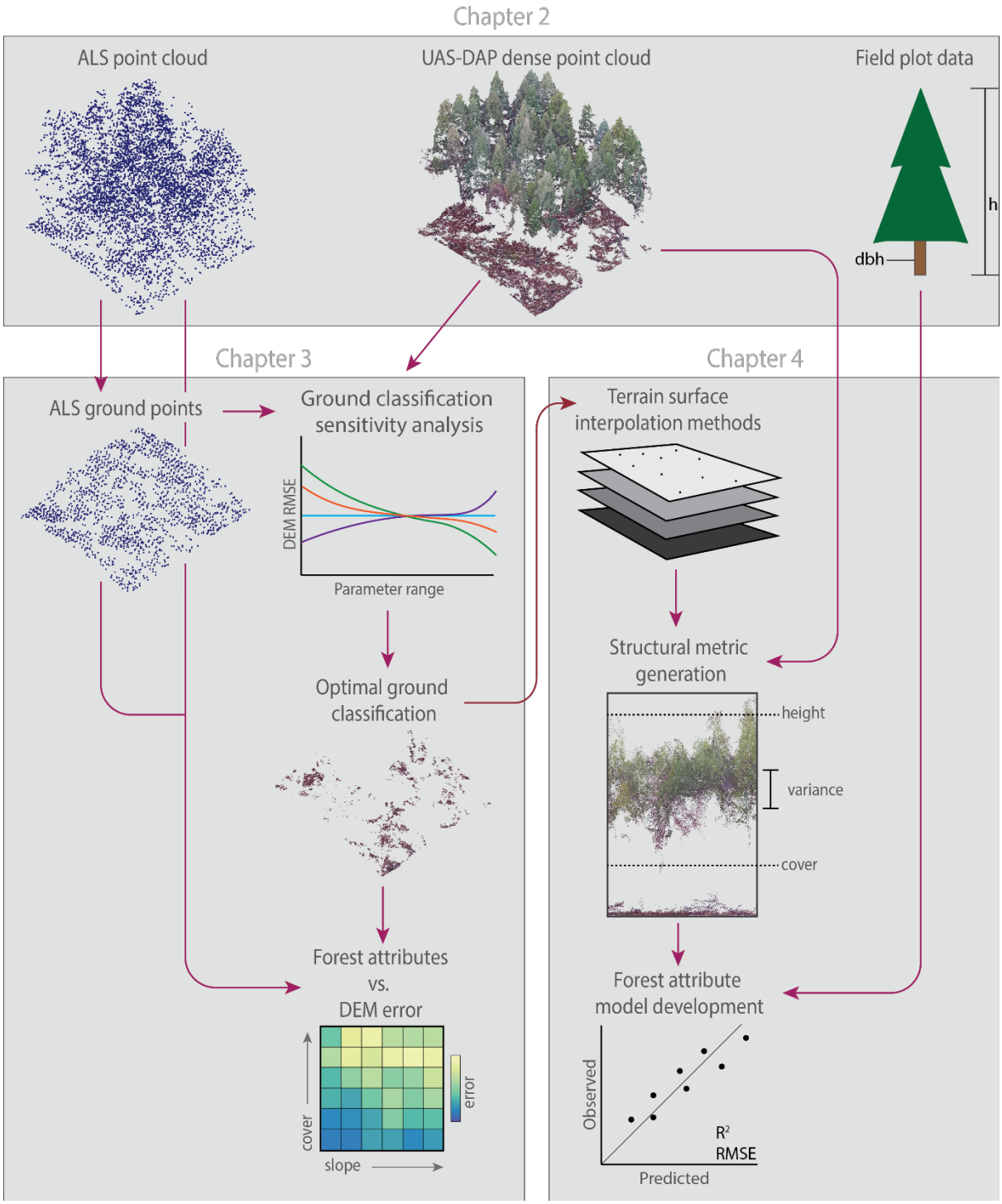


**Figure 1.5-1. Conceptual workflow diagram of data and analysis Chapters 2, 3 and 4.**

# Chapter 2: Study site & data

## 2.1 Study site

Terrain modelling and forest inventory estimation studies were conducted within three study areas (Figure 2.1-1) located within the University of British Columbia Alex Fraser Research Forest (AFRF) Gavin Lake Block, about 50 km northeast of Williams Lake, BC, Canada, herein referred to as Gavin Lake Block. In addition to ALS data availability, sites were chosen to represent the range of forest density and terrain complexity of BC's interior plateau physiographic region. The Gavin Lake Block transitions west to east from the Sub-boreal Spruce (SBS) to the Interior Cedar - Hemlock (ICH) Biogeoclimatic Ecosystem Classification (BEC) zones. Annual precipitation respective to each BEC zone 527 mm and 664 mm and mean-annual temperatures are 3.7 °C and 4.5 °C. (Day 2007). Forest structure of the Gavin Lake Block is also a product of frequent wildfires and logging activity dating back to the 1940's (Day 2007). Upon visiting the site in the fall of 2017, the forest stands were dominated by mature conifers with small patches of deciduous species. According to Klinka, 2004, tree species in decreasing abundance are Douglas-fir (*psuedotsuga menziesii var. glauca* (56%)), hybrid spruce (*Picea Glauca x engelmannii* (15%)), western redcedar (*Thuja plicata* (10%)), lodgepole pine (*Pinus contorta* (9%)), and trembling aspen (*Populus tremuloides* (6%)). The combined areas lie between 700-1250 m above mean sea level with varying terrain slopes up to 68° and a mean slope of 16°. The location and elevation of the three AAS-DAP flight areas (A, B and C) are shown in Table 2.1-1 and displayed as maps in Figures 2.1-1 and 2.1-2 below.

**Table 2.1-1. Location, elevation and size of the three data acquisition areas located in the Gavin Lake Block of interior British Columbia.**

| Study area | Centroid Location (Latitude, Longitude) | Mean Elevation AMSL (m) | Size (ha) |
|---|---|---|---|
| A | -121.8006, 52.4487 | 858 | 131 |
| B | -121.7723, 52.4481 | 926 | 116 |
| C | -121.7328, 52.44883 | 1156 | 123 |

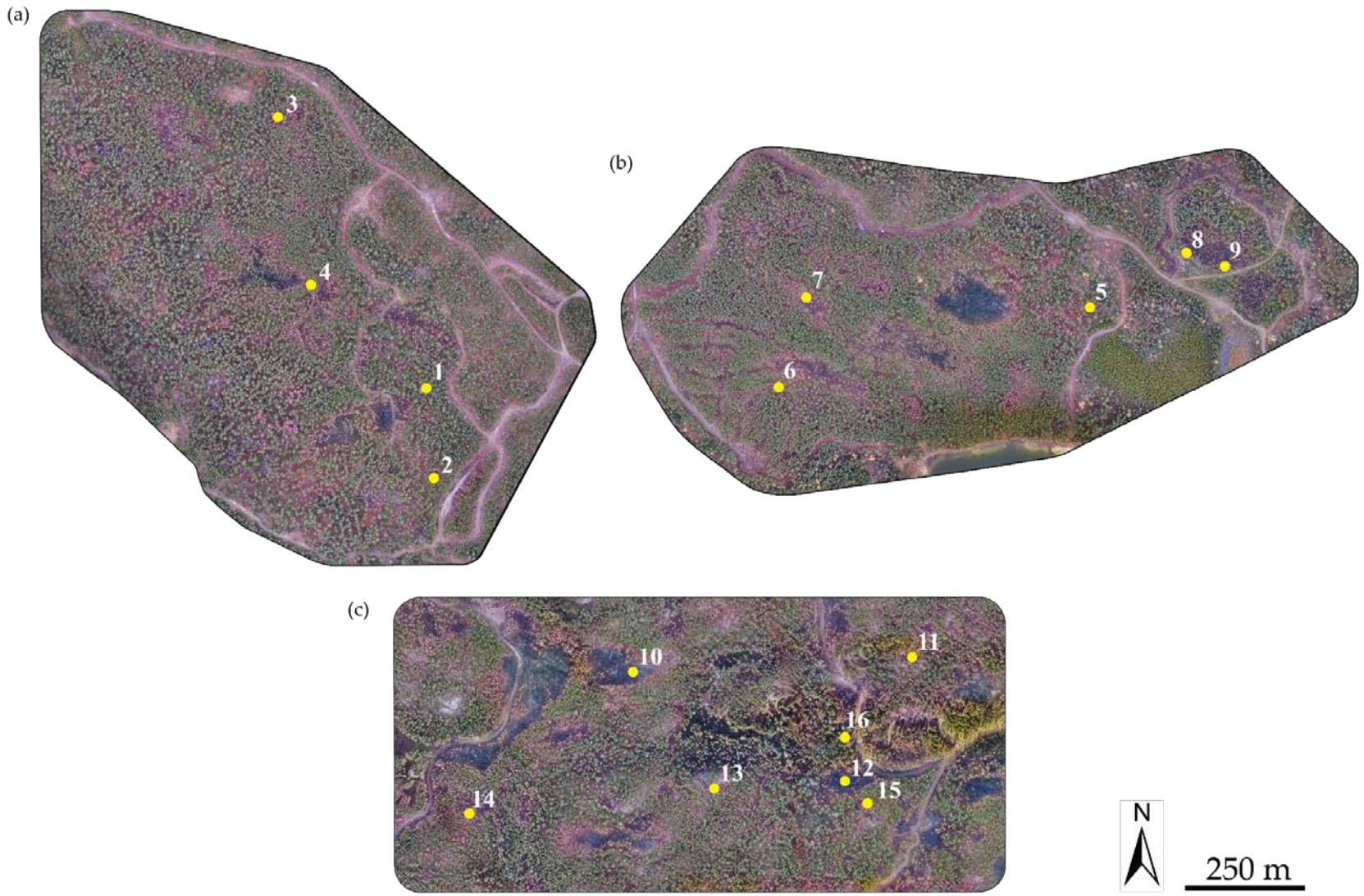


**Figure 2.1-1. AAS acquired orthomosaics of study areas A, B and C (a, b, and c) respectively overlaid with field plot locations labeled with Plot ID (see Table 2.2-1)**

A number of non-contiguous wildfires affected sizeable portions of the Gavin Lake Block with heterogeneous severity in the summer of 2017 prior to AAS data acquisition. As a result, portions of the study areas consisted of dead or dying trees along with scorched ground and tree stems. Where the fire intensity was higher, remaining standing trees had limited or no foliage. These areas are identifiable in Figure 2.1-1 as patches of dark grey and black. To quantify the proportional burned area within the study areas, relative differenced normalized burn ratio (RdNBR) was divided into low, moderate and high fire severity classes from Landsat Thematic Mapper / Enhanced Thematic Mapper+ imagery (Soverel, Perrakis, and Coops 2010). The proportion of fire severity classes aggregated over the three study areas was 28.9%, 14.5% and 5.4% for low, moderate and high respectively.

## 2.2 Field measurements

A total of 16 fixed radius (12.6 m) forest inventory plots were established within the AFRF Gavin Lake Block in October 2017. Plots were distributed using stratified random sampling based on the aforementioned classes of the RdNBR fire severity layer and canopy cover defined as the fraction of all returns > 2 m height from the ALS data to represent the variation in forest structure conditions present in the area. Upon visiting the site, two field plots were in areas of severe fire damage with minimal remaining above-ground biomass and were excluded from the analysis. The collected information for the field plots is summarized in Table 2.2-1. All live trees with diameter at breast height (DBH) greater than 10 cm were included. The mean height of measured trees was 16.3 m. Plot-centre locations were measured using differential global positioning system (DGPS) techniques with an Ashtech ProMark 120. The location of each tree was calculated using horizontal distance

and azimuth readings taken from the centre of each plot using a TruPulse 360B laser rangefinder. Tree heights were measured in the field using a Vertex III Hypsometer and Transponder while tree species was determined visually. Allometric relationships derived by Ung, Bernier, and Guo (2008) were utilized to estimate plot-level individual-tree biomass which were converted to $V_{stem}$ using wood density relationships established by Gonzalez (1990).

**Table 2.2-1. Summary of field plot measurements conducted in the study areas located in the Gavin Lake Block of interior British Columbia**.

| Plot ID | Tree Count | | Species Count | | | | | | DBH (cm) | | Height (m) | | $V_{stem}$ ($m^3$) | | $H_{Lorey}$ (m) |
|---|---|---|---|---|---|---|---|---|---|---|---|---|---|---|---|
| | Per Plot | Per ha | At | Bp | Fd | Fs | Pl | Sx | Mean | SD | Mean | SD | Per Plot | Per ha | |
| 1 | 33 | 660 | | | 24 | 1 | | 8 | 23.3 | 8.5 | 19.7 | 4.5 | 13.4 | 269 | 22.4 |
| 2 | 44 | 880 | | 1 | 37 | | 6 | | 18.7 | 4.4 | 18.2 | 3.1 | 10.1 | 203 | 19.3 |
| 3 | 29 | 580 | 1 | 5 | 8 | 2 | | 13 | 26.6 | 20.0 | 22.2 | 5.0 | 21.3 | 426 | 27.8 |
| 4 | 64 | 1280 | | | 64 | | | | 24.1 | 6.3 | 22.4 | 3.1 | 27.6 | 551 | 23.6 |
| 5 | 24 | 480 | 2 | 11 | 7 | | | 4 | 24.5 | 9.2 | 20.0 | 5.4 | 10.9 | 217 | 22.8 |
| 6 | 49 | 980 | | | 49 | | | | 21.8 | 8.4 | 18.4 | 3.1 | 14.7 | 295 | 20.0 |
| 7 | 17 | 340 | | | 15 | | 2 | | 18.7 | 5.5 | 14.1 | 4.0 | 3.0 | 59 | 15.7 |
| 8 | 27 | 540 | | 3 | | | 7 | 17 | 13.8 | 3.0 | 13.6 | 4.0 | 3.0 | 60 | 14.7 |
| 9 | 48 | 960 | | 1 | 2 | | 18 | 27 | 13.6 | 3.3 | 13.8 | 5.1 | 5.7 | 113 | 15.0 |
| 10 | 58 | 1160 | 1 | | 56 | | | 1 | 19.6 | 5.1 | 15.9 | 4.2 | 11.9 | 239 | 17.2 |
| 11 | 15 | 300 | | | 14 | | 1 | | 24.3 | 9.7 | 11.5 | 2.6 | 2.9 | 57 | 12.3 |
| 12 | 32 | 640 | | | 30 | 1 | | 1 | 23.0 | 7.0 | 17.2 | 6.2 | 10.4 | 208 | 19.9 |
| 13 | 32 | 640 | | | 30 | 2 | | | 19.9 | 5.7 | 11.3 | 2.5 | 4.3 | 86 | 12.3 |
| 14 | 40 | 800 | | | 39 | | | 1 | 20.1 | 8.1 | 15.1 | 2.4 | 8.3 | 165 | 16.8 |
| 15 | 54 | 1080 | | | 41 | 5 | 4 | 4 | 18.9 | 5.2 | 14.0 | 3.9 | 9.6 | 192 | 15.4 |
| 16 | 39 | 780 | | | 39 | | | | 19.7 | 5.5 | 13.5 | 4.2 | 6.7 | 134 | 15.1 |

Species names abbreviations: **At** - Trembling Aspen (*Populus tremuloides*), **Bp** - Paper Birch (*betula papyrifera*), **Fd** - Douglas Fir (*psuedotsuga menziesii var. glauca*), **Fs** - Subalpine Fir (*Abies lasiocarpa*), **Pl** - Lodgepole Pine (*Pinus contorta var. latifolia*), **Sx** - Sitka Spruce (*Picea sitchensis*) or White Spruce (*Picea glauca*) or Engelmann Spruce (*Picea engelmannii*)

## 2.3 Remote sensing data

### 2.3.1 AAS image acquisition

AAS-DAP data acquisitions were conducted within the AFRF Gavin Lake block from 21 to 24 October 2017 using a DJI Phantom IV quadcopter AAS equipped with a compact RGB digital camera. Each of the study areas (A, B and C) were flown on a single day with up to eight individual flights to cover each area. Weather conditions were predominantly clear sky with minimal cloud coverage. No precipitation was observed during any acquisitions. The specifications of the Phantom AAS along with employed flight parameters and image-overlap settings are presented in Table 2.3-1.

**Table 2.3-1. AAS specifications of the DJI Phantom 4 and parameters used for image acquisition.**

| **System Specifications** | |
|---|---|
| **Aircraft** | |
| Max Flight Time | 28 min |
| Navigation | GPS & GLONASS |
| GPS Positional Accuracy | 0.5m (z), 1.5 m (x,y) |
| Transmission Range | 5 km |
| **Camera** | |
| Sensor | 1/2.3” CMOS |
| ISO Range | 100–1600 (photo) |
| Electronic Shutter Speed | 1/8000s |
| FOV | 94° |
| Aperture | f/2.8 |
| Image Size | 4000 × 3000 |
| **Acquisition Parameters** | |
| Altitude | 120 m (AGL) |
| Terrain Following | 30 m SRTM * |
| Image Overlap | 90% Forward, 85% Lateral |
| Image Capture Interval | 2.5 s |
| Write to Disk Speed | 10 Mb/s |

*****Shuttle radar topography mission

### 2.3.2 AAS-DAP point cloud generation

AAS images were compiled for point-cloud generation using Pix4Dmapper Pro version 4.1.24 (Pix4D, 2018) software for each study area separately. Images were first aligned and optimized using the on-board inertial measurement unit and GNSS/GPS followed by tie-point pixel identification within overlapping images. The number of calibrated images used was 2117, 1890 and 1882 for areas A, B and C respectively. Settings employed for point-cloud generation were default image scale and 'optimal' point density, and the minimum number of images matches was set to three. Average processing time for point cloud generation between the three study areas was 5.1 h and the average point-cloud density was 95 points per $m^2$.

### 2.3.3 AAS-DAP point-cloud georeferencing

Point-cloud data captured from aerial platforms can be either directly georeferenced with onboard GPS systems or using a network of ground control points (GCP) with precise 3D coordinates. Ten GCPs were evenly distributed within each study site (Figure 2) resulting in an average density of 1 GCP per 13 ha. The location of each GCP was measured using differential GPS techniques with the Ashtech ProMark 120 by averaging one reading per second for five minutes. The Ashtech ProMark 120 is capable of DGPS accuracy of <0.30 m + 1 ppm (Spectra Precision 2012). One GCP in area A was discarded due to high vertical root-mean-square-error (RMSE) reported by the GPS unit at the site. Images containing GCPs were identified, then GCP tagged. The number of images containing GCPs, RMSE of GPS measurements and GCP image identification are presented in Table 2.3-2.

**Table 2.3-2. Ground sampling distance (GSD), mean horizontal and vertical RMSE ($RMSE_{xy}$, $RMSE_z$) acquired from the DGPS measurements of GCP used for georeferencing the DAP point-cloud, and GCP image identification RMSE averaged per study site.**

| AAS Flight Area | | GPS | | | GCP Image Identification Accuracy | | | |
|---|---|---|---|---|---|---|---|---|
| **Site** | **Mean GSD (cm)** | **# of GCP** | **Mean $RMSE_{xy}$ (m)** | **Mean $RMSE_z$ (m)** | **# of Marked Images** | **Mean RMSE X (m)** | **Mean RMSE Y (m)** | **Mean RMSE Z (m)** |
| A | 4.69 | 9 | 1.382 | 1.964 | 204 | 0.088 | 0.082 | 0.114 |
| B | 4.88 | 10 | 1.662 | 2.874 | 101 | 0.483 | 0.724 | 2.507 |
| C | 4.97 | 10 | 0.617 | 0.882 | 105 | 1.026 | 2.309 | 3.320 |

### 2.3.4 Airborne laser scanning data

ALS data were acquired over the Gavin Lake Block in 2008 at a point density of 4-6 points per $m^2$ using 50% lateral overlap (Coops, Duffe, and Koot 2010). A 1 m × 1 m resolution DEM was generated from the ground-classified returns and used in height normalization necessary for deriving ALS canopy cover. A 1 m × 1 m resolution terrain slope raster was also generated from the ALS-DEM.

# Chapter 3: Evaluation of ground surface models derived from autonomous aerial systems with digital aerial photogrammetry in a disturbed conifer forest

## 3.1 Introduction

The analysis of 3D point-cloud data typically involves the separation of terrain from vegetation object components. This process will be referred to herein as ground classification and allows the point cloud to be normalized according to height above ground, thus facilitating the measurement of 3D forest metrics. The accuracy of such classification varies according to terrain complexity (Meng et al. 2010; Yan et al. 2017); therefore, DEM generation that accounts for surface variability is necessary to ensure accurate estimates of forest structure. Both DAP and ALS point clouds provide accurate, continuous top-of-crown measurements; however, the ability for DAP to describe forest structure decreases with distance below the canopy surface. Furthermore, DAP is prone to producing voids in the point cloud where trees found in matching photos may occlude each other (Barnard, Fischler, and Barnard 1982). The disparity of terrain coverage between ALS and DAP generally increases with canopy height (Gatziolis et al. 2015). Nevertheless, the low cost and increased repeatability of DAP relative to ALS for stand-level applications shows significant potential (Goodbody, Coops, Hermosilla, Tompalski, and Pelletier 2018; Smith, Carrivick, and Quincey 2015). Recent studies indicate that accurate DEM generation from the unsupervised classification of DAP point clouds under open forest canopies is achievable (Kachamba et al. 2017; Guerra-Hernández et al. 2017; Goodbody, Coops, Hermosilla, Tompalski, and Pelletier 2018; Guerra-Hernández et al. 2018). For example (Guerra-

Hernández et al. 2017) used 20 high precision GPS checkpoints and found RMSE of 0.046 m, 0.018 m and 0.033 m in the X, Y and Z directions respectively.

To answer questions 1a) and 1b) outlined in Section 1.5, this chapter (1) obtained terrain-modelling results typical of a low-cost AAS-DAP acquisition in a mountainous forest environment, (2) established optimal parameters of three ground-point classification algorithms, and (3) compared DAP terrain-modelling accuracies under various terrain-slope and canopy-cover conditions. Evaluation of the AAS-DAP terrain models was carried out against commercially provided ALS ground points.

## 3.2 Methods

This chapter was carried out in five steps: photogrammetric processing, georeferencing, ground filter sensitivity analysis, forest structure and terrain stratification and performance evaluation (Figure 3.2-1). First, AAS images from three acquisitions were processed to generate photogrammetric point clouds. The point clouds were then georeferenced using GCPs followed by a systematic sensitivity analysis of three ground-point classification algorithms to determine optimal parameters resulting in a single ground-classified point cloud for each algorithm. Finally, performance evaluation was carried out to assess the accuracy of subsequently generated DEMs under various terrain-slope and canopy-cover classes.

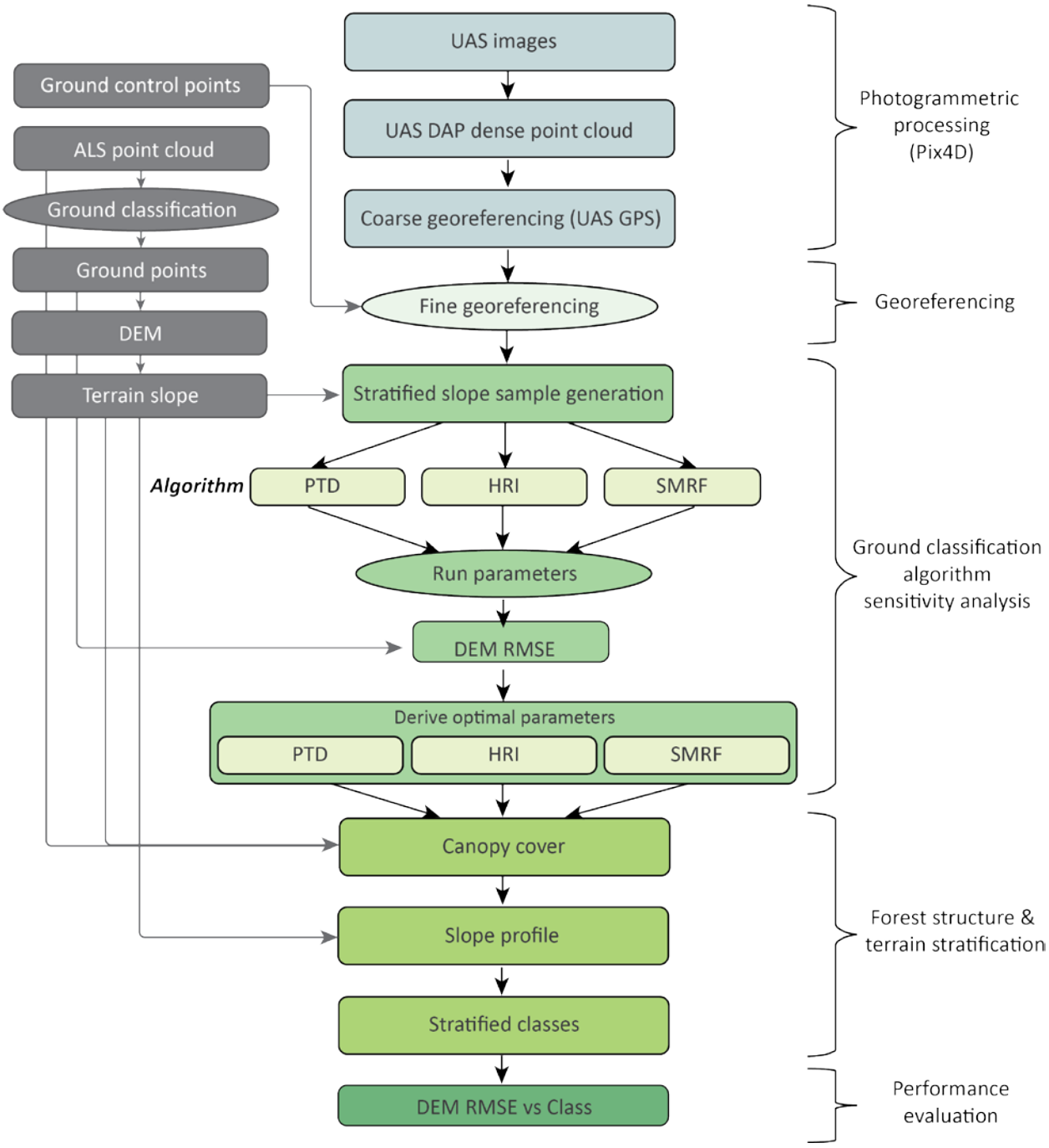


**Figure 3.2-1. Schematic workflow of DAP point cloud generation, filter sensitivity analysis and DEM error assessment.**

### 3.2.1 AAS-DAP Ground-point classification and DEM generation

Ground classification routines can be broadly categorized into surface-based, morphology-based and slope-based (W. Zhang et al. 2016). Surface-based algorithms can be further subdivided into progressive triangulated irregular network densification (PTD) and interpolation-based algorithms (Asghar 2017; Jat and Serre 2016, 2018). This chapter tested three published, academically licensed or open-source ground-point selection methods, all designed for ALS data. The two best performing algorithms according to results from Sithole & Vosselman (Sithole and Vosselman 2004) are tested in this chapter. They are PTD (Axelsson 1999, 2000), followed by the hierarchical robust interpolation (HRI) algorithm (Kraus and Pfeifer 1998). The third method is the simple morphological filter (SMRF) (Pingel, Clarke, and Mcbride 2013), first proposed by Kilian et al. (1996) and later implemented by Zhang et al. (Keqi Zhang et al. 2003). The PTD and SMRF algorithms are primarily designed for the ground classification of urban environments with a mix of natural and man-made surface elements while the HRI method is designed for wooded areas (Kraus and Pfeifer 1998).

The PTD algorithm (Axelsson 1999, 2000) and its modifications for the improved handling of surface discontinuities (J. Zhang and Lin 2013), first generates a sparse triangulated irregular network (TIN) based on seed points (lowest points) within cells of a gridded point-cloud (Axelsson 2000). After seed points are established, the remaining points are used to iteratively densify the initial TIN based on thresholds of normal distance and angle to nearest facets and nodes respectively of the sparse TIN (Axelsson 2000). The PTD method has been shown to produce better results when compared to other methods (Montealegre, Lamelas, and De

La Riva 2015a; Asghar 2017) and is implemented in the commercial point-cloud classification software, Terrascan (2016).

The HRI algorithm (Kraus and Pfeifer 1998), is based on linear-least-squares and is designed for removing non-ground ALS measurements of forested environments. The method begins by computing an equally-weighted surface ($Z_i$) through z-values of all points, and is presumed to lie between the true terrain and canopy top surfaces. Under the assumption that points with larger negative residuals with respect to $Z_i$ are more likely to be true terrain points, residual-based weights are computed. $Z_i$ is then updated iteratively until the specified number of iterations is reached (Kraus and Pfeifer 1998). Upon each iteration, points are assigned a weight value according to the following equation:

$$p_i = \begin{cases} 1 & v_i \leq g \\ \dfrac{1}{1 + (a(v_i - g)^b)} & g < v_i \leq g + w \\ 0 & g + w < v_i \end{cases} \quad (1)$$

Where *a*, *b*, *g* and *w* are parameters of the HRI method and $p_i$ is assigned weight where points with residuals $v_i$ greater than $g + w$ with respect to the current ground-surface estimation are assigned as non-ground points.

The SMRF is a computationally simplified method stemming from the work of Kilian et al. (1996), implemented by Zhang et al. (2003)**,** and establishes a performance baseline for the morphological filtering approach (Pingel, Clarke, and Mcbride 2013). The algorithm consists of four steps and four required parameters in addition to the 3D coordinates of points. The initial step is similar to that of the PTD algorithm where lowest points within a gridded point cloud are isolated to generate an initial minimum surface represented as a raster rather than a TIN.

Algorithm parameters are the cell-size of the initial minimum raster surface, a slope value that dictates terrain vs. object classification upon each iteration, and minimum and maximum window radii controlling the opening operation. An additional optional parameter, cut is dependent on provisional DEM slope calculations and operates under the assumption that terrain vs. object distance thresholds should be more liberal in areas of steeper slope.

For the final DEM surface generation, the ALS and DAP ground points were converted to a TIN surface, and a 1 m × 1 m raster DEM using memory efficient TIN-streaming technology based on three parallel processes (Isenburg et al. 2006).

### 3.2.2 Ground classification algorithm sensitivity analysis

All three examined ground classification methods require parameterization, with key parameters likely to be different between DAP and ALS-derived point clouds. Therefore, a sensitivity analysis was conducted by varying parameters to derive a single set of optimal parameters for each classification method. Given the strong influence of terrain slope on the results of ground filtering (Hodgson et al. 2005; Meng et al. 2010), the study areas were stratified into three terrain-slope classes; gentle (0–11°), moderate (11–17°) and high (17–39°) based on the ALS-DEM. Three 1 ha (100 m x 100 m) samples were randomly placed within each slope class and a 25 m buffer was incorporated around samples to eliminate edge artifacts during the TIN-based DEM generation. Next, for each tested algorithm (Table 3.2-1), a range of parameter values (Table 3.2-2) were tested for each sample. *Step*, *cell* and *cell* of the PTD, HRI and SMRF algorithms respectively serve as the spatial resolution of the classification input area and were therefore varied from 1 to 25 m in 7 steps. The maximum value of *step*, *cell* and *cell* of the PTD,

HRI and SMRF methods was limited to 25 m for two reasons. First, values >25 m tended to leave large gaps in the distribution of ground points even when they existed. Second, to avoid problematic edge artifacts, larger initial search footprints require a larger point-cloud dataset and therefore compromise the ability to stratify the samples and require exponentially more processing time. Therefore analysis was limited to 1 ha (100 m x 100 m) samples and 25 m search footprints. For the remaining parameters, default values from the original authors were used as the median of the varied range. Parameters without default values were varied in equal steps. The *cut* parameter of the SMRF method is a large structuring element designed for removing large continuous objects on relatively flat terrain (Pingel, Clarke, and Mcbride 2013) and therefore was not varied and held at its default value of 0. As a result, 23,625, 45,927 and 25,515 unique runs were undertaken to produce DAP-DEMs for the PTD, HRI and SMRF methods respectively.

**Table 3.2-1. Chosen ALS ground-point classification algorithms tested on DAP point clouds and their respective parameters and software implementations.**

| Publication | Class | Key Method | Tested Parameters | Software Implementation |
|---|---|---|---|---|
| (Axelsson 1999, 2000) | Surface | PTD | step-size, initial search intensity, bulge, spike, ground offset | LAStools |
| (Kraus and Pfeifer 1998) | Surface | HRI | cell-size, tolerance distance, a, b, g, w, iterations | FUSION |
| (Pingel, Clarke, and Mcbride 2013) | Morphological | SMRF | cell-size, cut-net size, elevation scalar, slope, elevation threshold, max window size | Point Data Abstraction Library (PDAL) |

**Table 3.2-2. Ground classification algorithms, parameter descriptions and values used for testing on 1 ha stratified samples.**

| Method | Parameter | Description | Values |
|---|---|---|---|
| PTD | step | initial grid resolution for assigning TIN seed points (m) | 1, 5, 9, 13, 17, 21, 25* |
| | intensity | initial ground point search intensity | coarse, fine, hyper-fine |
| | bulge | positive height coarse TIN surface can bulge during refinement (m) | 0.1, 0.6, 1.1, 1.6, 2.1 |
| | spike | height threshold to remove localized positive vertical spikes (m) | 0.1, 0.6, 1.1, 1.6, 2.1 |
| | offset | positive vertical offset from ground estimate to include points (m) | 0.1, 0.6, 1.1, 0.6, 2.1 |
| HRI | cell | cell-size used for intermediate surface models (m) | 1, 5, 9, 13, 17, 21, 25 |
| | g | see Equation (1). | −2.2, −2.0*, −1.8 |
| | w | | 2.25, 2.5*, 2.75 |
| | a | | 0.9, 1.0*, 1.1 |
| | b | | 3.6, 4.0*, 4.4 |
| | tolerance | vertical tolerance for final classification of ground points | 0.1, 1.1, 2.1 |
| | iterations | number of iterations for classification logic | 3, 5*, 7 |
| SMRF | cell | grid cell resolution of ground point search (m) | 1, 5, 9, 13, 17, 21, 25 |
| | slope | slope threshold to exclude adjacent ground points (%) | 0.05, 0.10, 0.15*, 0.20, 0.25 |
| | scalar | scaling value to be multiplied by slope of provisional DEM | 0.75, 1.00, 1.25*, 1.50, 1.75 |
| | threshold | vertical distance from provisional DEM to include points (m) | 0.1, 0.5*, 0.9 |
| | window | max search radius for including points in the provisional DEM (m) | 10, 14, 18*, 22, 26 |
| | cut | spacing of minimum values used for removing large objects (m) | 0* |

*algorithm default value.

### 3.2.3 Ground classification algorithm accuracy assessment

The RMSE and the signed elevation differences, referred to as DEM bias, were calculated for each sensitivity analysis iteration using the vertical residual between the DAP-DEM surfaces and ALS ground points. RMSE was calculated according to the following equation:

$$RMSE = \sqrt{\frac{\sum_{i=1}^{n} ALS_z - DAPDEM_z}{n}} \quad (2)$$

where $ALS_z$ is the elevation of the ALS ground point and $DAPDEM_z$ is the elevation of the 1 m x 1 m resolution DAP-DEM raster surface and *n* is the number of ALS ground points. Anticipating that some runs would yield DAP-DEMs with incomplete sample coverage, 99% of ALS ground points were required to overlap with the DAP-DEM to provide a valid RMSE. Then, for each 1 ha sample, RMSE values within the first percentile were extracted from which the most occurring value of each parameter was designated as the optimal parameter for each algorithm.

### 3.2.4 DEM accuracy under various canopy cover and terrain slope conditions

Once optimum values were found for each method, the resulting DEMs and their RMSE with respect to ALS ground points were compared to canopy cover and terrain slope classes computed in 25 m × 25 m cells (Figures 3.3-1 and 3.3-2). Terrain slope and canopy cover classes were defined using a single stratification across the three study areas from the full ALS point clouds and 1 m x 1 m resolution ALS-DEMs respectively. Each grid cell was assigned a mean terrain slope and canopy cover value. Traditionally, canopy cover has been defined as fraction of points above breast height (1.3 m) (Korhonen et al. 2011) or 2 m (Nilsson 1996). However, an increased height threshold of 6 m was chosen due to the abundance of tall stands (>20 m) across

all study areas to represent the range of canopy cover classes. Canopy cover and terrain slope were defined at the 25 m × 25 m cell level and each divided into six classes across the aggregated study areas. The best performing classification method was defined as the algorithm which produced DAP-DEMs with RMSE <1.5 over the largest proportional area. The threshold of 1.5 m represents approximately 10% of the mean tree height found in the study areas according to the field measurements (Section 2.2). Finally, a random forests regression tree algorithm was used to model RMSE to estimate the relative influence of terrain slope and canopy cover.

## 3.3 Results

### 3.3.1 Ground classification algorithm sensitivity analysis results

Proportion of valid DAP-DEMs generated during the sensitivity analysis were 99.9%, 94.9% and 91.8% for the PTD, HRI and SMRF methods respectively. In order to isolate a given parameter's relative influence on RMSE (Figure 3.3-4), each parameter was varied across its range while the remaining parameters were held constant at the mean of their range. For example, the *step* parameter curve of the PTD method shown in Figure 3.3-4 represents algorithm runs where *step* was employed with values 1, 5, 9, 13, 17, 21, and 25 m with *bulge* of 1.1 m, *offset* of 1.1 m, *spike* of 1.1 m and 'fine' *intensity.*

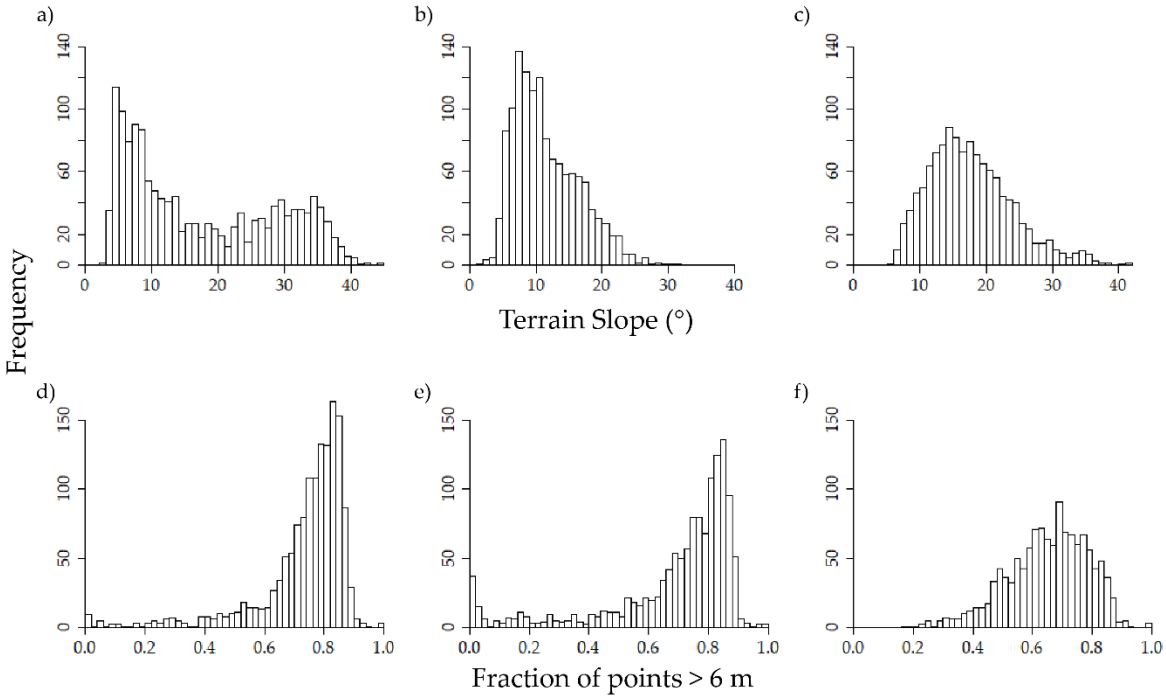


**Figure 3.3-1. Distribution of area-based ALS derived terrain slope and canopy cover per study area A (a,d), B (b,e), and C (c,f) defined at 25 m × 25 m cell resolution.**

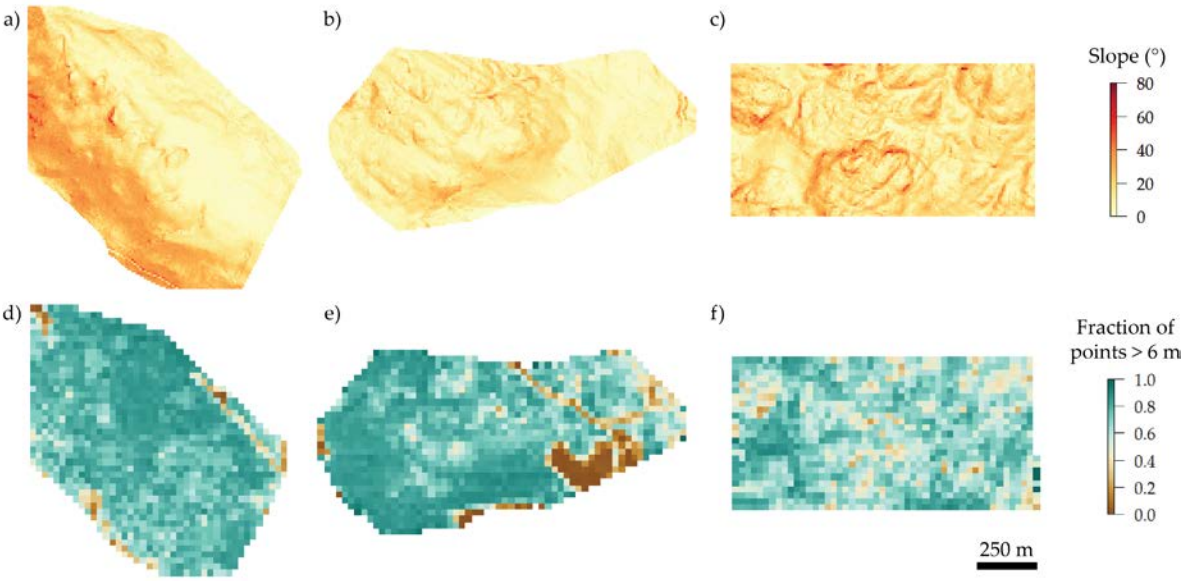


**Figure 3.3-2. Spatial distribution of the 1 m × 1 m resolution ALS derived slope layer for areas A, B and C respectively (a–c), and canopy cover (d–f) defined at 25 m × 25 m cell resolution.**

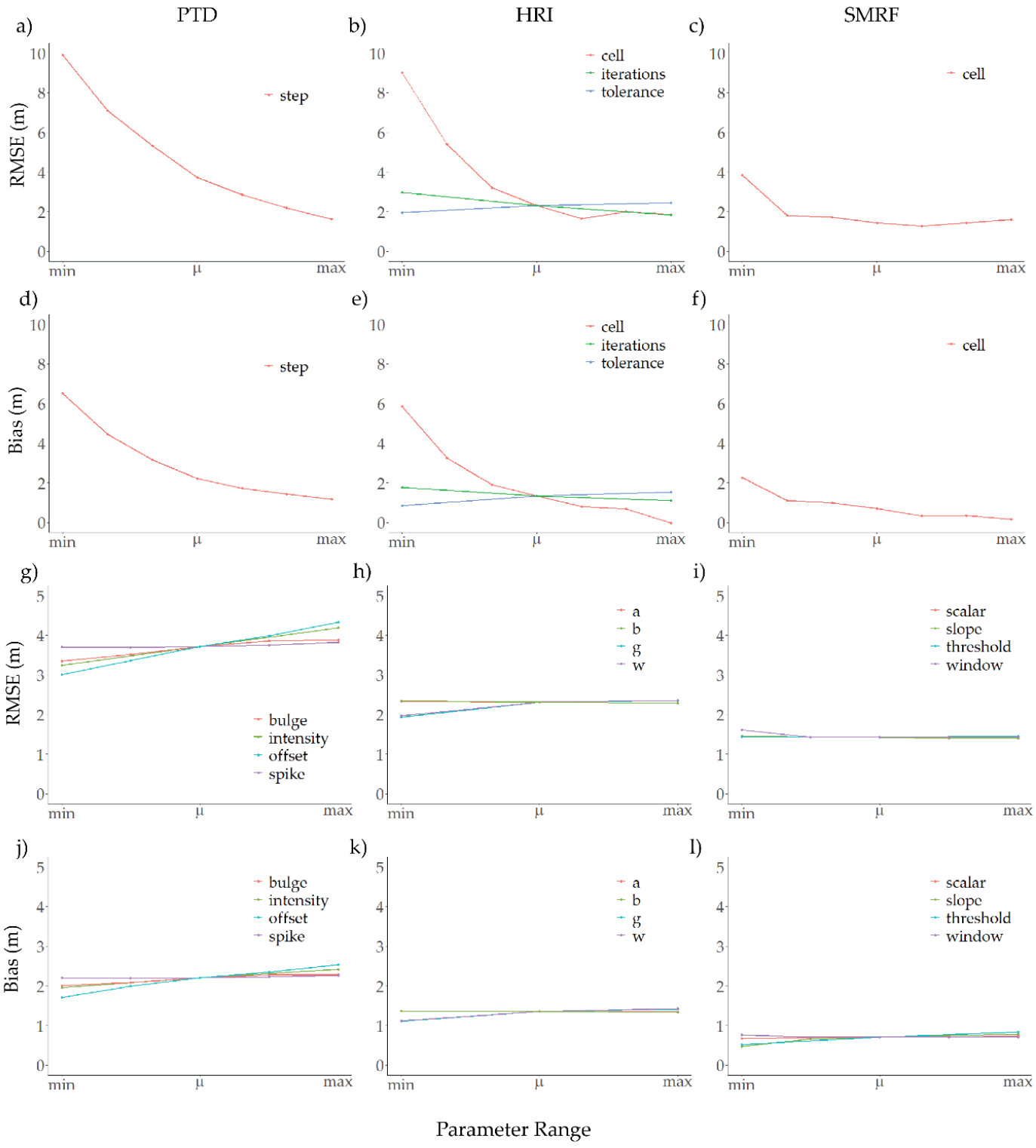


**Figure 3.3-3. Sensitivity analysis results of ALS ground points vs. DAP DEM surface elevations using ground classification methods PTD (a,d,g,j); HRI (b,e,h,k); and SMRF (c,f,i,l). Varied parameter ranges are combined in a relative scale.**

The PTD *step* parameter defines the grid-cell size used in designating initial low points and therefore had the greatest range in RMSE of any method-parameter combination. RMSE steadily decreased with increasing values of the *step* parameter while the *offset*, *intensity* and *bulge* parameters, in decreasing order, had a far smaller inverse effect on RMSE. The *spike* parameter, designed to remove localized positive vertical spikes in the estimated ground surface, had almost no effect on RMSE. The *cell* parameter of the HRI method influenced RMSE similar to that of PTD's *step* parameter; however, it reached a minimum RMSE using *cell* of 17 m. Increasing the number of iterations, represented by the *iteration* parameter, had a relatively smaller effect of reducing RMSE. The *tolerance* parameter yielded lower RMSE when set to the minimum tested value of 0.1 m. For the SMRF method, RMSE decreased most from a *cell* value of 1 m to 5 m and continued to decrease until a minimum was reached at a *cell* value of 17 m similar to the HRI method, while the remaining parameters show very little effect on RMSE. Optimal parameters for each tested classification method (Table 3.3-1) were found by isolating most occurring value within the first percentile of RMSE values for each method while Figure 3.3-4 shows a sample transect of AAS-DAP ground classification results from study area A. For all methods, default parameter values were not found in any of the optimal parameter sets.

**Table 3.3-1. Optimal parameters found for each ground-classification algorithm tested.**

| Method | Parameter | Optimal Value |
|---|---|---|
| PTD | step | 21 |
| | intensity | coarse |
| | bulge | 0.1 |
| | spike | 0.1 |
| | offset | 0.1 |
| HRI | cell | 17 |
| | g | −2.2 |
| | w | 2.25 |
| | a | 1.1 |
| | b | 4.4 |
| | tolerance | 0.1 |
| | iterations | 7 |
| SMRF | cell | 21 |
| | slope | 0.05 |
| | scalar | 0.75 |
| | threshold | 0.1 |
| | window | 22 |
| | cut | 0 |

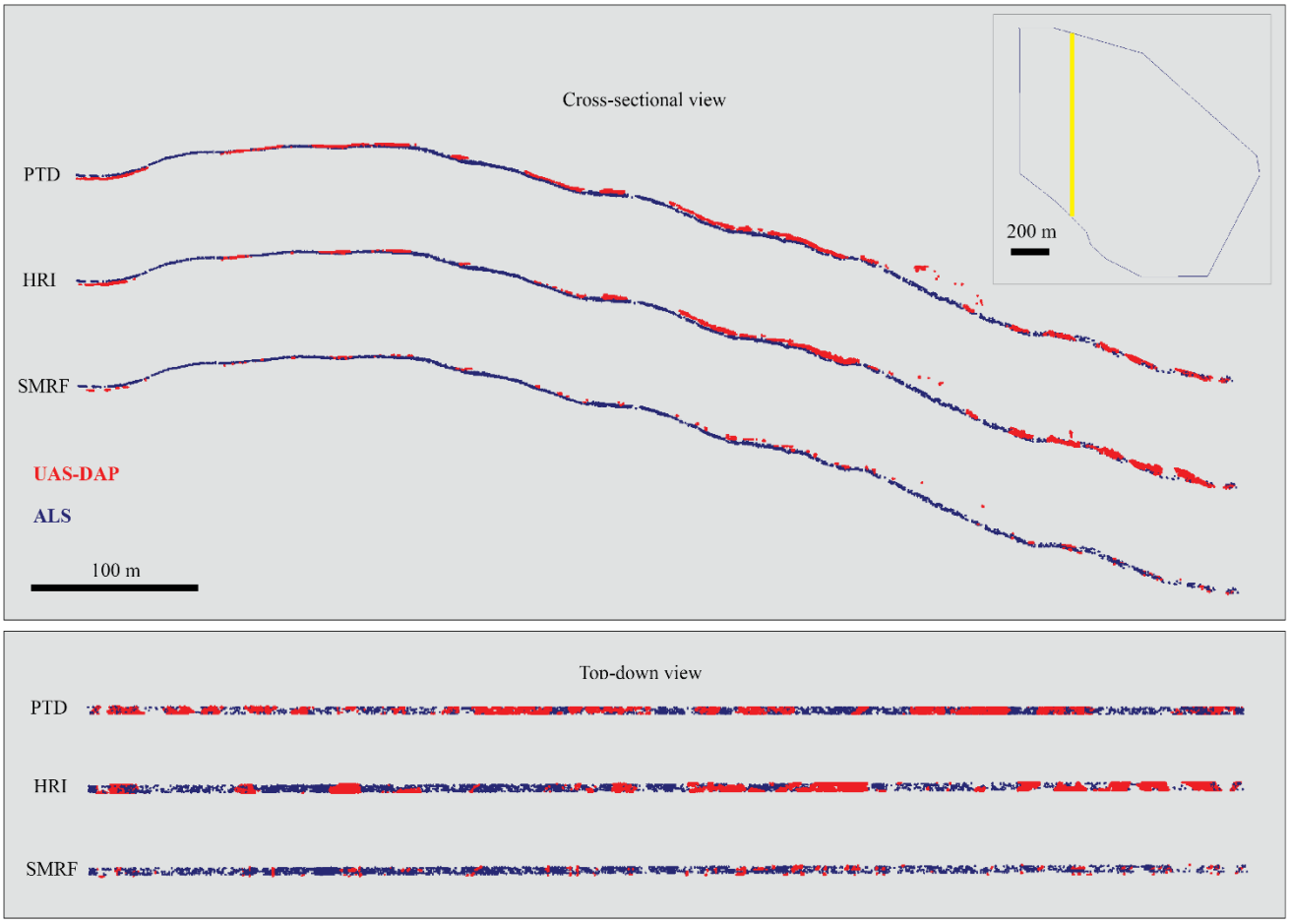


**Figure 3.3-4. Cross-sectional and top-down views of a 5 m wide transect taken from area A comparing ground classification results using optimal parameters of each tested algorithm. AAS-DAP and ALS ground classified points are shown in red and blue respectively.**

### 3.3.2 DEM results under various canopy cover and terrain slope

Figure 3.3-5 and Figure 3.3-6 show the spatial distribution of DEM RMSE and DEM bias respectively across the three study areas. Mean proportion of 25 m cells with RMSE <1.5 m across the three study areas was 56.5%, 51.6% and 52.3% for the PTD, HRI and SMRF methods respectively while individual study areas had a range from 42.3% to 72.1%. Therefore based on the criteria defined in Section 3.2.4, PTD was found to be the best performing method. Mean

canopy cover for these areas was 0.67, 0.68 and 0.68 for the PTD, HRI and SMRF methods respectively. Large contiguous areas of high RMSE and positive bias existed in areas A and B for all three methods where high canopy cover contributed to the inclusion of canopy points in the terrain model. Figure 3.3-7 shows the distribution of RMSE across the six stratified classes of terrain slope and canopy cover for each study area. The trend of RMSE increasing with both canopy cover and terrain slope classes is more pronounced in areas A and B relative to area C (Figure 3.3-7). A random forest model of RMSE using optimal parameters of the PTD method found the relative variable importance of canopy cover to be approximately three times that of terrain slope.

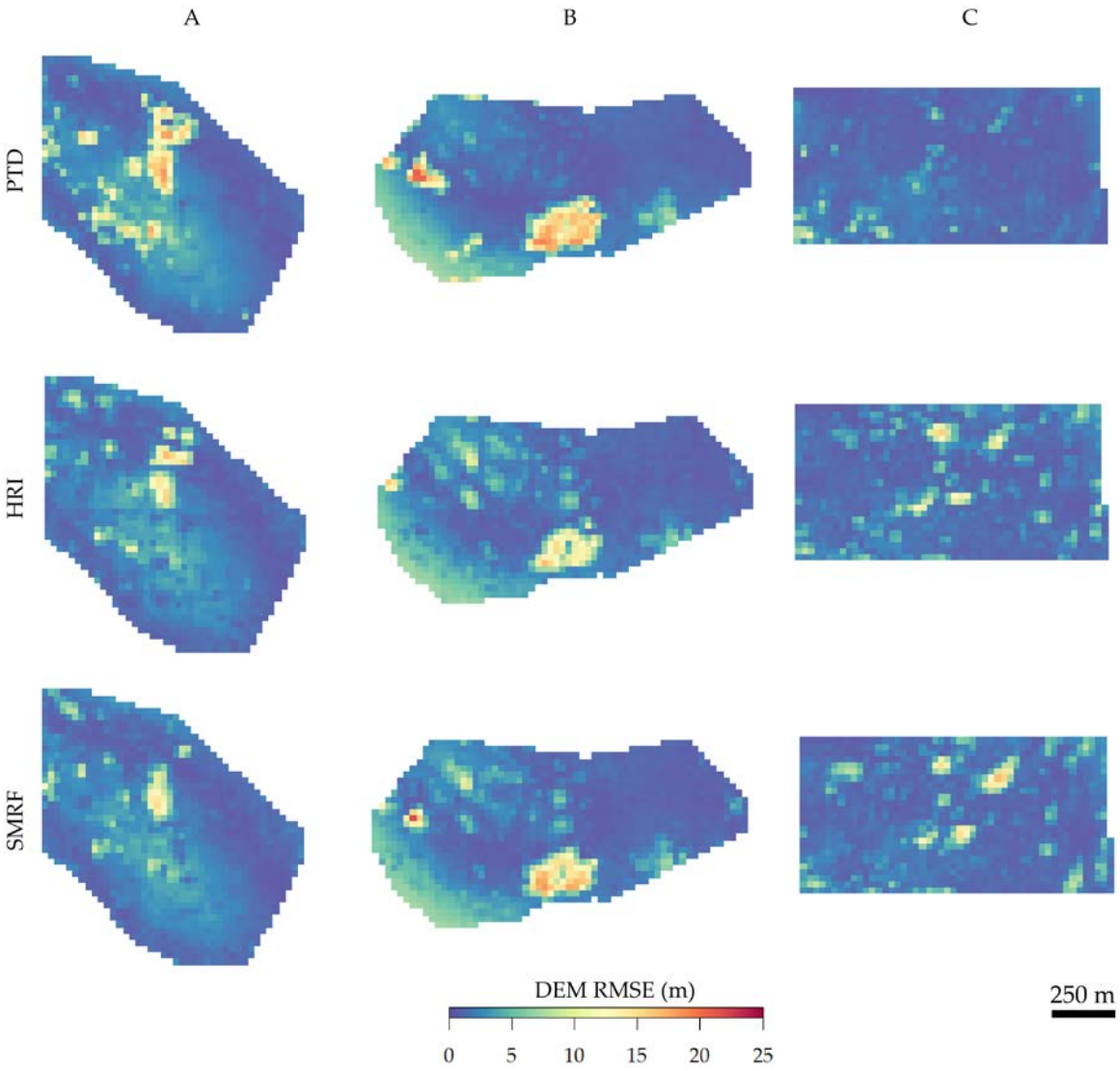


**Figure 3.3-5. Spatial distribution of the ALS vs. DAP-DEM RMSE averaged using 25 × 25 m cells for the three study areas A, B and C and ground classification methods PTD, HRI and SMRF.**

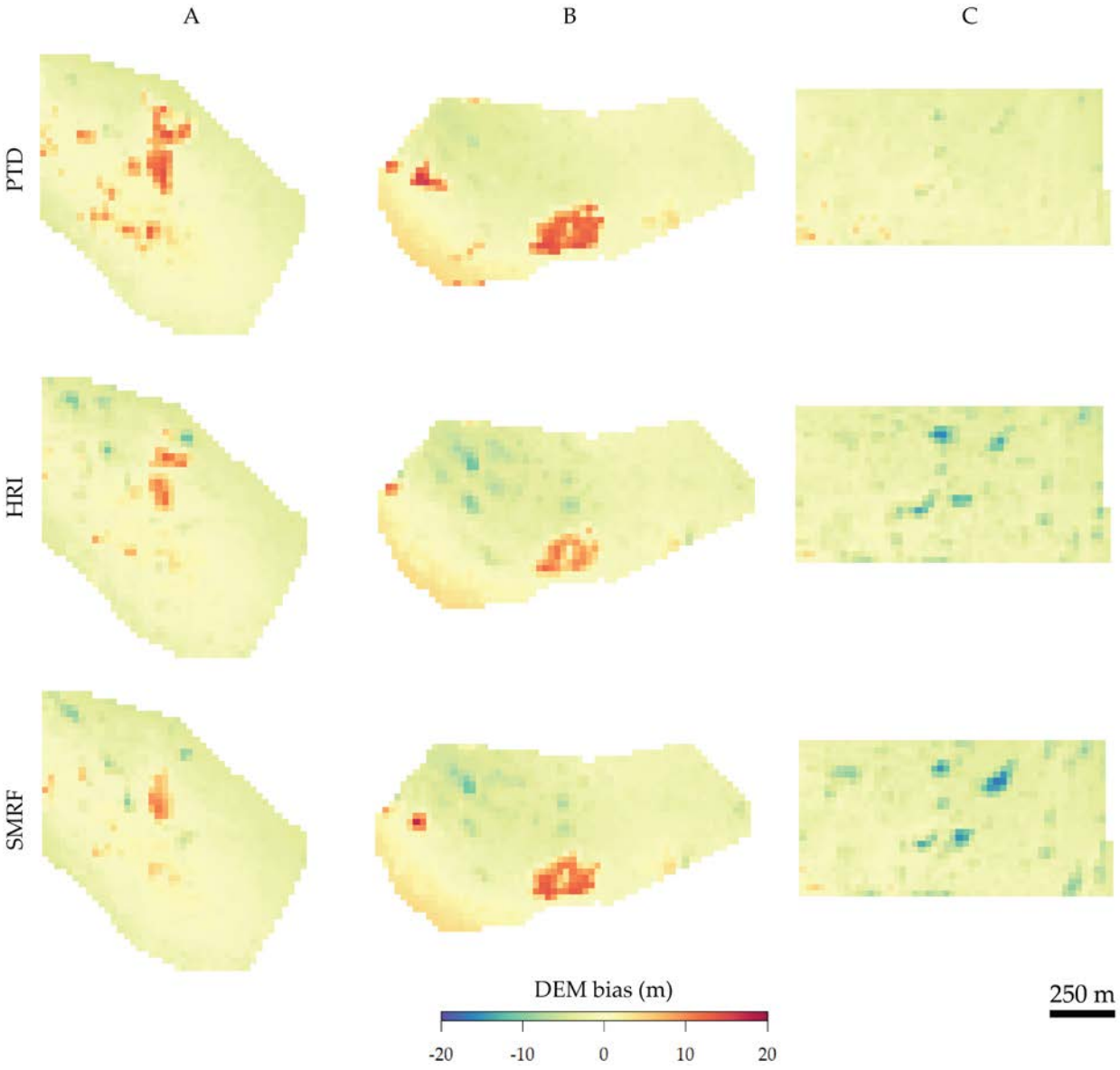


**Figure 3.3-6. Spatial distribution of the ALS vs. DAP-DEM bias averaged using 25 × 25 m cells for the three study areas A, B and C and ground classification methods PTD, HRI and SMRF.**

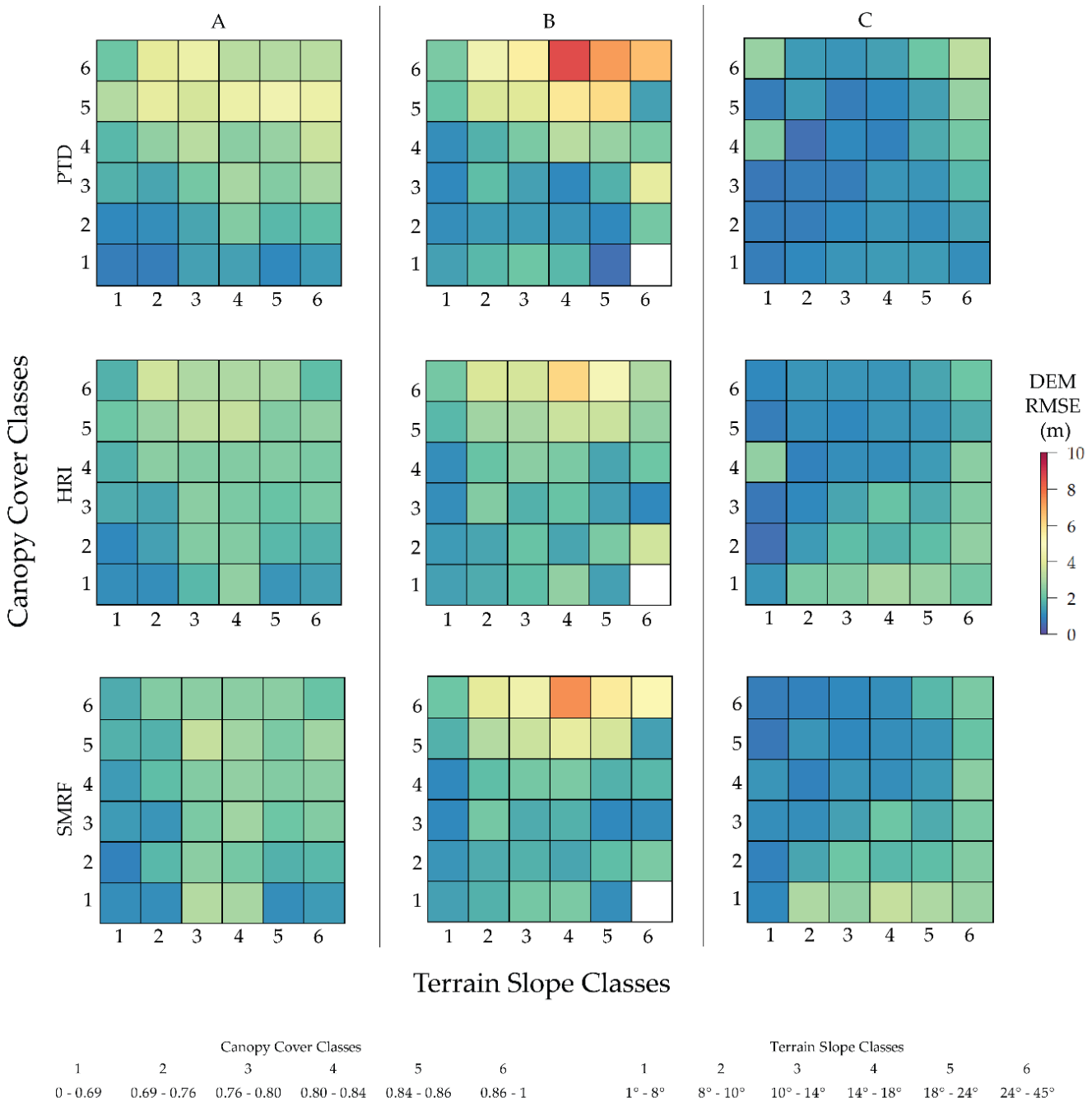


**Figure 3.3-7. DEM RMSE vs. stratified classes of terrain slope and canopy cover for the three study areas (A, B and C) and ground classification algorithms tested (PTD, HRI and SMRF) and their respective optimal parameterizations found in Section 3.1. The strata combining terrain slope class 6 and canopy cover class 1 was not represented in area B an is denoted by the white square.**

## 3.4 Discussion

This chapter examined the achievable terrain-modelling accuracy of a low-cost AAS-DAP data acquisition. Optimal parameters of three ground classification algorithms, designed for ALS point clouds, were determined using a sensitivity analysis and the variation in terrain-modelling accuracy was analyzed across local terrain slope and canopy cover conditions. It should be acknowledged that the ALS ground points used as the reference are subject to errors as stated in Section 1.2, therefore compounding errors associated with the DAP-DEM. The use of survey grade reference ground points such as in (Hodgson and Bresnahan 2004) is ideal; however, the equipment and time spent in the field are costly. Therefore the centimeter precision of modern ALS data (Davenport, Holden, and Gurney 2004; Hodgson and Bresnahan 2004) and the relatively larger errors associated with DAP-DEM in forested environments warrant the use of ALS ground points as reference and has been carried out by (Goodbody, Coops, Hermosilla, Tompalski, and Pelletier 2018).

Optimal parameter values for each method differed from the default algorithm values indicating that forested environments, may require a unique set of parameter values to produce an accurate DAP-DEM. The *step*, *cell* and *cell* parameters of the PTD, HRI and SMRF methods respectively specify the two-dimensional footprint for the initial search for ground points and had the greatest influence on DEM RMSE. Given the many ground classification algorithms that employ this fundamental step (Axelsson 1999, 2000; Keqi Zhang et al. 2003; Kraus and Pfeifer 1998; Pingel, Clarke, and Mcbride 2013; W. Zhang et al. 2016), the agreement between optimal *step*, *cell* and *cell* values of ~20 m indicate an initial search resolution likely appropriate for conifer stands of the ICH and SBS BEC zones.

Following the sensitivity analysis, errors of the DAP-DEMs generated employing optimal parameters were compared to stratified classes of terrain slope and canopy cover derived from ALS point-clouds. The relative importance of canopy cover was found to be approximately three times that of terrain slope when using optimal parameters of the best performing PTD classification method. Although it appears that further increases in the PTD *step* parameter may reduce RMSE according to Figure 3.3-4, the optimal *step* value was found to be 21 m rather than the maximum tested value of 25 m according to the criteria outlined in Section 3.2.3.

The analysis found that 57% of the terrain was modeled with an RMSE <1.5 m. With this, assuming a mean tree height of 15 m, DEM error may contribute an error of 10% or less in these areas. Similar to this chapter's findings, Iizuka et al. (2018) generated terrain models within a forested environment from a AAS-DAP point cloud and found normalized tree heights to be estimated with a minimum RMSE of 1.712 m. Similarly, Guerra-Hernández et al. (2018) estimated tree heights with RMSE of 1.82 m using a AAS-DAP point cloud normalized by an ALS-DEM. In another comparison, (Goodbody, Coops, Hermosilla, Tompalski, and Pelletier 2018) were able to produce DAP derived ground models within low cover deciduous forests where the mean error reported was 0.01 m with a standard deviation of 0.14 m. While the results show a significant portion of the terrain was modeled adequately, large errors (>10 m) persist in areas of high canopy cover >0.8. These are areas where DAP was unable to register ground in areas larger than the defined initial search extent of the ground classification algorithms. In these areas, the algorithm misclassifies a fraction of canopy points as ground leading to a large over estimation in terrain elevation. Similar to results from this chapter, Guerra-Hernández et al. (2018) report terrain height overestimation of >±2.0 m in areas of where slope was >20% and

canopy cover >60%. Nevertheless, this chapter finds that there is potential for operationally acceptable DAP-DEM derivation where mean canopy cover is lower than around 0.7.

# Chapter 4: Effect of Ground Surface Interpolation Methods on the Accuracy of Forest Attribute Modelling using Autonomous Aerial Systems-based Digital Aerial Photogrammetry

## 4.1 Introduction

In Chapter 3, an analysis was conducted to gather optimal ground classification results from the AAS-DAP point cloud. This was done to establish a terrain surface from which metrics that quantify the vertical distribution of points can be used to model forest attributes. Stand-level height and stem volume can be modelled using a combination of existing species-specific allometric growth models and the area-based approach (ABA) (S Magnussen and Boudewyn 2011; Vastaranta et al. 2012; Tompalski et al. 2015; Tuominen et al. 2015; Goodbody et al. 2017; Tompalski et al. 2018). Structural metrics derived from point clouds and subsequent modelling efforts are critically dependent on underlying terrain models used to normalize heights of vegetation objects (Bater and Coops 2009). To generate a terrain surface from point-cloud data, first a subset of points must be classified as ground from which a continuous surface is interpolated. The numerous existing algorithms designed to carry out each of these individual steps introduces a significant challenge DEM optimization given unique forest stand characteristics. Relative to ALS, image-based DAP point clouds are susceptible to occlusion by the forest canopy rendering terrain difficult to model. As a result, 3D points normalized by the terrain will likely be inaccurate, which in turn will have an impact on deriving the metrics necessary for modelling forest attributes.

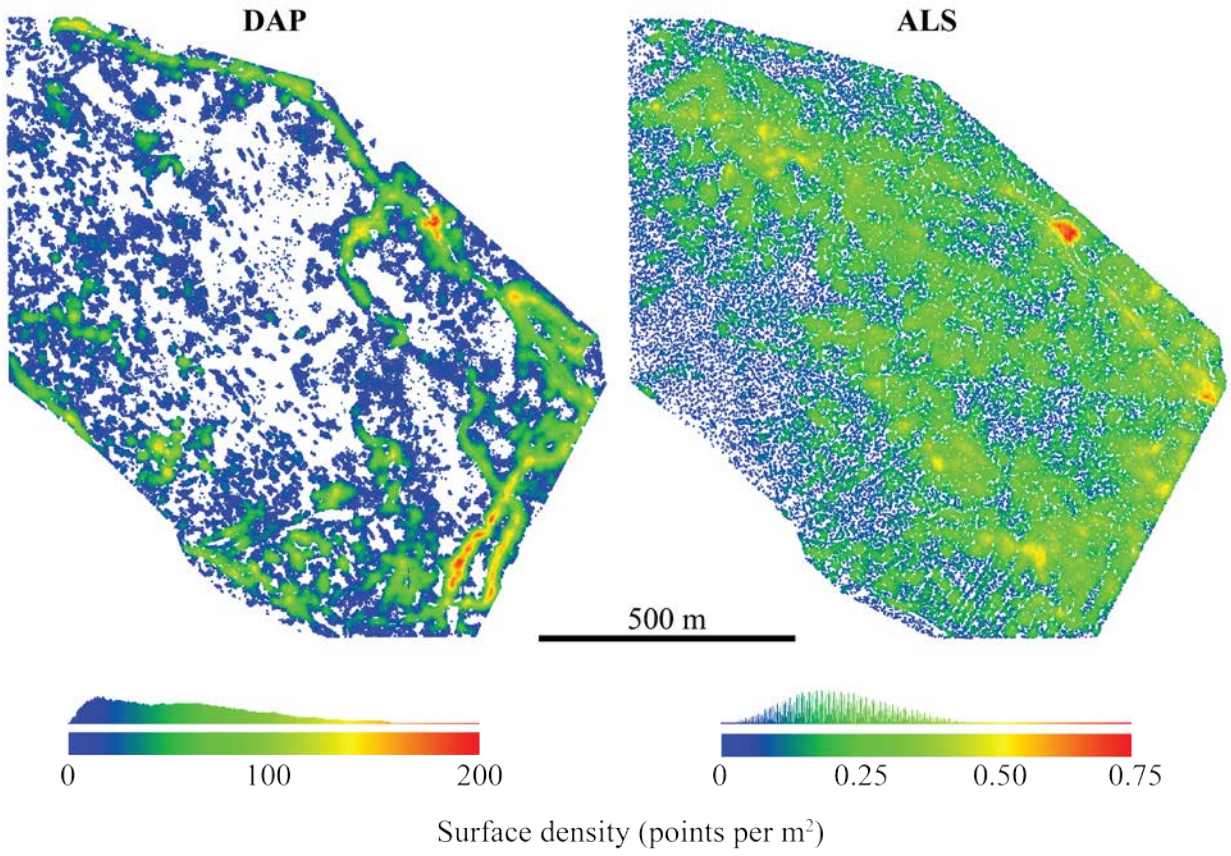


**Figure 4.1-1. DAP ground points classified using PTD and ALS ground points colourized by the surface density of points derived from a 10 m search radius for study area A.**

In order to assess the effects of different interpolation routines, a single ground-point classification using PTD (Figure 4.1-1), identified as ideal for the environment in Chapter 3 (Graham et al. 2019), was used as input for multiple common interpolation methods to derive a range of continuous terrain surfaces from AAS-DAP. Second, terrain models were used to normalize the heights of the AAS-DAP point-clouds and calculate structural metrics commonly used in ABA estimates of forest inventory. Third, a stepwise selection approach was employed to model mean tree height ($H_{mean}$), Lorey's height ($H_{Lorey}$) and stem volume per hectare ($V_{stem}$) based on the AAS-DAP structural metrics. The results

from this chapter are important in highlighting the influence of terrain surface interpolation and can potentially improve results of forest attribute modelling from AAS-DAP.

## 4.2 Methods

A flow diagram of the processing workflow is shown in Figure 4.2-1 and consists of 6 steps: 1) photogrammetric processing, 2) georeferencing, 3) ground classification and DEM surface interpolation, 4) forest metric generation, 5) stepwise model selection and 6) model error assessments. Steps 1 and 2 are outlined in Chapter 2 while steps 3-6 are detailed below.

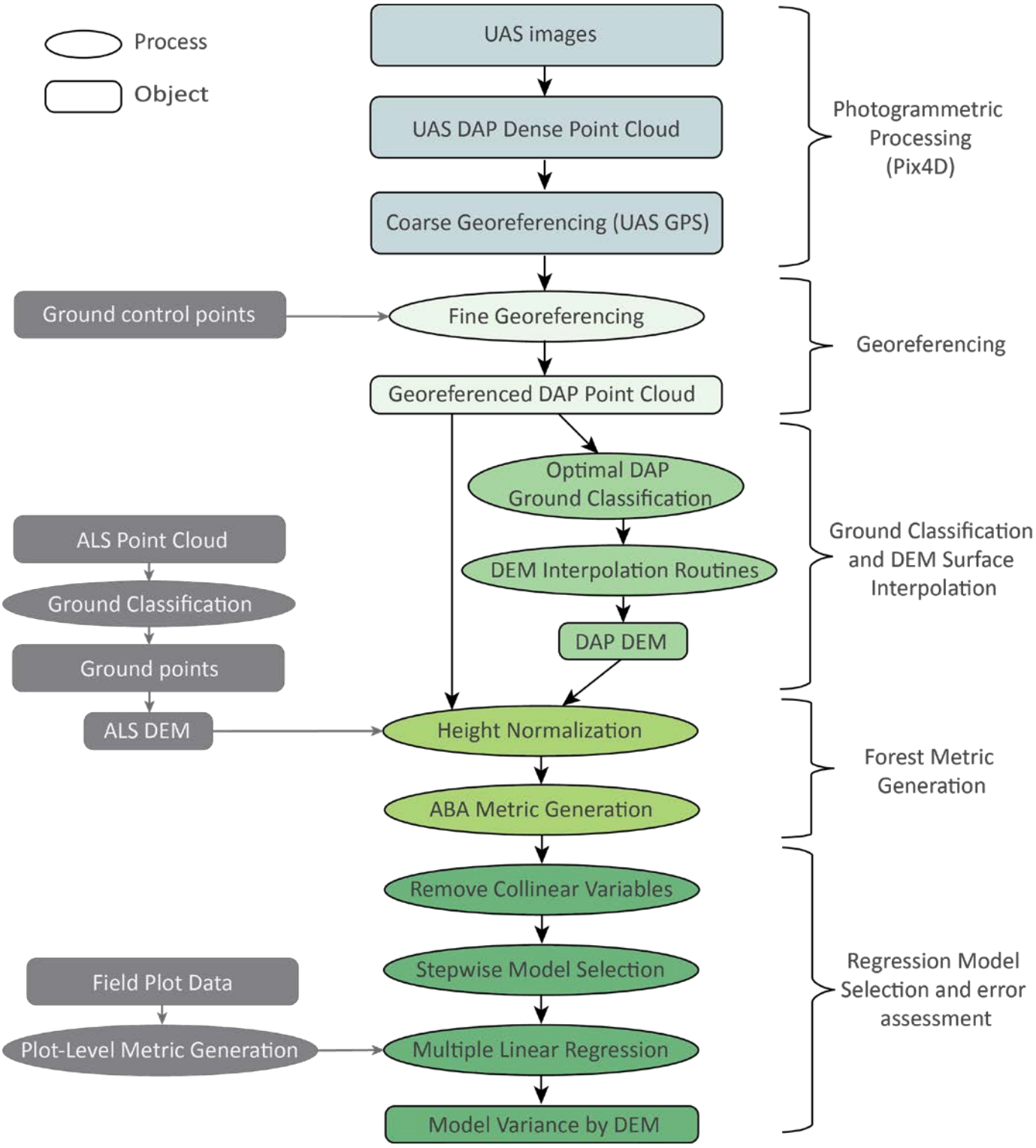


**Figure 4.2-1. Schematic workflow for assessing the accuracy of forest attribute modelling against terrain surface modelling.**

### 4.2.1 DEM Interpolation

Regular grid elevations and TINs are two dominant methods of representing terrain surfaces (Hutchinson and Gallant 1999; Ali and Mehrabian 2009). Surface interpolation methods can be broadly categorized as exact or inexact methods where surfaces are respectively either fit through every data point or a trend surface (Maguya, Junttila, and Kauranne 2013). Inexact methods of interpolation were not included as their increased complexity does not necessarily improve results (Bater and Coops 2009). In addition, the preservation of the input ground-point elevations in the continuous terrain model is desirable, given that the optimal ground points were identified through a sensitivity analysis (Graham et al. 2019). The selection of interpolation methods tested in this chapter is influenced by the predominance of terrain modelling studies using ALS data. In this analysis, four exact methods of surface interpolation were tested and are detailed in Table 4.2-1: TIN, inverse-distance weighted (IDW), natural neighbour (NATN), and spline with tension (SPLT). These interpolation methods were then used to define continuous gridded elevation values.

TIN-based interpolation is adaptable to a range of terrain structures and varying data densities, and is therefore commonly implemented (Yunfei et al. 2002; Aschoff, Thies, and Spiecker 2004; Wallace et al. 2016; Stereńczak et al. 2016); however, capacity to characterize curved and sloped terrain can be limited in some cases (Hutchinson and Gallant 1999). TIN surfaces can be more efficient than grid-based surfaces by varying the density of points needed based on the ruggedness of the terrain (Ali and Mehrabian 2009). As a result of the applicability of TINs in terrain modelling from ALS data, significant computational efficiencies were

introduced to TIN-derived raster DEM generation. One example is TIN streaming and is the minimization of data transfer between disk and memory where finalized triangles are written to disk in subsets at each algorithm iteration (Isenburg et al. 2006). K-nearest neighbour IDW is another commonly used point cloud terrain surface interpolation method (Ben-Arie et al. 2009; Maguya, Junttila, and Kauranne 2013; Razak et al. 2013; Montealegre, Lamelas, and De La Riva 2015b). Values at interpolated locations are determined using *k* number of nearest data points which influence the estimation based on proximity. Montealegre et al. (2015b) tested six interpolation methods and found that IDW generated the most accurate ALS-DEMs in terms of mean-absolute-error at both 1 and 2 m resolutions. NATN is a data dependent, parameter-free interpolation routine based on Voronoi tessellation of points and is therefore widely applicable and simple to implement (Sibson 1981). Values at the interpolated point locations are assigned based on changes in area to the new tessellation when including the interpolated point location (Razak et al. 2013). SPLT fits a surface of minimized curvature with the ability to model acute changes in elevation such as ridges and streams (Razak et al. 2013) and is also simple to parameterize (Mitásova and Mitás 1993). The tension parameter of SPLT controls the degree of curvature allowed in the interpolated surface where larger values yield more gradual curves in the surface (Godone and Garnero 2013).

**Table 4.2-1. Summary of DEM surface interpolation routines used on the DAP ground points**

| Method Name | Acronym | Key Parameters | References | Software |
|---|---|---|---|---|
| Triangulated Irregular Network | TIN | Delaunay Triangulation | (Isenburg et al. 2006) | LASTools |
| K-Nearest Neighbour Inverse Distance Weighting | IDW | Number of nearest neighbours (k) = 10<br>Power for inverse-distance weighting (p) = 2 | | R |
| Natural Neighbour | NATN | | (Sibson 1981) | ArcGIS |
| Spline with Tension | SPLT | Tension weight (w) = 0.1 | (Franke 1982) | ArcGIS |

### 4.2.2 Metric generation for height and volume modelling

To generate structural forest metrics, the DAP point cloud elevations were normalized using each of the four DEM surface interpolation methods (TIN, IDW, NATN, and SPLT). Following height normalization, metrics were generated for each cell of a 25 m resolution regular grid. Similar to (Bouvier et al. 2015; Tompalski et al. 2015; Goodbody et al. 2016), predictor metrics describing the vertical distribution of the point cloud in each cell were divided into three categories: height-based, cover-based and vertical variability-based. Metrics used as input to the model selection process are detailed in Table 4.2-2.

**Table 4.2-2. Structural metrics used as independent variables for modelling forest attributes.**

| Metric Type | Metric Abbreviation | Description |
|---|---|---|
| Height | *p50* | 50th percentile of point heights above ground |
| | *p75* | 75th percentile of point heights above ground |
| | *p90* | 90th percentile of point heights above ground |
| | *max* | Maximum point height above ground |
| Cover | *frc2* | Fraction of points > 2m above ground |
| | *frc6* | Fraction of points > 6m above ground |
| | *frc10* | Fraction of points > 10m above ground |
| | *frcMean* | Fraction of points > mean height above ground |
| Variance | *sd* | Standard deviation of point heights above ground |
| | *cv* | Coefficient of variation of point heights above ground |

Ordinary least-squares (OLS) regression models were developed between field measurements and metrics derived from the vertical distribution of DAP point clouds to perform ABA estimations of stem volume and tree height. To include the potential predictive contribution of each metric type (Table 4.2-2), combinations of independent variables were tested using a bidirectional stepwise selection method based on AIC. For each dependent variable and terrain surface, the model selection process permitted ≤3 independent variables, one from each metric type. A threshold Pearson's correlation coefficient of >0.75 was used to eliminate collinear independent variables. As a result, 32 models were generated for each dependent variable and terrain surface, from which the best performing model was determined by the lowest AIC value. It has been shown that biomass and volume are best represented with multiplicative power models (Means et al. 1999;

Ketterings et al. 2001; Hollaus et al. 2007; Tompalski et al. 2015); therefore, logarithmic transformations applied to both independent and dependent variables were also tested in the stepwise selection process. To account for the systematic bias introduced by log transformation, predictions from the back-transformed models were multiplied by a bias correction factor (BCF) (Sprugel 1983) based on the standard error estimate (SEE) and is calculated as:

$$SEE = \sqrt{\frac{\sum_{i=1}^{N}(\log(obs_i) - \log(pred_i))^2}{N - p}} \quad (2)$$

$$BCF = \exp(SEE^2/2)$$

where *obs* and *pred* are the field measured and predicted forest attribute values respectively, *N* is the number of plots and *p* is the number of predictor variables. Models with the lowest AIC values were selected as best performing models and used to generate wall-to-wall ABA prediction grids for $H_{mean}$, $H_{Lorey}$ and $V_{stem}$. Comparison of AIC values between linear and log-transformed models was carried out according to (Akaike, 2006, p. 224). To quantify differences in modelling results between the DAP-DEM terrain surfaces, a Kruskal-Wallis with Dunn's posthoc test was conducted to test if the predicted height and stem volume values were significantly different depending on the terrain surface used. In addition, 95% confidence intervals using a t-distribution around each model coefficient were calculated and compared.

## 4.3 Results

Overall, there were only small variations in the metric distributions between the DAP-DEM surface interpolation routines (Figure 4.3-1). In comparison to using the ALS-DEM for height normalization, the value of the *p90* height metric were overestimated between 15 and 25 m and underestimated at values above 25 m. The distribution of height metrics generated using the IDW surface interpolation method and DAP ground points showed the least deviation from the metrics generated using the ALS-DEM. Fractional cover metrics yielded the largest discrepancy between the ALS and DAP height normalization methods where the ALS derived metric was more left-skewed. Increases in the height threshold used to define percent cover yielded better agreement between the DAP and ALS derived cover metric distributions. Distributions of metrics *frcMean* and *sd* derived from the IDW surface showed the least deviation from those derived from the ALS.

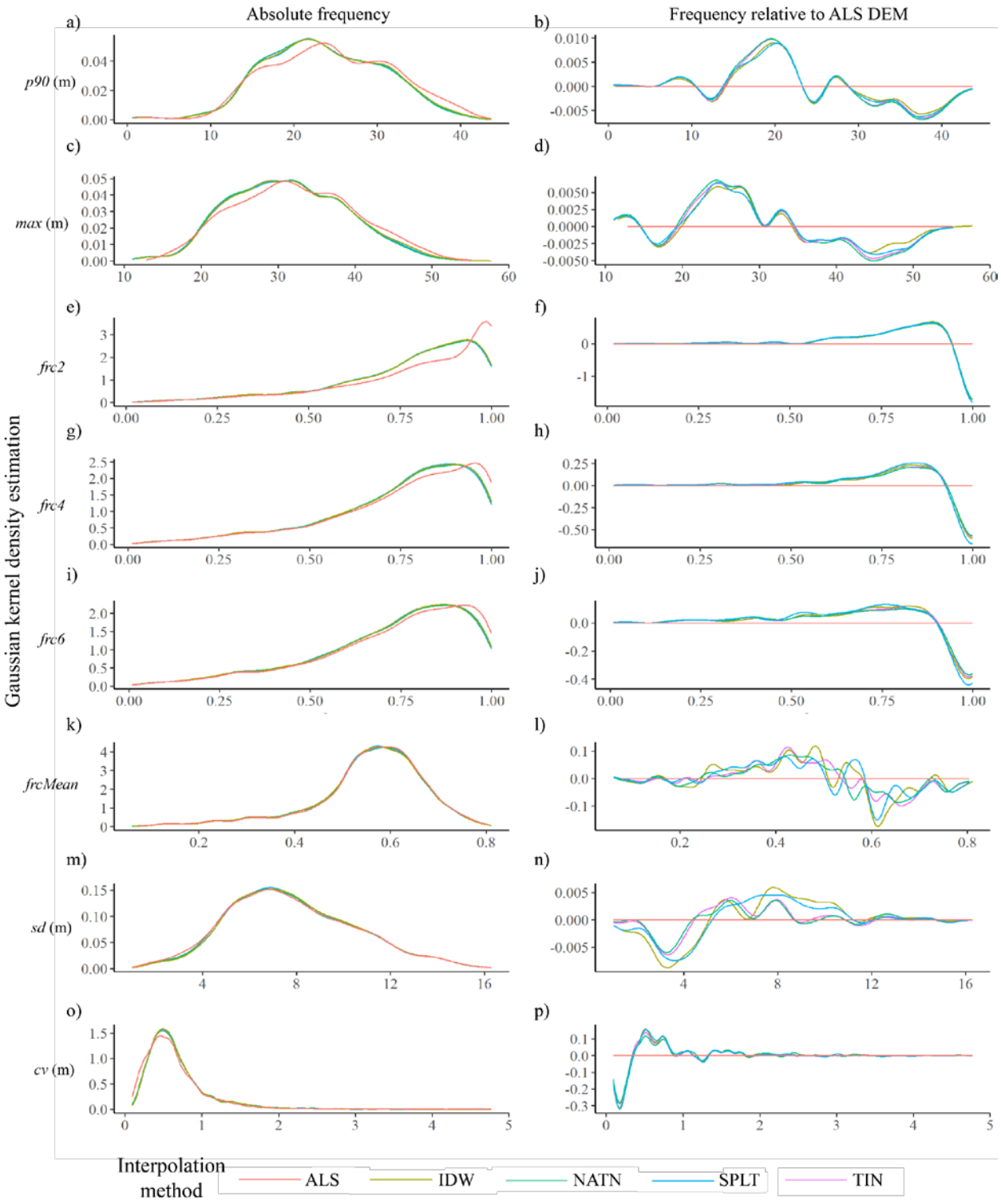


**Figure 4.3-1. Absolute and relative frequency distributions of DAP Point-cloud metrics selected for modelling forest attributes using Gaussian kernel density estimation. Curves represent metrics derived from different terrain surfaces used for point cloud height normalization. Frequencies relative to metrics derived from height normalization using the ALS-DEM are also shown.**

For all dependent forest variables, log-log transformed models outperformed linear models according to the stepwise selection process based on AIC (Table 4.3-1). With the exception of the ALS-DEM, $H_{mean}$ was modelled using only the *max* height metrics while cover and variance were more prevalent among models for $H_{Lorey}$ and $V_{stem}$. The models using ALS-DEM normalized point cloud structural metrics had consistently higher adjusted $R^2$ and lower AIC and RMSE compared to those from the four different DAP-DEM surfaces. The mean RMSE using DAP-DEM surfaces for forest attributes $H_{mean}$, $H_{Lorey}$ and $V_{stem}$ were respectively 7.29%, 5.04% and 26.66%. Among the models using metrics derived from DAP-DEMs, TIN had the lowest AIC and RMSE for $H_{mean}$ and $H_{Lorey}$ while performance of selected models for $V_{stem}$ were nearly identical with the exception of IDW, which had reduced relative performance based on AIC, adjusted $R^2$ and RMSE.

**Table 4.3-1. Parameters for best performing models based on AIC values for each DAP-DEM, ALS-DEM, and field metric. Best performing models per DAP-DEM terrain surface are in bold. All models represent the log-log forms. *p < 0.05. **p < 0.01. ***p < 0.001.**

| DEM Surface Method | Predicted Attribute | Height Metric | Coef. | Cover Metric | Coef. | Variance Metric | Coef. | AIC | Adjusted $R^2$ | RMSE % | RMSE (m, $m^3ha^{-1}$) |
|---|---|---|---|---|---|---|---|---|---|---|---|
| **ALS** | $H_{mean}$ | ***max**** | **1.05** | ***frc2**** | **-0.13** | ***sd*** | **-0.07** | **-10.61** | **0.96** | **4.43** | **0.73** |
| IDW | | *max**** | 0.93 | | | | | -0.51 | 0.87 | 7.63 | 1.24 |
| NATN | | *max**** | 1.01 | | | | | -1.48 | 0.88 | 7.20 | 1.17 |
| SPLT | | *max**** | 0.95 | | | | | -0.34 | 0.88 | 7.42 | 1.21 |
| TIN | | *max**** | 0.98 | | | | | -2.61 | 0.89 | 6.91 | 1.13 |
| **ALS** | $H_{Lorey}$ | ***max**** | **1.15** | ***frc2**** | **-0.13** | | | **-20.09** | **0.98** | **3.24** | **0.59** |
| IDW | | *max**** | 1.10 | *frc2* | -0.08 | | | -7.75 | 0.96 | 4.89 | 0.89 |
| NATN | | *max**** | 1.17 | *frcMean** | -0.12 | | | -5.89 | 0.94 | 5.52 | 1.00 |
| SPLT | | *max**** | 1.09 | *frcMean* | -0.11 | | | -5.35 | 0.95 | 5.21 | 0.95 |
| TIN | | *max**** | 1.09 | *frcMean* | -0.10 | *sd* | 0.08 | -8.82 | 0.96 | 4.54 | 0.82 |
| **ALS** | $V_{stem}$ | ***p90**** | **1.92** | ***frcMean*** | **-0.37** | | | **50.34** | **0.90** | **19.15** | **41.04** |
| IDW | | *p90**** | 1.96 | | | | | 70.16 | 0.79 | 29.14 | 59.62 |
| NATN | | *p90**** | 2.69 | *frc2* | -0.51 | *sd* | 0.80 | 70.33 | 0.84 | 25.71 | 52.62 |
| SPLT | | *p90**** | 2.05 | | | | | 68.28 | 0.84 | 25.99 | 53.19 |
| TIN | | *p90**** | 2.70 | *frc2* | -0.50 | *sd* | 0.13 | 70.00 | 0.84 | 25.79 | 52.77 |

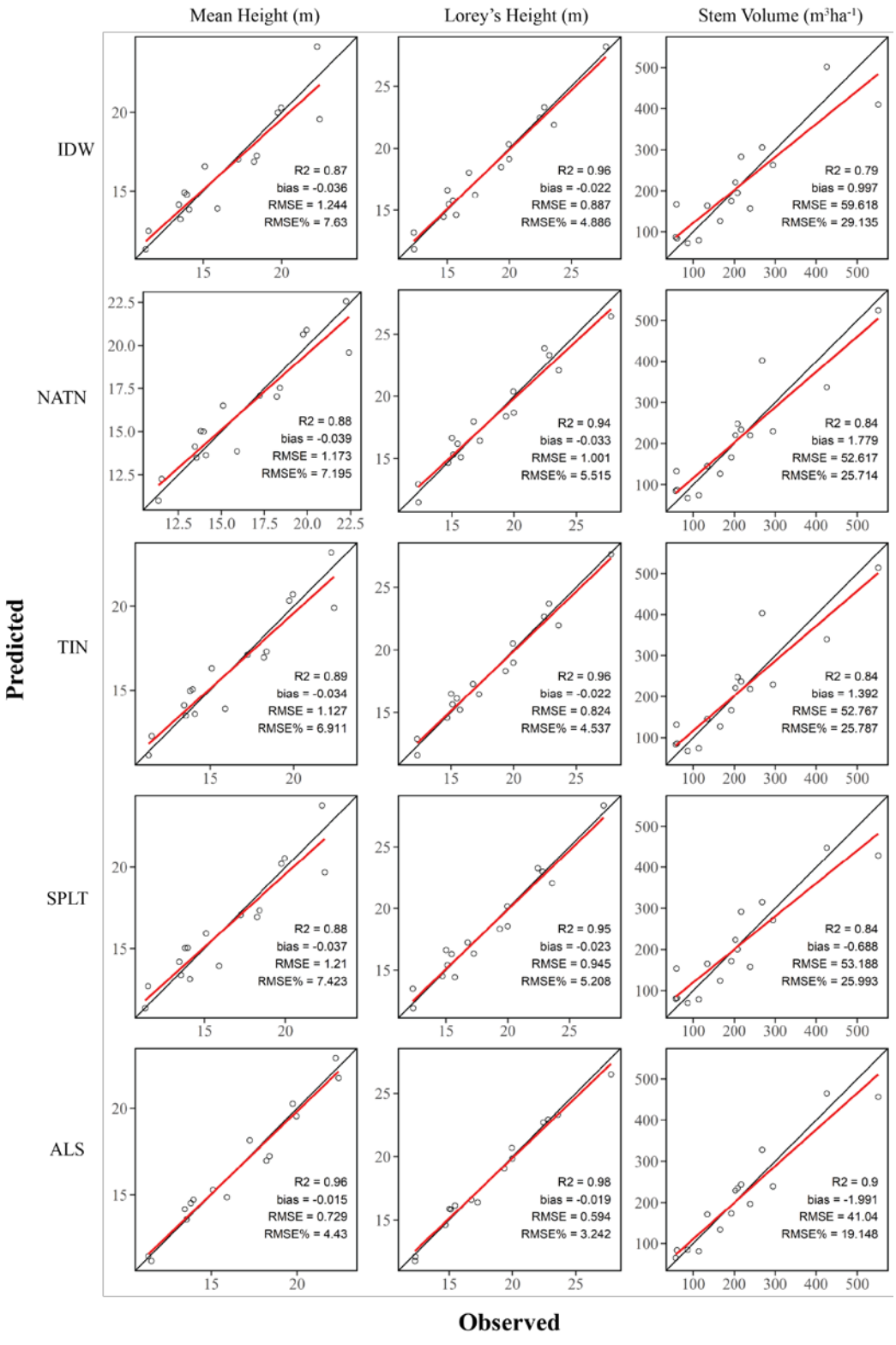


**Figure 4.3-2. One to one scatter plots of modelled predicted against observed plot level forest attributes.**

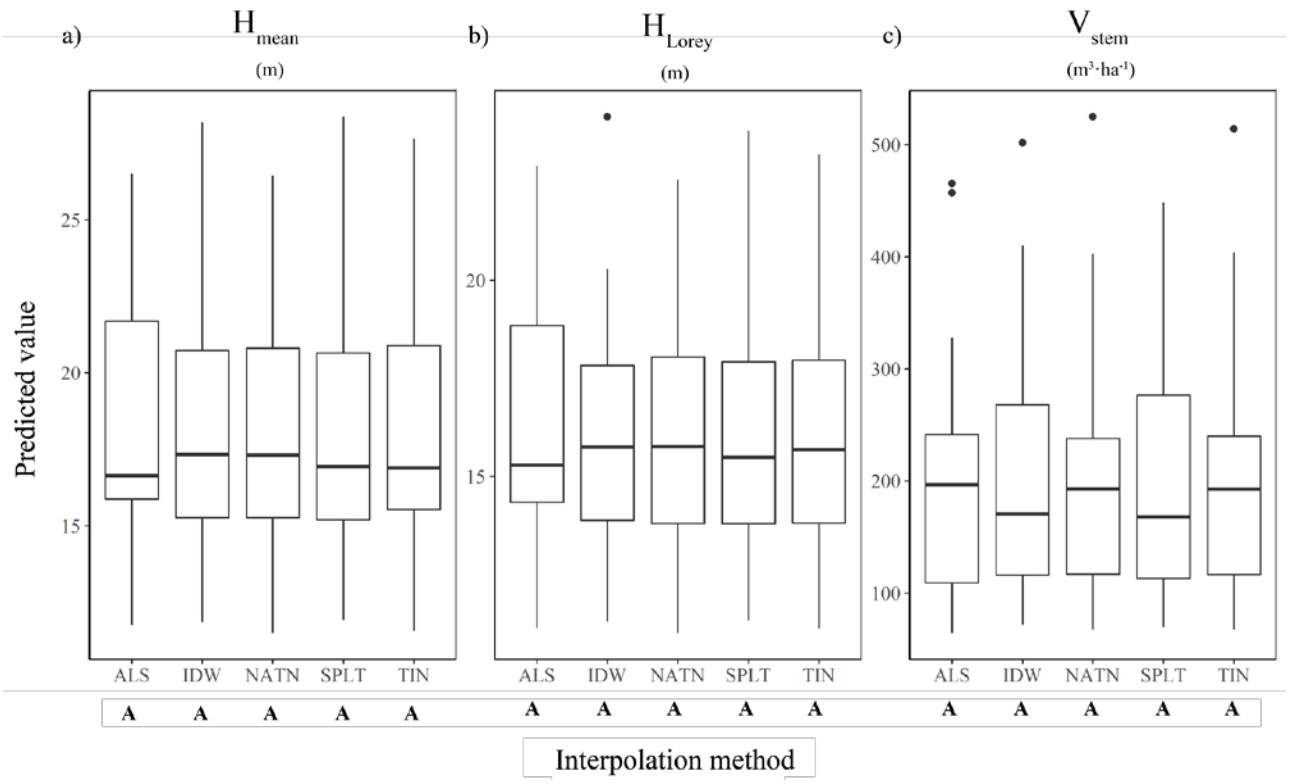


**Figure 4.3-3. Boxplots displaying the distribution of predicted forest attributes (a-c) according to the models in Table 4. Prediction groups which share the same letter are not significantly different according to the Kruskal-Wallis with Dunn's posthoc test.**

The distribution of predicted forest attribute values seen in Figure 4.3-3 were similar across the terrain surface interpolation methods, however the mean of predictions using the ALS-DEM were lower than those from DAP-DEMs for all three dependent variables. A Kruskal-Wallis with Dunn's posthoc test found no significant difference between the groups of predictions for all three dependent variables at $\alpha = 0.05$.

**Table 4.3-2. Parameters for models which match predictor variables included in the best performing found in Table 4.3-1. All models shown represent the log-log transformed model form and models with changed predictor variables with respect to Table 4.3-1 are shown in bold. *p < 0.05. **p < 0.01. ***p < 0.001.**

| DEM Surface Method | Predicted Attribute | Height Metric | Coef. | Cover Metric | Coef. | Variance Metric | Coef. | AIC | Adjusted $R^2$ | RMSE % | RMSE (m, $m^3ha^{-1}$) |
|---|---|---|---|---|---|---|---|---|---|---|---|
| ALS | $H_{mean}$ | *max**** | 1.05 | *frc2** | -0.13 | *sd* | -0.07 | -10.61 | 0.96 | 4.43 | 0.73 |
| **IDW** | | ***max***** | **0.95** | ***frc2*** | **-0.05** | ***sd*** | **0.03** | **1.88** | **0.87** | **7.60** | **1.24** |
| **NATN** | | ***max***** | **1.06** | ***frc2*** | **-0.05** | ***sd*** | **0.00** | **1.30** | **0.89** | **7.10** | **1.16** |
| **SPLT** | | ***max***** | **0.98** | ***frc2*** | **-0.05** | ***sd*** | **0.01** | **2.66** | **0.88** | **7.41** | **1.21** |
| **TIN** | | ***max***** | **1.01** | ***frc2*** | **-0.05** | ***sd*** | **0.01** | **0.07** | **0.89** | **6.84** | **1.12** |
| ALS | $H_{Lorey}$ | *max**** | 1.05 | *frc2**** | -0.13 | | | -20.09 | 0.98 | 3.24 | 0.59 |
| IDW | | *max**** | 1.15 | *frc2* | -0.13 | | | -7.75 | 0.96 | 4.89 | 0.89 |
| **NATN** | | ***max***** | **1.10** | ***frc2*** | **-0.08** | | | **-3.46** | **0.93** | **5.96** | **1.08** |
| **SPLT** | | ***max***** | **1.18** | ***frc2*** | **-0.07** | | | **-4.09** | **0.95** | **5.21** | **0.94** |
| **TIN** | | ***max***** | **1.12** | ***frc2*** | **-0.07** | | | **-6.65** | **0.95** | **5.06** | **0.92** |
| ALS | $V_{stem}$ | *p90**** | 1.14 | *frcMean* | -0.07 | | | 50.34 | 0.90 | 19.15 | 41.04 |
| **IDW** | | ***p90***** | **1.15** | ***frcMean*** | **-0.13** | | | **72.12** | **0.79** | **29.45** | **60.27** |
| **NATN** | | ***p90***** | **1.92** | ***frcMean*** | **-0.37** | | | **72.60** | **0.79** | **29.44** | **60.25** |
| **SPLT** | | ***p90***** | **1.98** | ***frcMean*** | **-0.07** | | | **70.23** | **0.84** | **26.00** | **53.20** |
| **TIN** | | ***p90***** | **2.13** | ***frcMean*** | **-0.11** | | | **72.09** | **0.80** | **28.37** | **58.05** |

Models for which independent variables differ between Table 4.3-1 and Table 4.2-2 show small increases and decreases in AIC and adjusted $R^2$ respectively. The mean difference in AIC and adjusted $R^2$ for these models was respectively 2.27 and -0.01 while the associated mean increases in %RMSE was 0.67 %. The largest increase in AIC was 3.00 in the model difference for $H_{mean}$ using

the SPLT DAP-DEM. Models for $H_{mean}$ had an average reduction in %RMSE of -0.05% when adding both cover and variance metrics in the model.

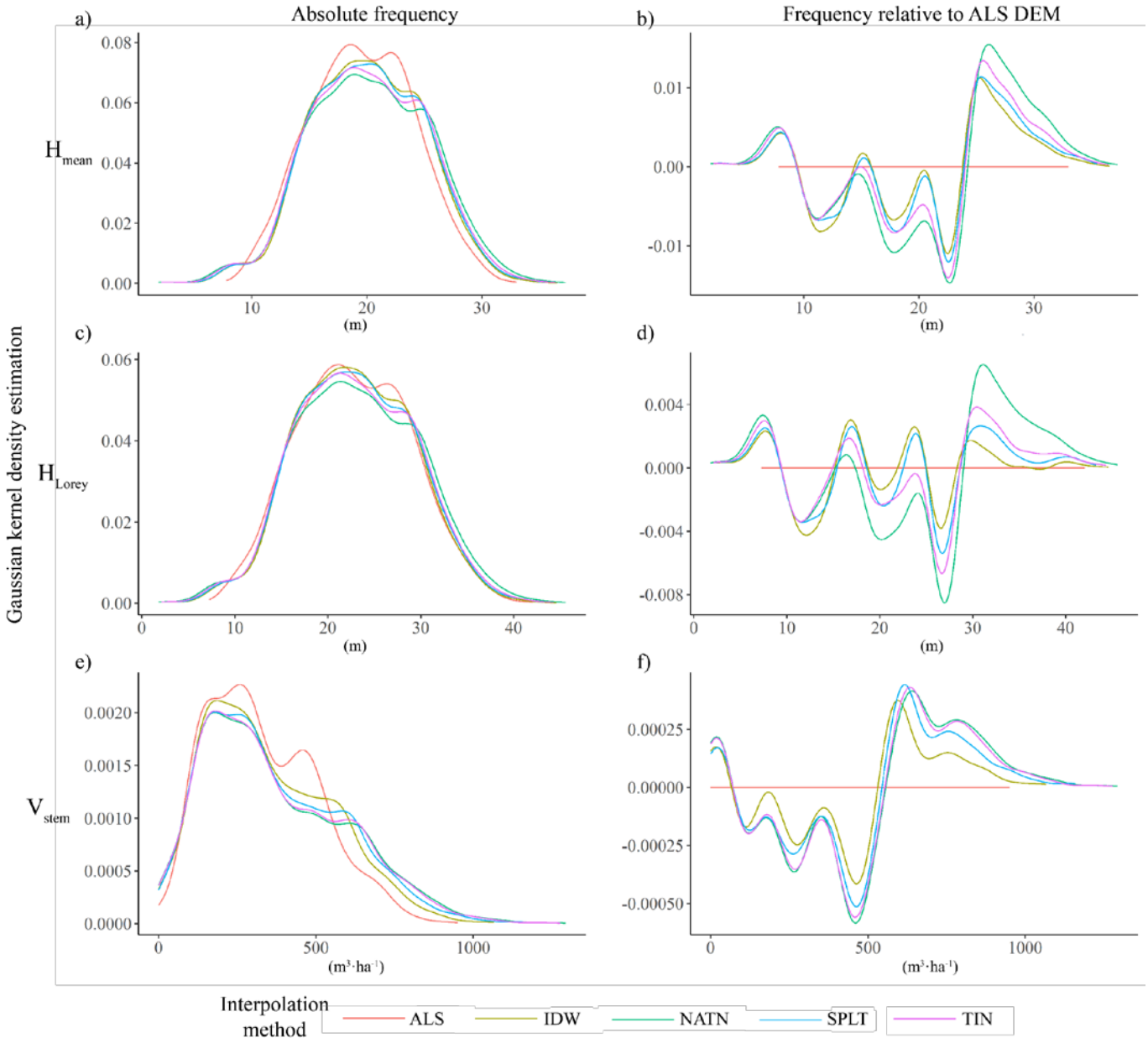


**Figure 4.3-4. Absolute and relative frequency distributions of forest attributes predicted using Table 5 visualized with Gaussian kernel density estimation. Curves represent metrics derived from different terrain surfaces used for point cloud height normalization. Frequencies relative to metrics derived from height normalization using the ALS-DEM are also shown.**

The absolute and relative frequencies of the all three forest attribute predictions (Figure 4.3-4) show that relative to the ALS-DEM, predictions using DAP-DEMs tended to overestimate the higher values. In particular, the NATN method is consistently the furthest from the ALS based predictions for both $H_{mean}$ and $H_{Lorey}$, while predictions based on the IDW method are closest.

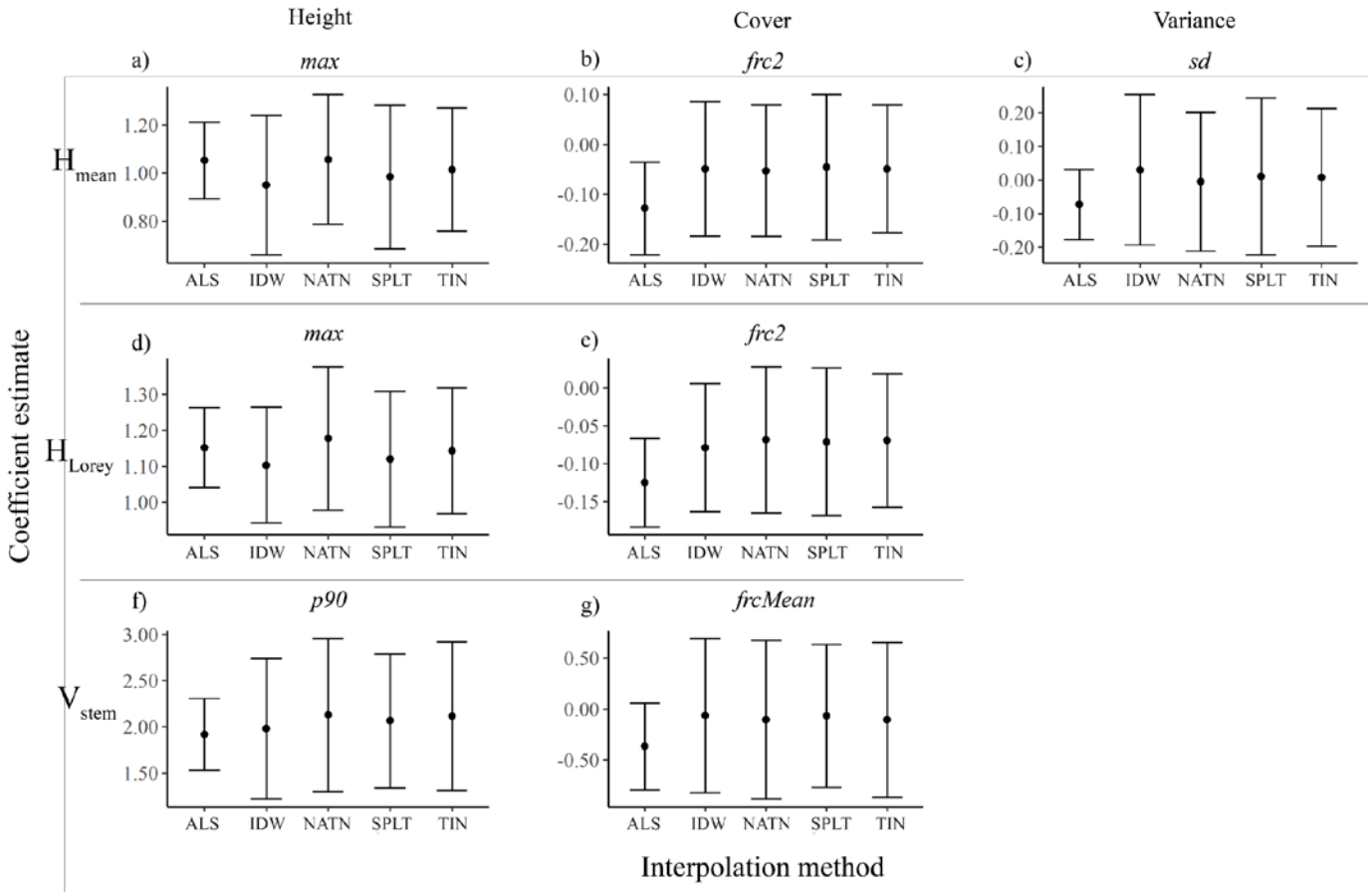


**Figure 4.3-5. Whisker plots displaying the 95% confidence interval of the model coefficients from Table 5 for $H_{mean}$ and $H_{Lorey}$ and $V_{stem}$ coefficients from Table 4.**

Confidence intervals of coefficients derived from models using ALS-DEM normalization have consistently narrower ranges than those using DAP-DEM normalization (Figure 4.3-5); however, complete overlap in the interval ranges is observed for between DAP- and ALS-DEM

derived model coefficients with the exception of the cover metric involved in the $H_{mean}$ and $H_{Lorey}$ models.

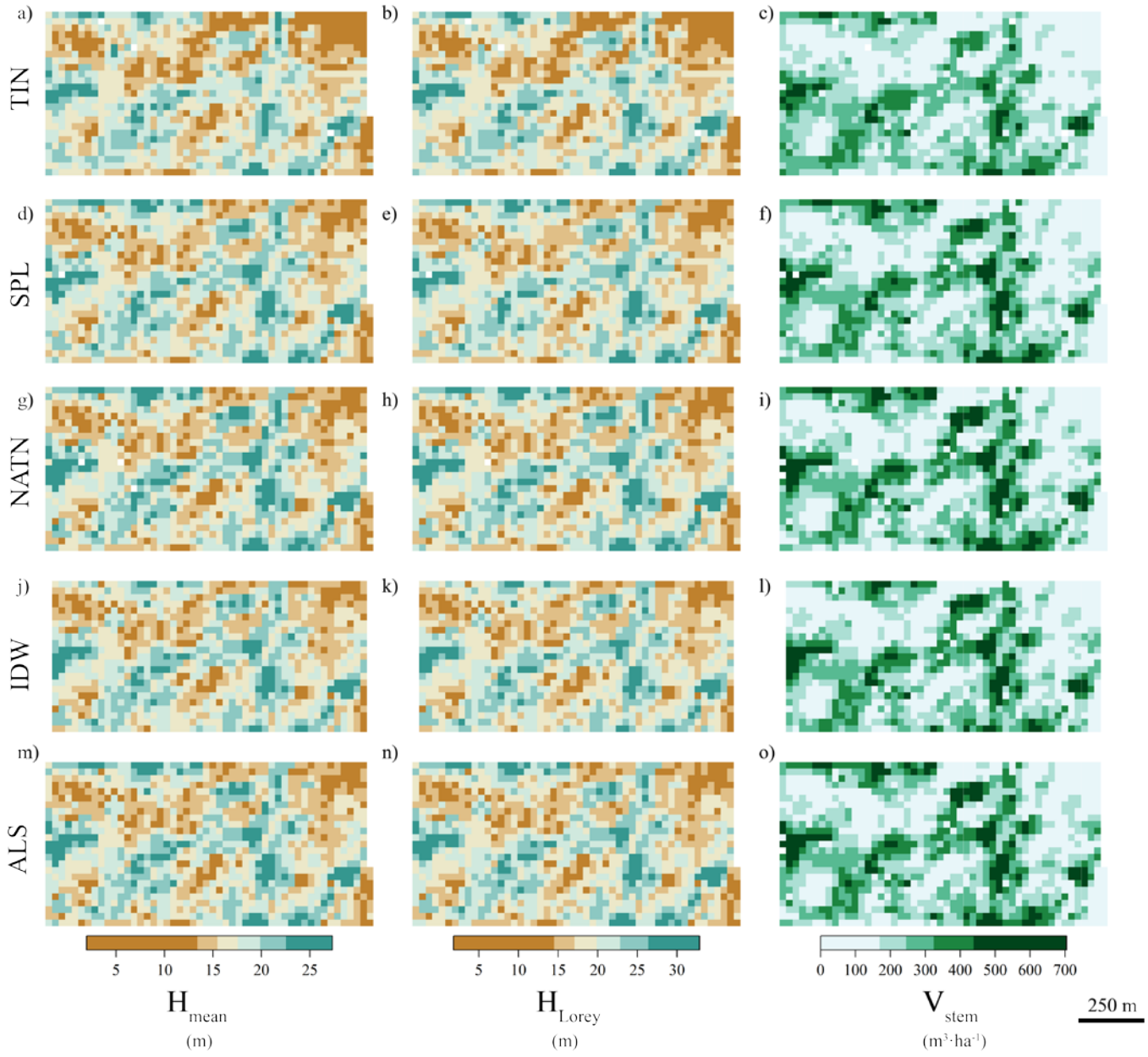


**Figure 4.3-6. Area based forest attribute predictions of $H_{mean}$, $H_{Lorey}$, and $V_{stem}$ for each terrain surface using 25 m x 25 m cells in area C.**

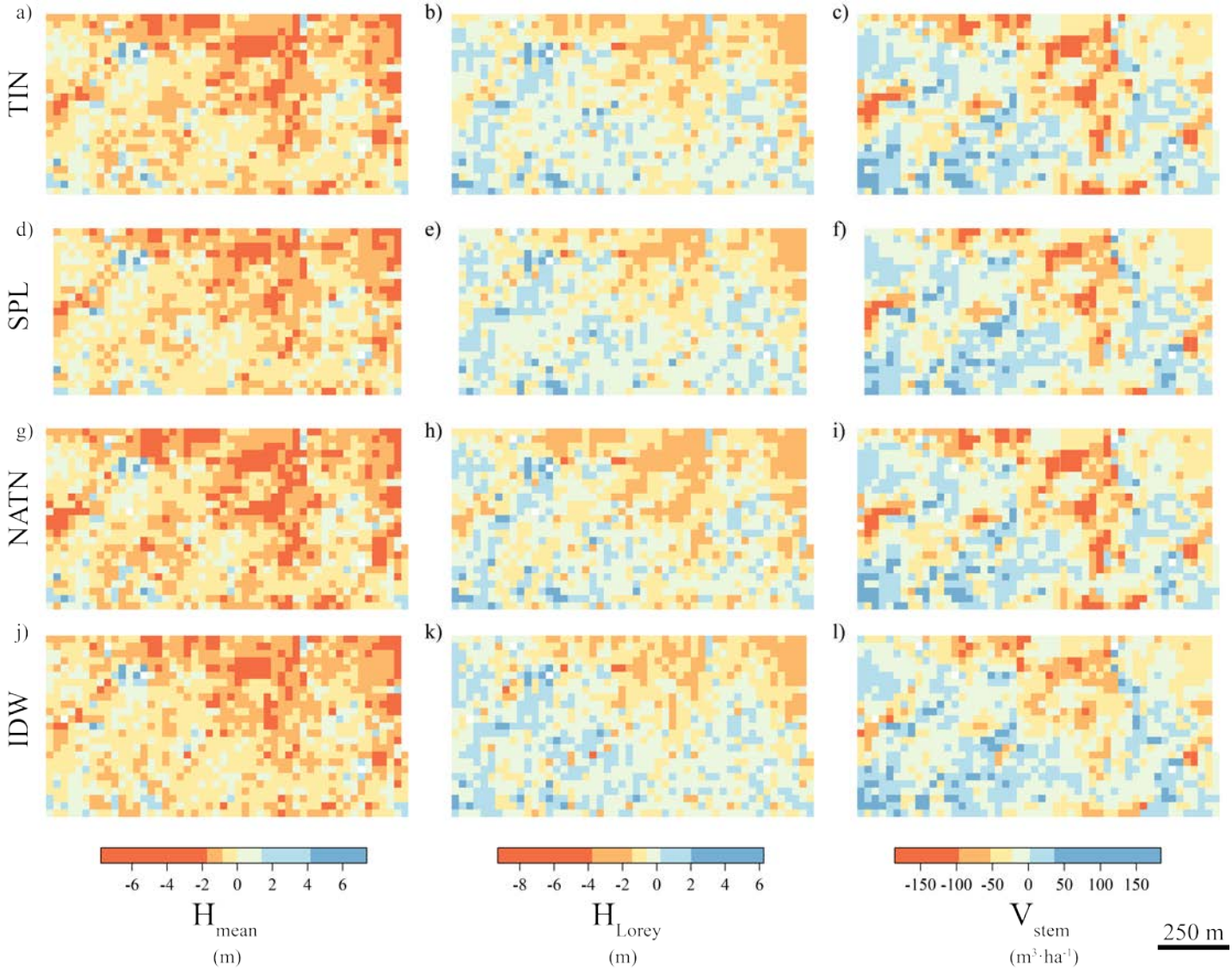


**Figure 4.3-7. Differences between the ALS-DEM and DAP-DEM normalized area-based forest attribute predictions using a 25 x 25 m cell size and each of the tested DAP-DEM interpolation methods using $H_{mean}$, $H_{Lorey}$, and $V_{stem}$ models from Table 4.3-2.**

## 4.4 Discussion

Of the interpolation methods tested to generate terrain surfaces from DAP point clouds, there was not a consistent method which outperformed the others when compared to the ALS-DEM derived models; however, the frequency distribution of predictions derived from the IDW DAP-DEM were appear to be closest to those derived using the ALS-DEM according to Figure 4.3-4 and aligns with findings from (Montealegre, Lamelas, and De La Riva 2015b). Given the small variation in the forest attribute modelling accuracies across the interpolation methods used to generate DAP-DEMs, the processing time may become a limiting factor when choosing between the methods, especially when considering either larger areas or higher DAP point-cloud densities. The respective cumulative times to conduct DEM generation for the three flight areas per interpolation method were 0.22, 0.76, 0.36 and 0.04 hours for IDW, NATN, SPL and TIN respectively.

Point-cloud structural metric generation from DAP terrain models showed that height metrics were overestimated from low to moderate stand heights (~15-30m) and underestimated in tall stands (>30m) in comparison to those derived using the ALS-DEM. A likely explanation for this result is that within shorter forest stands, DAP point-clouds have greater ability to model the terrain surface compared to areas with taller stands, given similar stem densities, due to less aboveground biomass. Therefore, DAP terrain models within tall stands have a tendency to overestimate the terrain elevation compared to the ALS-DEM as noted by the positive relationship shown below in Figure 4.4-1. Fractional cover metric distribution discrepancies between DAP and ALS terrain surface normalization may likely be explained by a small proportion of cells where terrain was considerably overestimated, therefore leading to an

underestimation of high cover cells using DAP terrain normalization. Predictions of height and volume derived from these metrics showed and inverse relationship where taller stands tended to be overestimated by using terrain surfaces from DAP relative to ALS and may be a result of over-compensation by the model fit.

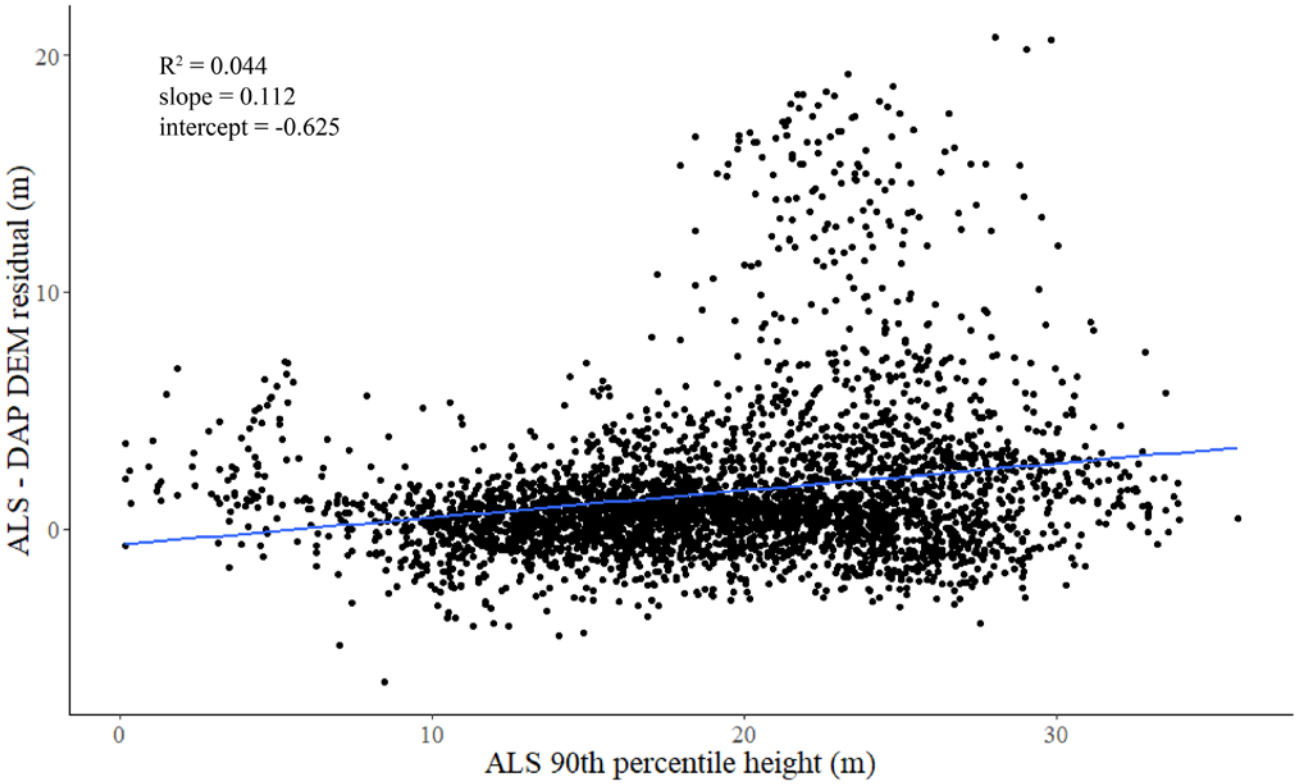


**Figure 4.4-1. Residual between the ALS-DEM and DAP-DEM using TIN interpolation as a function of the 90$^{th}$ percentile of height derived from the ALS point cloud with regression line.**

The best performing forest attribute models for $H_{mean}$, $H_{Lorey}$ and $V_{stem}$ using DAP-DEMs yielded mean RMSE values of 1.19 m (7.29%), 0.92 m (5.04%) and 54.55 $m^3 \cdot ha^{-1}$ (26.66%) respectively across the four DAP-DEM surfaces tested. Model performance was higher when using the ALS-DEM for point cloud height normalization with RMSE values of 0.73 m (4.43%), 0.59 m (3.24%) and 37.31 m (18.24%). Stem volume model performance was considerably

lower than mean height and Lorey's height and is likely due to the reliance on species-specific allometric equations and therefore an additional compounding source of error. Similarly, Puliti et al. (2015) found RMSE values for $H_{Lorey}$ and $V_{stem}$ of 1.4 m and 38.3 $m^3 \cdot ha^{-1}$ respectively when using metrics from a AAS-DAP point cloud normalized by an ALS-DEM within conifer stands of south-eastern Norway. Furthermore, Krause et al. (2019) modelled tree height with an RMSE value of 0.48 m (2.78%) using a DEM derived from field measured control points within a Scots Pine plantation. The close agreement between forest attribute modelling accuracies found in this chapter and those found in the aforementioned studies highlights the predictive capacity for metrics derived from point clouds normalized by DAP-DEM surfaces. Lastly, an entirely nadir image network was tested in this thesis; however, Wallace et al. (2019) report that composite network consisting of nadir and oblique imagery can reduce DEM RMSE by up to 11 cm, presenting the potential for further improvements in forest attribute modelling using point clouds normalized by DAP-DEM surfaces

# Chapter 5: Conclusion

Chapter 3 demonstrated the current capacity of low-cost AAS-DAP terrain modelling results within the interior forests of central BC. It was found that DEMs derived from AAS-DAP point clouds using existing ALS ground classification algorithms are comparable to ALS derived DEMs in a limited capacity largely due to the lack of ground points registered using DAP under dense forest canopies as well as canopy points incorrectly classified as ground. Of the ground classification methods tested, PTD was able to model terrain accurately over a marginally larger area than HRI and SMRF methods. Subsequently, the expectation was confirmed that DAP-DEM error is largely influenced by a combination of terrain slope and canopy cover and that canopy cover is more influential on error than terrain slope.

Chapter 4 evaluated the ABA forest attribute modelling capacity of a consumer-grade optical imaging AA. A well-established modelling approach using ALS point clouds which relies on the derivation of a continuous terrain surface was performed using AAS-DAP data. By testing four interpolation methods to derive continuous terrain surfaces from the DAP point-cloud, it was found that $H_{mean}$, $H_{Lorey}$ and $V_{stem}$ were modelled with accuracies lower yet comparable to those using an ALS-DEM. Between the AAS-DAP DEM interpolation methods used, a consistent leader was not established based on the model parameters and no significant difference was between the distribution of predictions. Nevertheless, I confirm that forest height and stem volume can be predicted with reasonable accuracy using an ABA commonly employed on ALS data.

## 5.1 Key findings

Timely, accurate forest inventories informed by remotely sensed data can be used towards optimizing the value of forest resources (Woods et al. 2011; Holopainen et al. 2014). Recent advances in laser scanning and photogrammetric reconstruction technologies provide 3D point cloud data products with the ability to register forest structure. ALS datasets are commercially established means of describing forest structure at large spatial scales (White, Wulder, Varhola, et al. 2013); however, the associated acquisition costs are high, limiting the average revisit time to approximately 10 years (White, Wulder, Vastaranta, et al. 2013). More frequent data are often needed for supply-chain optimization desirable for commercial harvesting (Goodbody et al. 2017) or for rapid changes to forest structure such as disturbance/harvest and proceeding successional regeneration (Goodbody, Coops, Hermosilla, Tompalski, and Crawford 2018). These forest-related applications may be most effectively monitored using AAS-DAP, especially for fine-scale applications.

The principal objective of this thesis was to analyze the capacity for AAS-DAP to generate an operational inventory of a conifer forest in interior BC, Canada. Using the ABA to model forest attributes, gathering predictive structural metrics from point-cloud data requires a continuous terrain surface to establish vegetation heights above ground (Næsset 2002). In Chapter 3, using commercially provided ALS ground points as reference, a sensitivity analysis of three algorithms designed for the ground classification of ALS data was conducted on the AAS-DAP point-cloud. Using optimal AAS-DAP ground points established in Chapter 3, Chapter 4 investigated the influence of common interpolation methods for deriving a continuous terrain

surface. Predictive models for $H_{mean}$, $H_{Lorey}$ and $V_{stem}$ were then developed using structural point-cloud metrics calculated from the range of generated terrain surfaces.

### 5.1.1 AAS-DAP terrain model optimization

The ground classification of ALS point-clouds has been extensively researched resulting in both proprietary and open-source algorithm implementations. Therefore, three algorithms designed for terrain-point classification of ALS points were applied to AAS-DAP point-clouds. The distribution of DAP-DEM errors were compared to stratified classes of canopy cover and terrain slope defined by the ALS data set.

- The effect of algorithm parameters for ground classification of AAS-DAP points was demonstrated. This serves as a platform from which ideal algorithm parameters can be more easily estimated for future data acquisitions.
- Using three ground classification algorithms, ~40 - 70% of the study areas was characterized by DAP-DEM RMSE of <1.5 m; however, isolated areas with RMSE and BIAS values > 10 m are present even when using optimal parameters due to the inclusion of canopy points in the ground classification.
- Using the leading algorithm, 56% of the aggregated study area terrain was modeled with RMSE <1.5 m
- Canopy cover was found to be approximately three times more influential on DAP-DEM RMSE than terrain slope

### 5.1.2 Influence of terrain surface interpolation on forest inventory estimation

The modelling of forest attributes to produce an operational forest inventory has been extensively explored using ALS data. Chapter 4 of this thesis explored the transferability of these methods to the AAS-DAP platform. This method relies on establishing a terrain surface for the height normalization of forest elements. Using an optimal set of ground points established in Chapter 3, common surface interpolation methods were implemented to produce a range of final terrain products from AAS-DAP.

- Using only DAP point cloud, predictive models for forest attributes $H_{mean}$, $H_{Lorey}$ and $V_{stem}$ had mean RMSE values 1.19 m (7.29%), 0.92 m (5.04%) and 54.55 $m^3 \cdot ha^{-1}$ (26.66%) respectively among the four DAP-DEM interpolation methods used.
- Forest attribute modelling accuracies were consistently higher by a small amount when using the ALS-DEM to normalize point-cloud vegetation heights.
- Between the four terrain surfaces derived from DAP and one from ALS, no statistically significant difference was found between model parameter coefficients or distributions of wall-to-wall predictions for $H_{mean}$, $H_{Lorey}$ and $V_{stem}$; however, the IDW interpolation method produced predictions most similar to those from the ALS-DEM

## 5.2 Implications

This research demonstrates that dense point clouds generated from consumer grade AAS-DAP hold potential in conducting both terrain reconstruction and subsequent operational forest inventories over the study area. Despite some limitations (Section 5.4), operationally useful

terrain models were generated from DAP point clouds for large portions of the study site. Though RMSE >10 m was found in certain areas of the AAS-DAP terrain models over dense forest canopies, resulting area-based structural point-cloud metrics were used to predict plot-level forest attributes with errors comparable to predictions developed using ALS terrain models. The findings presented here highlight the utility of AAS-DAP as a tool for performing timely, cost-effective forest inventories at the forest stand level.

The range of forest conditions found within the chosen AFRF study area are typical of BC's ICH and SBS BEC zones, which account for 17% of total provincial land mass ("Biogeoclimatic Ecosystem Classification (BEC) Map" 2018). As previously mentioned, the AFRF study areas were disturbed by wildfire in the months prior to image acquisition, potentially reducing canopy foliage and therefore ground occlusion, providing the opportunity for a case study unique to stands disturbed by wildfire. Given recent catastrophic forest disturbances from the mountain pine beetle and wildfire across BC, there is a demand from forest managers for the timely collection of structural information in disturbed forests. For the many forest-related natural resource management agencies around the province, the relatively low cost of AAS deployment compared to ALS opens new possibilities for such data collection. Findings from this thesis are specific to the AFRF Gavin Lake Block; however, results have been shown to improve in relatively more open forest stands and less complex topography (Jensen and Mathews 2016). Therefore, this thesis provides insight into the feasibility of AAS-DAP derived forest inventories over boreal and temperate forest biomes, which respectively account for 24.2% and 21.8% of global forests (Crowther et al. 2015).

## 5.3 Operational outcomes

Based on findings presented in this thesis, I make key operational recommendations for using AAS-DAP for forest inventory applications. Due to the inability for ground classification algorithms to remove all canopy points within dense canopy cover in Chapter 3, terrain models built from AAS-DAP require careful manual inspection or validation against an independently verified terrain data source where possible. In order to maximize the utility of ground classification algorithms, the optimal parameters are likely to vary, even among different conifer forests. Nevertheless, the agreement between *step, cell* and *cell* values of ~20 m for PTD, HRI and SMRF algorithms found in Chapter 3 indicate an initial search resolution likely appropriate for conifer stands of the ICH and SBS BEC zones. Additionally, only small differences were found in performance between the proprietary PTD and open-source HRI and SMRF methods. In particular, ground classifications using the SMRF algorithm were least sensitive to changes in parameter values and therefore, may have similar performance in different conifer environments.

Chapter 4 demonstrated that structural point-cloud metrics can be used to develop models for forest attributes $H_{mean}$, $H_{Lorey}$ and $V_{stem}$ summarized at the plot-level from field-measured tree height and DBH. It is recommended that plots are distributed using a stratified random sampling technique using a priori knowledge of forest structure (Corona and Fattorini 2008). Results from Chapter 4 show that height attributes were predicted with higher accuracies using less complex models than those for stem volume. The differences in stem volume predictions derived from ALS and AAS-DAP terrain surfaces shows that a relatively large variation in predictions can exist. Therefore, stem volume models may be enhanced with the incorporation of spectral metrics. Given that there were no significant differences found between

predictions from different DAP-DEM interpolated surfaces, the TIN interpolation method is recommended given its relatively faster processing speed.

This thesis is a result of collaboration between the University of British Columbia Faculty of Forestry and FYBR Solutions Inc. and exemplifies the transfer of technology from academia into commercial operations. This partnership hopes to serve as a template for future research collaborations. In addition to the analyses presented in Chapters 3 & 4, research innovations provided to FYBR Solutions Inc. include a sampling framework for testing AAS-DAP ground classification performance over a range of landscape types and an automated method to register multi-temporal point-cloud entities. As the capabilities of consumer-grade AAS-DAP platforms and processing techniques increases, this thesis serves as a benchmark for future research.

## 5.4 Limitations

There are a few notable limitations of the AAS platform for forest inventory analysis which factored into this study. As previously mentioned, limitations of the current consumer-grade AAS-DAP platform used in this thesis are the spatial coverage, georeferencing accuracy and susceptibility to occlusion. The maximum spatial coverage of any remote sensing platform changes with altitude and is inversely proportional to spatial resolution. In this thesis, images were acquired over ~300 ha in three days of flight resulting in an average point cloud density of 95 points/$m^2$ and GSD of 5 cm. Of the DAP acquisition parameters, flying altitude was restricted by local regulations to 122 m AGL while flight speed was restricted by the rate at which images are written to disk (5 Mb/s) and the desired image capture interval. In addition, there was a need to relocate the take-off point multiple times to maintain visual line of sight with the AAS. In

comparison to a flat study site, terrain following the mountainous topography of the AFRF required additional power to climb and descend reducing the efficiency of each flight. Up to eight readily charged batteries and corresponding takeoffs and landings were necessary in order to replace the battery. Lastly, there was further potential to optimize flights for hours with acceptable lighting conditions. As result of these restrictions and logistical shortcomings, ~100 ha was captured per day of flight was acquired in this case study. Therefore, it should be noted, that given these acquisition conditions, the realizable spatial coverage of consumer grade AAS-DAP could have been significantly enhanced.

This thesis assumes the canopy cover and terrain slope derived from ALS acquired in 2008 are adequate descriptions for analysis with DAP data acquired in 2017. A degree of change to forest structure between the acquisitions should be acknowledged. Therefore, a smaller temporal gap may have enhanced the relationship between canopy cover and the RMSE in Chapter 3. Georeferencing accuracy of AAS-DAP depends on the on-board GPS capability of the platform as well as remotely detected registration with GCPs measured in the field. The precision of GPS point measurement is known to be reduced within coniferous forests (Deckert and Bolstad 1996; Næsset 1999; Reutebuch et al. 2003). Therefore the error of GCP locations in complex forested terrain, such as in this region, may have reduced the agreement between DAP-DEMs and ALS points and therefore inflated RMSE. Tomaštík et al. (2017) tested of a range of GCP configurations using a total station in three ~1 ha plots situated in flat, open canopy forests and report a mean vertical RMSE of ~0.1 m. Similarly, Jensen and Mathews (Jensen and Mathews 2016) used eight GCP over ~15 ha where the landscape transitioned from savannah to closed canopy woodlands and found a mean estimated error of <0.15 m. Given these

comparisons, future analyses involving the fusion of AAS-DAP and ancillary spatial data over relatively dense conifer forests requires a more precise direct or indirect georeferencing method for AAS-DAP point clouds to achieve similar accuracies.

## 5.5 Future Research

Future research should be conducted towards optimizing the utility of AAS-DAP in a range of forest-related applications. The majority of studies to date which investigate the use of AAS-DAP are conducted in urban environments (Z. Zhang et al. 2018), open forests (Jensen and Mathews 2016) or plantations (Guerra-Hernández et al. 2018). Considering that a large portion of global forest resources are complex conifer ecosystems (Crowther et al. 2015), exploration of cost-effective remote sensing techniques such as AAS-DAP are justified. This thesis aimed to address the lack of studies conducted within conifer stands of British Columbia, Canada; however, supplementary research is needed in these environments. Given that the classification of ground returns from ALS data has been thoroughly examined in peer reviewed literature, the development of a terrain classification algorithm specific to AAS-DAP datasets should be investigated.

One solution towards precise AAS-DAP dataset alignment is to deploy a more precisely measured GCP network using sub-centimeter precision differential GPS elevations collected from a total station (Simpson et al. 2017); however, defining and mapping the forest floor is challenging and the associated cost of such equipment and field work is high. Another viable solution is the inclusion of higher precision GPS equipment onboard AASs, however this may erode the low-cost advantage of the AAS-DAP approach. A third potential solution is the co-registration of the DAP point cloud with an independent, precisely georeferenced spatial dataset

such as an ALS point cloud or an accurate road network layer with a high degree of spatial detail and coverage. For instance, automated alignment of point-cloud datasets has been demonstrated using the iterative closest point (ICP) algorithm (Men, Gebre, and Pochiraju 2011; Gressin et al. 2013; Kai Zhang, Li, and Zhang 2014).

This thesis generated only structural metrics used to predict forest attributes in Chapter 4; however, the inclusion of spectral information may enhance inventory prediction accuracies. Consumer-grade AAS imaging systems are restricted to RGB bands which have some capacity in describing vegetation, such as small crops (Bendig et al. 2014) and deciduous forests (Chianucci et al. 2016); however, future research should be conducted by employing sensors capable of measuring near-infrared portions of the spectrum as for they have been widely proven to provide detail on forest health. Combinatory metrics consisting of both structural and spectral criteria may also improve prediction accuracy. A simple example of this could be the fraction of green vegetation points above a height threshold. Lastly, metrics generated without the use of terrain height normalization are currently being explored (Giannetti et al. 2018) and should be further researched to reduce the dependence of remotely sensing forest inventories on terrain modelling.

The versatility and cost-effectiveness of the AAS-DAP remote sensing platform present many avenues for future research. Moreover, software tools used to analyze point-cloud data are concurrently becoming more complex and efficient and increasingly available at little or no cost as result of the globally trending open-source software movement. Wall-to-wall applications for AAS-DAP are limited to the stand-level; however, systematically distributed AAS acquisitions over a landscape can serve as a cost-effective forest inventory sampling method and have been

recently investigated as alternatives to wall-to-wall ALS acquisitions of similar scale (Puliti et al., 2017). Similarly, fusion of ancillary satellite spectral information and partial-coverage UAV DAP as sample training data has also been tested in assessing insect defoliation (Cardil et al., 2017). Given the outlined possibilities for future research, the low-cost AAS platform serves as a promising tool of choice for detailed surveys of small forested areas (Wallace et al., 2012).

**Bibliography**

Akaike, Hirotugu. 2006. “On the Likelihood of a Time Series Model.” *The Statistician* 27 (3/4): 217. https://doi.org/10.2307/2988185.

Alaback, P.G., and S. Saunders. 2013. “Disturbance Ecology of the Temperate Rainforests of Southeast Alaska and Adjacent British Columbia.” In *North Temperate Rainforests: Ecology and Conservation*, 73–88. https://books.google.ca/books?hl=en&lr=&id=WzcgDAAAQBAJ&oi=fnd&pg=PA73&dq=Natural+disturbance+patterns+in+the+temperate+rainforests+of+southeast+Alaska+and+adjacent+British+Columbia&ots=rsE10xVz0s&sig=NHtNiFbJay4CFi2B_XDgrFg1tRE.

Ali, Tarig, and Ali Mehrabian. 2009. “A Novel Computational Paradigm for Creating a Triangular Irregular Network (TIN) from LiDAR Data.” *Nonlinear Analysis, Theory, Methods and Applications* 71 (12): e624–29. https://doi.org/10.1016/j.na.2008.11.081.

Aschoff, T, M Thies, and H Spiecker. 2004. “Describing Forest Stands Using Terrestrial Laser-Scanning.” In *XXth ISPRS Congress: Proceedings of Commission V*, 237–41. http://www.cartesia.es/geodoc/isprs2004/comm5/papers/556.pdf.

Asghar, Umair. 2017. “Landslide Mapping from Analysis of UAV-SFM Point Clouds.” University of British Columbia. https://doi.org/10.14288/1.0357952.

Axelsson, Peter. 1999. “Processing of Laser Scanner Data—Algorithms and Applications.” *ISPRS Journal of Photogrammetry and Remote Sensing* 54: 138–47. https://doi.org/10.1016/S0924-2716(99)00008-8.

———. 2000. “DEM Generation from Laser Scanner Data Using Adaptive TIN Models.” *International Archives of Photogrammetry and Remote Sensing* 33 (Part B4): 110–17. https://doi.org/10.1016/j.isprsjprs.2005.10.005.

Baltsavias, Emmanuel P. 1999. “A Comparison between Photogrammetry and Laser Scanning.” *ISPRS Journal of Photogrammetry and Remote Sensing* 54 (2–3): 83–94. https://doi.org/10.1016/S0924-2716(99)00014-3.

Barnard, Stephen T, Martin A Fischler, and S T Barnard. 1982. “Computational Stereo.” https://doi.org/10.1145/356893.356896.

Barnes, Alex. 2016. “2015 Economic State of the B.C. Forest Sector.” https://www2.gov.bc.ca/assets/gov/farming-natural-resources-and-industry/forestry/forest-industry-economics/economic-state/2015_economic_state_of_bc_forest_sector.pdf.

———. 2018. “2017 Economic State of the B.C. Forest Sector.” http://citeseerx.ist.psu.edu/viewdoc/download?doi=10.1.1.398.4123&rep=rep1&type=pdf.

Bater, Christopher W, and Nicholas C Coops. 2009. “Evaluating Error Associated with Lidar-Derived DEM Interpolation.” *Computers and Geosciences* 35 (2): 289–300. https://doi.org/10.1016/j.cageo.2008.09.001.

Ben-Arie, Joshua R., Geoffrey J. Hay, Ryan P. Powers, Guillermo Castilla, and Benoît St-Onge. 2009. “Development of a Pit Filling Algorithm for LiDAR Canopy Height Models.” *Computers and Geosciences* 35 (9): 1940–49. https://doi.org/10.1016/j.cageo.2009.02.003.

Bendig, Juliane, Andreas Bolten, Simon Bennertz, Janis Broscheit, Silas Eichfuss, Georg Bareth,

Juliane Bendig, et al. 2014. “Estimating Biomass of Barley Using Crop Surface Models (CSMs) Derived from UAV-Based RGB Imaging.” *Remote Sensing* 6 (11): 10395–412. https://doi.org/10.3390/rs61110395.

Bengtsson, Jan, Sven G Nilsson, Alain Franc, and Paolo Menozzi. 2000. “Biodiversity, Disturbances, Ecosystem Function and Management of European Forests.” *Forest Ecology and Management* 132 (1): 39–50. https://doi.org/10.1016/S0378-1127(00)00378-9.

“Biogeoclimatic Ecosystem Classification (BEC) Map.” 2018. 2018. https://catalogue.data.gov.bc.ca/dataset/bec-map-historic-versions.

Bleiker, Kathy. 2017. “Mountain Pine Beetle (Factsheet).” Natural Resources Canada. 2017. https://www.nrcan.gc.ca/forests/fire-insects-disturbances/top-insects/13397.

Bohlin, Jonas, Jörgen Wallerman, and Johan E.S. Fransson. 2012. “Forest Variable Estimation Using Photogrammetric Matching of Digital Aerial Images in Combination with a High-Resolution DEM.” *Scandinavian Journal of Forest Research* 27 (7): 692–99. https://doi.org/10.1080/02827581.2012.686625.

Bouvier, Marc, Sylvie Durrieu, Richard A. Fournier, and Jean Pierre Renaud. 2015. “Generalizing Predictive Models of Forest Inventory Attributes Using an Area-Based Approach with Airborne LiDAR Data.” *Remote Sensing of Environment*. Elsevier. https://doi.org/10.1016/j.rse.2014.10.004.

Burton, Philip J. 2010. “Striving for Sustainability and Resilience in the Face of Unprecedented Change: The Case of the Mountain Pine Beetle Outbreak in British Columbia.”

*Sustainability* 2 (8): 2403–23. https://doi.org/10.3390/su2082403.

Chen, Qi, Peng Gong, Dennis Baldocchi, and Yong Q. Tian. 2013. "Estimating Basal Area and Stem Volume for Individual Trees from Lidar Data." *Photogrammetric Engineering & Remote Sensing* 73 (12): 1355–65. https://doi.org/10.14358/pers.73.12.1355.

Chianucci, Francesco, Leonardo Disperati, Donatella Guzzi, Daniele Bianchini, Vanni Nardino, Cinzia Lastri, Andrea Rindinella, and Piermaria Corona. 2016. "Estimation of Canopy Attributes in Beech Forests Using True Colour Digital Images from a Small Fixed-Wing UAV." *International Journal of Applied Earth Observation and Geoinformation* 47: 60–68. https://doi.org/10.1016/j.jag.2015.12.005.

Clapuyt, Francois, Veerle Vanacker, and Kristof Van Oost. 2016. "Reproducibility of UAV-Based Earth Topography Reconstructions Based on Structure-from-Motion Algorithms." *Geomorphology* 260: 4–15. https://doi.org/10.1016/j.geomorph.2015.05.011.

Coops, Nicholas C, Jason Duffe, and Cathy Koot. 2010. "Assessing the Utility of Lidar Remote Sensing Technology to Identify Mule Deer Winter Habitat." *Canadian Journal of Remote Sensing* 36 (2): 81–88. https://doi.org/10.5589/m10-029.

Corona, Piermaria, and Lorenzo Fattorini. 2008. "Area-Based Lidar-Assisted Estimation of Forest Standing Volume." *Canadian Journal of Forest Research* 38 (11): 2911–16. https://doi.org/10.1139/X08-122.

Crowther, Thomas W, Henry B Glick, K. R. Covey, C. Bettigole, Daniel S Maynard, Stephen M Thomas, J. R. Smith, et al. 2015. "Mapping Tree Density at a Global Scale." *Nature* 525

(7568): 201–5. https://doi.org/10.1038/nature14967.

Culbert, Patrick D, Volker C Radeloff, Curtis H Flather, Josef M Kellndorfer, Chadwick D Rittenhouse, and Anna M Pidgeon. 2013. “The Influence of Vertical and Horizontal Habitat Structure on Nationwide Patterns of Avian Biodiversity.” *The Auk* 130 (4): 656–65. https://doi.org/10.1525/auk.2013.13007.

Davenport, Ian J., Nick Holden, and Robert J. Gurney. 2004. “Characterizing Errors in Airborne Laser Altimetry Data to Extract Soil Roughness.” In *IEEE Transactions on Geoscience and Remote Sensing*, 42:2130–41. https://doi.org/10.1109/TGRS.2004.834648.

Day, Ken. 2007. *History of the UBC Alex Fraser Research Forest (1987-2007) - Excerpts from Management and Working Plan # 3*. http://www.forestry.ubc.ca/resfor/afrf/Reports_Index.htm.

Deckert, Christopher, and Paul V Bolstad. 1996. “Forest Canopy, Terrain, and Distance Effects on Global Positioning System Point Accuracy.” *Photogrammetric Engineering and Remote Sensing.* 62 (3): 317–21. https://www.asprs.org/wp-content/uploads/pers/1996journal/mar/1996_mar_317-321.pdf.

Fonstad, Mark A., James T. Dietrich, Brittany C. Courville, Jennifer L. Jensen, and Patrice E. Carbonneau. 2013. “Topographic Structure from Motion: A New Development in Photogrammetric Measurement.” *Earth Surface Processes and Landforms* 38 (4): 421–30. https://doi.org/10.1002/esp.3366.

Franke, Richard. 1982. “Smooth Interpolation of Scattered Data by Local Thin Plate Splines.”

*Computers and Mathematics with Applications* 8 (4): 273–81. https://doi.org/10.1016/0898-1221(82)90009-8.

Frey, Julian, Kyle Kovach, Simon Stemmler, Barbara Koch, Julian Frey, Kyle Kovach, Simon Stemmler, and Barbara Koch. 2018. "UAV Photogrammetry of Forests as a Vulnerable Process. A Sensitivity Analysis for a Structure from Motion RGB-Image Pipeline." *Remote Sensing* 10 (6): 912. https://doi.org/10.3390/rs10060912.

Gatziolis, Demetrios, Jean F Lienard, Andre Vogs, and Nikolay S Strigul. 2015. "3D Tree Dimensionality Assessment Using Photogrammetry and Small Unmanned Aerial Vehicles." Edited by Han Y.H. Chen. *PLOS ONE* 10 (9): e0137765. https://doi.org/10.1371/journal.pone.0137765.

Giannetti, Francesca, Gherardo Chirici, Terje Gobakken, Erik Næsset, Davide Travaglini, and Stefano Puliti. 2018. "A New Approach with DTM-Independent Metrics for Forest Growing Stock Prediction Using UAV Photogrammetric Data." *Remote Sensing of Environment* 213 (August): 195–205. https://doi.org/10.1016/j.rse.2018.05.016.

Gillis, M D, P Boudewyn, K Power, and Glenda Russo. 2010. "Development of Canada's National Forest Inventory." In *National Forest Inventories: Pathways for Common Reporting*, 97–111. https://doi.org/10.1007/978-90-481-3233-1.

Gillis, MD, and DG Leckie. 1993. "Forest Inventory Mapping Procedures across Canada." *Petawawa National Forestry Institute*. Vol. 114. Chalk River, Ontario: Petawawa National Forestry Institute. http://www.cfs.nrcan.gc.ca/publications/?id=4365.

Godone, Danilo, and Gabriele Garnero. 2013. “The Role of Morphometric Parameters in Digital Terrain Models Interpolation Accuracy: A Case Study.” *European Journal of Remote Sensing* 46 (1): 198–214. https://doi.org/10.5721/EuJRS20134611.

Gonzalez, J.S. 1990. “Wood Density of Canadian Tree Species.” No. NOR-X-315. http://cfs.nrcan.gc.ca/pubwarehouse/pdfs/11744.pdf.

Goodbody, Tristan R.H., Nicholas C. Coops, Txomin Hermosilla, Piotr Tompalski, and Gaetan Pelletier. 2018. “Vegetation Phenology Driving Error Variation in Digital Aerial Photogrammetrically Derived Terrain Models.” *Remote Sensing* 10 (10): 1554. https://doi.org/10.3390/rs10101554.

Goodbody, Tristan R.H., Nicholas C Coops, Txomin Hermosilla, Piotr Tompalski, and Patrick Crawford. 2018. “Assessing the Status of Forest Regeneration Using Digital Aerial Photogrammetry and Unmanned Aerial Systems.” *International Journal of Remote Sensing* 39 (15–16): 5246–64. https://doi.org/10.1080/01431161.2017.1402387.

Goodbody, Tristan R.H., Nicholas C Coops, Piotr Tompalski, Patrick Crawford, and Ken J.K. Day. 2017. “Updating Residual Stem Volume Estimates Using ALS- and UAV-Acquired Stereo-Photogrammetric Point Clouds.” *International Journal of Remote Sensing* 38 (8–10): 2938–53. https://doi.org/10.1080/01431161.2016.1219425.

Goodbody, Tristan R H, Nicholas C Coops, Piotr Tompalski, Patrick Crawford, and Ken J K Day. 2016. “Updating Residual Stem Volume Estimates Using ALS-and UAV-Acquired Stereo-Photogrammetric Point Clouds Updating Residual Stem Volume Estimates Using ALS-and UAV-Acquired Stereo-Photogrammetric Point Clouds.” *International Journal of*

*Remote Sensing* 38 (8–10): 2938–53. https://doi.org/10.1080/01431161.2016.1219425.

Graham, Alexander, Nicholas C. Coops, Michael Wilcox, and Andrew Plowright. 2019. "Evaluation of Ground Surface Models Derived from Unmanned Aerial Systems with Digital Aerial Photogrammetry in a Disturbed Conifer Forest." *Remote Sensing* 11 (1): 84. https://doi.org/10.3390/rs11010084.

Gressin, Adrien, Clément Mallet, Jér Ôme Demantké, and Nicolas David. 2013. "Towards 3D Lidar Point Cloud Registration Improvement Using Optimal Neighborhood Knowledge." *ISPRS Journal of Photogrammetry and Remote Sensing* 79 (May): 240–51. https://doi.org/10.1016/j.isprsjprs.2013.02.019.

Guerra-Hernández, Juan, Diogo N Cosenza, Luiz Carlos, Estraviz Rodriguez, Margarida Silva, Margarida Tomé, Ramón A Díaz-Varela, Eduardo González-Ferreiro, Eduardo González, and Luiz Carlos Estraviz Rodriguez. 2018. "Eucalyptus Plantations." *International Journal of Remote Sensing* 39: 5211–35. https://doi.org/10.1080/01431161.2018.1486519.

Guerra-Hernández, Juan, Eduardo González-Ferreiro, Vicente Monleón, Sonia Faias, Margarida Tomé, Ramón Díaz-Varela, Juan Guerra-Hernández, et al. 2017. "Use of Multi-Temporal UAV-Derived Imagery for Estimating Individual Tree Growth in Pinus Pinea Stands." *Forests* 8 (8): 300. https://doi.org/10.3390/f8080300.

Harwin, Steve, and Arko Lucieer. 2012. "Assessing the Accuracy of Georeferenced Point Clouds Produced via Multi-View Stereopsis from Unmanned Aerial Vehicle (UAV) Imagery." *Remote Sensing* 4 (6): 1573–99. https://doi.org/10.3390/rs4061573.

Helava, U V. 1978. “Digital Corellation in Photogrammetric Instruments” Vol. 34. https://ac.els-cdn.com/0031866378900200/1-s2.0-0031866378900200-main.pdf?_tid=995335bb-87cf-4853-9120-632c03c61ab7&acdnat=1537813205_696eef73b368b28edaeefb9cf6489a1d.

Herrero-Huerta, Mónica, Beatriz Felipe-García, Soledad Belmar-Lizarán, David Hernández-López, Pablo Rodríguez-Gonzálvez, and Diego González-Aguilera. 2016. “Dense Canopy Height Model from a Low-Cost Photogrammetric Platform and LiDAR Data.” *Trees - Structure and Function* 30 (4): 1287–1301. https://doi.org/10.1007/s00468-016-1366-9.

Hickey, Gordon M, and John L Innes. 2008. “Indicators for Demonstrating Sustainable Forest Management in British Columbia, Canada: An International Review.” *Ecological Indicators* 8 (2): 131–40. https://doi.org/10.1016/j.ecolind.2006.11.005.

Hodgson, Michael E., and Patrick Bresnahan. 2004. “Accuracy of Airborne Lidar-Derived Elevation: Empirical Assessment and Error Budget.” *Photogrammetric Engineering and Remote Sensing* 70 (3): 331–39. https://doi.org/10.14358/PERS.70.3.331.

Hodgson, Michael E., John Jensen, George Raber, Jason Tullis, Bruce A. Davis, Gary Thompson, and Karen Schuckman. 2005. “An Evaluation of Lidar-Derived Elevation and Terrain Slope in Leaf-off Conditions.” *Photogrammetric Engineering & Remote Sensing* 71 (7): 817–23. https://doi.org/10.14358/PERS.71.7.817.

Holopainen, Markus, Mikko Vastaranta, Juha Hyyppä, Markus Holopainen, Mikko Vastaranta, and Juha Hyyppä. 2014. “Outlook for the Next Generation’s Precision Forestry in Finland.” *Forests* 5 (7): 1682–94. https://doi.org/10.3390/f5071682.

Hutchinson, M F, and J C Gallant. 1999. “Representation of Terrain.” *Geographical Information Systems* 1: 105–24. https://frew.eri.ucsb.edu/private/ESM263/week/7/Representation_of_terrain.pdf.

Iizuka, Kotaro, Taichiro Yonehara, Masayuki Itoh, and Yoshiko Kosugi. 2018. “Estimating Tree Height and Diameter at Breast Height (DBH) from Digital Surface Models and Orthophotos Obtained with an Unmanned Aerial System for a Japanese Cypress (Chamaecyparis Obtusa) Forest.” *Remote Sensing* 10 (1): 13. https://doi.org/10.3390/rs10010013.

Isenburg, Martin, Yuanxin Liu, Jonathan Shewchuk, Jack Snoeyink, and Tim Thirion. 2006. “Generating Raster DEM from Mass Points Via TIN Streaming.” In , 186–98. https://doi.org/10.1007/11863939_13.

Jat, Prahlad, and Marc L. Serre. 2016. “Bayesian Maximum Entropy Space/Time Estimation of Surface Water Chloride in Maryland Using River Distances.” *Environmental Pollution* 219 (December): 1148–55. https://doi.org/10.1016/J.ENVPOL.2016.09.020.

Jat, Prahlad, and Marc L Serre. 2018. “A Novel Geostatistical Approach Combining Euclidean and Gradual-Flow Covariance Models to Estimate Fecal Coliform along the Haw and Deep Rivers in North Carolina.” *Stochastic Environmental Research and Risk Assessment* 32. https://doi.org/10.1007/s00477-018-1512-6.

Jensen, Jennifer L. R., and Adam J. Mathews. 2016. “Assessment of Image-Based Point Cloud Products to Generate a Bare Earth Surface and Estimate Canopy Heights in a Woodland Ecosystem.” *Remote Sensing* 8 (1): 50. https://doi.org/10.3390/rs8010050.

Kachamba, Daud Jones, Hans Ole Ørka, Erik Næsset, Tron Eid, and Terje Gobakken. 2017. "Influence of Plot Size on Efficiency of Biomass Estimates in Inventories of Dry Tropical Forests Assisted by Photogrammetric Data from an Unmanned Aircraft System." *Remote Sensing* 9 (6): 610. https://doi.org/10.3390/rs9060610.

Kerns, Becky K., and Alan Ager. 2007. "Risk Assessment for Biodiversity Conservation Planning in Pacific Northwest Forests." *Forest Ecology and Management* 246 (1 SPEC. ISS.): 38–44. https://doi.org/10.1016/j.foreco.2007.03.049.

Kilian, Johannes, Norbert Haala, and Englich Markus. 1996. "Capture and Evaluation of Airborne Laser Scanner Data." *International Archives of Photogrammetry and Remote Sensing* 31 (Part B3). http://www.isprs.org/proceedings/XXXI/congress/part3/383_XXXI-part3.pdf.

Klinka, K. 2004. "Site Identification Tools, Field Site Maps, and Polygon Summaries for the UBC Alex Fraser Research Forest." https://afrfforestry.sites.olt.ubc.ca/files/2018/11/SiteUnitsUBCAFRF_2018update_LowRes.pdf

Koch, Barbara, Ursula Heyder, and Holger Weinacker. 2013. "Detection of Individual Tree Crowns in Airborne Lidar Data." *Photogrammetric Engineering & Remote Sensing* 72 (4): 357–63. https://doi.org/10.14358/pers.72.4.357.

Korhonen, Lauri, Ilkka Korpela, Janne Heiskanen, and Matti Maltamo. 2011. "Airborne Discrete-Return LIDAR Data in the Estimation of Vertical Canopy Cover, Angular Canopy Closure and Leaf Area Index." *Remote Sensing of Environment* 115 (4): 1065–80.

https://doi.org/10.1016/j.rse.2010.12.011.

Korpela, Ilkka, and Perttu Anttila. 2004. “Appraisal Of The Mean Height Of Trees By Means Of Image Matching Of Digitised Aerial Photographs.” *Photogrammetric Journal of Finland* 19 (1): 23–36. https://foto.aalto.fi/seura/julkaisut/pjf/pjf_e/2004/PJF2004_Korpela_Anttila.pdf.

Kraus, K., and N Pfeifer. 1998. “Determination of Terrain Models in Wooded Areas with Airborne Laser Scanner Data.” *ISPRS Journal of Photogrammetry and Remote Sensing* 53 (4): 193–203. https://doi.org/10.1016/S0924-2716(98)00009-4.

Krause, Stuart, Tanja G.M. Sanders, Jan-Peter Mund, and Klaus Greve. 2019. “UAV-Based Photogrammetric Tree Height Measurement for Intensive Forest Monitoring.” *Remote Sensing* 11 (7): 758. https://doi.org/10.3390/rs11070758.

Kurz, W A, C C Dymond, G Stinson, G J Rampley, E T Neilson, A L Carroll, T Ebata, and L Safranyik. 2008. “Mountain Pine Beetle and Forest Carbon Feedback to Climate Change.” *Nature* 452 (7190): 987–90. https://doi.org/10.1038/nature06777.

Lane, S. N., T. D. James, and M. D. Crowell. 2000. “Application of Digital Photogrammetry to Complex Topography for Geomorphological Research.” *Photogrammetric Record* 16 (95): 793–821. https://doi.org/10.1111/0031-868X.00152.

Leckie, D G, and M D Gillis. 1995. “Forest Inventory in Canada with Emphasis on Map Production.” *Forestry Chronicle* 71 (1): 74–88. https://doi.org/10.5558/tfc71074-1.

Lierop, Pieter Van, Erik Lindquist, Shiroma Sathyapala, and Gianluca Franceschini. 2015. “Global Forest Area Disturbance from Fire, Insect Pests, Diseases and Severe Weather

Events.” https://doi.org/10.1016/j.foreco.2015.06.010.

Lim, Kevin, Paul Treitz, Michael Wulder, Benoît St-Onge, and Martin Flood. 2003. “LiDAR Remote Sensing of Forest Structure.” https://doi.org/10.1191/0309133303pp360ra.

Lucieer, Arko, Steven M.de Jong, and Darren Turner. 2014. “Mapping Landslide Displacements Using Structure from Motion (SfM) and Image Correlation of Multi-Temporal UAV Photography.” *Progress in Physical Geography* 38 (1): 97–116. https://doi.org/10.1177/0309133313515293.

Magnussen, S, and P Boudewyn. 2011. “Derivations of Stand Heights from Airborne Laser Scanner Data with Canopy-Based Quantile Estimators.” *Canadian Journal of Forest Research* 28 (7): 1016–31. https://doi.org/10.1139/x98-078.

Magnussen, Steen, E. Næsset, T. Gobakken, and G. Frazer. 2012. “A Fine-Scale Model for Area-Based Predictions of Tree-Size-Related Attributes Derived from LiDAR Canopy Heights.” *Scandinavian Journal of Forest Research* 27 (3): 312–22. https://doi.org/10.1080/02827581.2011.624116.

Magnussen, Steen, and Glenda Russo. 2012. “Uncertainty in Photo-Interpreted Forest Inventory Variables and Effects on Estimates of Error in Canada’s National Forest Inventory.” *Forestry Chronicle* 88 (4): 439–47. https://doi.org/10.5558/tfc2012-080.

Maguya, Almasi S., Virpi Junttila, and Tuomo Kauranne. 2013. “Adaptive Algorithm for Large Scale Dtm Interpolation from Lidar Data for Forestry Applications in Steep Forested Terrain.” *ISPRS Journal of Photogrammetry and Remote Sensing* 85 (November): 74–83.

https://doi.org/10.1016/j.isprsjprs.2013.08.005.

McElhinny, Chris, Phillip Gibbons, Cris Brack, and Juergen Bauhus. 2005. “Forest and Woodland Stand Structural Complexity: Its Definition and Measurement.” *Forest Ecology and Management* 218 (1–3): 1–24. https://doi.org/10.1016/J.FORECO.2005.08.034.

Means, Joseph E., Steven A. Acker, David J. Harding, J. Bryan Blair, Michael A. Lefsky, Warren B. Cohen, Mark E. Harmon, and W. Arthur McKee. 1999. “Use of Large-Footprint Scanning Airborne Lidar to Estimate Forest Stand Characteristics in the Western Cascades of Oregon.” *Remote Sensing of Environment* 67 (3): 298–308. https://doi.org/10.1016/S0034-4257(98)00091-1.

Men, Hao, Biruk Gebre, and Kishore Pochiraju. 2011. “Color Point Cloud Registration with 4D ICP Algorithm.” In *Proceedings - IEEE International Conference on Robotics and Automation*, 1511–16. IEEE. https://doi.org/10.1109/ICRA.2011.5980407.

Meng, Xuelian, Nate Currit, Kaiguang Zhao, Xuelian Meng, Nate Currit, and Kaiguang Zhao. 2010. “Ground Filtering Algorithms for Airborne LiDAR Data: A Review of Critical Issues.” *Remote Sensing* 2 (3): 833–60. https://doi.org/10.3390/rs2030833.

Mitásova, H, and L Mitás. 1993. “Interpolation by Regularized Spline with Tension: I. Theory and Implementation.” *Mathematical Geology* 25(6): 641–55. https://link.springer.com/content/pdf/10.1007%2FBF00893171.pdf.

Mohan, Midhun, Carlos Silva, Carine Klauberg, Prahlad Jat, Glenn Catts, Adrián Cardil, Andrew Hudak, et al. 2017. “Individual Tree Detection from Unmanned Aerial Vehicle (UAV)

Derived Canopy Height Model in an Open Canopy Mixed Conifer Forest." *Forests* 8 (9): 340. https://doi.org/10.3390/f8090340.

Montealegre, Antonio Luis, María Teresa Lamelas, and Juan De La Riva. 2015a. "A Comparison of Open - Source LiDAR Filtering Algorithms in a Mediterranean Forest Environment." *IEEE Journal of Selected Topics in Applied Earth Observations and Remote Sensing* 8 (8): 4072–85. https://doi.org/10.1109/JSTARS.2015.2436974.

———. 2015b. "Interpolation Routines Assessment in ALS-Derived Digital Elevation Models for Forestry Applications." *Remote Sensing* 7 (7): 8631–54. https://doi.org/10.3390/rs70708631.

Næsset, Erik. 1999. "Point Accuracy of Combined Pseudorange and Carrier Phase Differential GPS under Forest Canopy." *Canadian Journal of Forest Research* 29 (5): 547–53. https://doi.org/10.1139/x99-021.

———. 2002. "Determination of Mean Tree Height of Forest Stands by Digital Photogrammetry." *Scandinavian Journal of Forest Research* 17 (5): 446–59. https://doi.org/10.1080/028275802320435469.

Nie, Sheng, Cheng Wang, Hongcheng Zeng, Xiaohuan Xi, and Guicai Li. 2017. "Above-Ground Biomass Estimation Using Airborne Discrete-Return and Full-Waveform LiDAR Data in a Coniferous Forest." *Ecological Indicators* 78 (July): 221–28. https://doi.org/10.1016/j.ecolind.2017.02.045.

Niethammer, U, M R James, S Rothmund, J Travelletti, and M Joswig. 2012. "UAV-Based

Remote Sensing of the Super-Sauze Landslide: Evaluation and Results." *Engineering Geology* 128: 2–11. https://doi.org/10.1016/j.enggeo.2011.03.012.

Nilsson, Mats. 1996. "Estimation of Tree Heights and Stand Volume Using an Airborne Lidar System." *Remote Sensing of Environment* 56 (1): 1–7. https://doi.org/10.1016/0034-4257(95)00224-3.

Nowacki, Gregory, and Marc Kramer. 1998. "The Effects of Wind Disturbance on Temperate Rain Forest Structure and Dynamics of Southeast Alaska." *General Technical Report PNW-GTR-421*. https://www.fs.fed.us/pnw/pubs/pnw_gtr421.pdf.

Ota, Tetsuji, Miyuki Ogawa, Katsuto Shimizu, Tsuyoshi Kajisa, Nobuya Mizoue, Shigejiro Yoshida, Gen Takao, et al. 2015. "Aboveground Biomass Estimation Using Structure from Motion Approach with Aerial Photographs in a Seasonal Tropical Forest." *Forests* 6 (11): 3882–98. https://doi.org/10.3390/f6113882.

Patriquin, Mike N., Adam M. Wellstead, and William A. White. 2007. "Beetles, Trees, and People: Regional Economic Impact Sensitivity and Policy Considerations Related to the Mountain Pine Beetle Infestation in British Columbia, Canada." *Forest Policy and Economics* 9 (8): 938–46. https://doi.org/10.1016/J.FORPOL.2006.08.002.

Pingel, Thomas J, Keith C Clarke, and William A Mcbride. 2013. "An Improved Simple Morphological Filter for the Terrain Classification of Airborne LIDAR Data." *ISPRS Journal of Photogrammetry and Remote Sensing* 77: 21–30. https://doi.org/10.1016/j.isprsjprs.2012.12.002.

"Pix4Dmapper Pro Version 4.1.24." 2018. https://www.pix4d.com/.

Popescu, Sorin C, Randolph H Wynne, and Ross F Nelson. 2003. "Measuring Individual Tree Crown Diameter with Lidar and Assessing Its Influence on Estimating Forest Volume and Biomass." *Canadian Journal of Remote Sensing* 29 (5): 564–77. https://doi.org/10.5589/m03-027.

Pousette, John, and Chris Hawkins. 2006. "Prince George Timber Supply Area" 7 (2): 93–104.

Pozo, Susana Del, Pablo Rodríguez-Gonzálvez, David Hernández-López, and Beatriz Felipe-García. 2014. "Vicarious Radiometric Calibration of a Multispectral Camera on Board an Unmanned Aerial System." *Remote Sensing* 6 (3): 1918–37. https://doi.org/10.3390/rs6031918.

Puliti, Stefano, Hans Ole Ørka, Terje Gobakken, and Erik Næsset. 2015. "Inventory of Small Forest Areas Using an Unmanned Aerial System." *Remote Sensing* 7 (8): 9632–54. https://doi.org/10.3390/rs70809632.

Rahlf, Johannes, Johannes Breidenbach, Svein Solberg, Erik Naesset, and Rasmus Astrup. 2017. "Digital Aerial Photogrammetry Can Efficiently Support Large-Area Forest Inventories in Norway." *ForestryAn International Journal of Forest Research Forestry* 90: 710–18. https://doi.org/10.1093/forestry/cpx027.

Razak, Khamarrul Azahari, Michele Santangelo, Cees J. Van Westen, Menno W. Straatsma, and Steven M. de Jong. 2013. "Generating an Optimal DTM from Airborne Laser Scanning Data for Landslide Mapping in a Tropical Forest Environment." *Geomorphology* 190

(May): 112–25. https://doi.org/10.1016/j.geomorph.2013.02.021.

Reitberger, J., Cl. Schnörr, P. Krzystek, and U. Stilla. 2009. “3D Segmentation of Single Trees Exploiting Full Waveform LIDAR Data.” *ISPRS Journal of Photogrammetry and Remote Sensing* 64 (6): 561–74. https://doi.org/10.1016/j.isprsjprs.2009.04.002.

Reutebuch, Stephen E, Robert J McGaughey, Hans-Erik Andersen, and Ward W Carson. 2003. “Accuracy of a High-Resolution Lidar Terrain Model under a Conifer Forest Canopy.” *Canadian Journal of Remote Sensing* 29 (5): 527–35. https://doi.org/10.5589/m03-022.

Scrinzi, Gianfranco, Fabrizio Clementel, and Antonio Floris. 2015. “Angle Count Sampling Reliability as Ground Truth for Area-Based LiDAR Applications in Forest Inventories.” *Canadian Journal of Forest Research* 45 (4): 506–14. https://doi.org/10.1139/cjfr-2014-0408.

Seidel, Dominik, Martin Ehbrecht, and Klaus Puettmann. 2016. “Assessing Different Components of Three-Dimensional Forest Structure with Single-Scan Terrestrial Laser Scanning: A Case Study.” *Forest Ecology and Management* 381 (December): 196–208. https://doi.org/10.1016/j.foreco.2016.09.036.

Sibson, Robin. 1981. “Interpreting Multivariate Data.” In , edited by Vic Barnett, 21–36. Chichester: John Wiley & Sons, Ltd.

Simpson, Jake, Thomas Smith, Martin Wooster, Jake E. Simpson, Thomas E. L. Smith, and Martin J. Wooster. 2017. “Assessment of Errors Caused by Forest Vegetation Structure in Airborne LiDAR-Derived DTMs.” *Remote Sensing* 9 (11): 1101.

https://doi.org/10.3390/rs9111101.

Sithole, George, and George Vosselman. 2004. “Experimental Comparison of Filter Algorithms for Bare-Earth Extraction from Airborne Laser Scanning Point Clouds.” *ISPRS Journal of Photogrammetry and Remote Sensing* 59 (1–2): 85–101. https://doi.org/10.1016/j.isprsjprs.2004.05.004.

Smith, M W, J L Carrivick, and D J Quincey. 2015. “Structure from Motion Photogrammetry in Physical Geography.” *Progress in Physical Geography* 40 (2): 247–75. https://doi.org/10.1177/0309133315615805.

Soverel, Nicholas O, Daniel D.B. Perrakis, and Nicholas C Coops. 2010. “Estimating Burn Severity from Landsat DNBR and RdNBR Indices across Western Canada.” *Remote Sensing of Environment* 114 (9): 1896–1909. https://doi.org/10.1016/j.rse.2010.03.013.

Spectra Precision. 2012. “ProMark ™ 120.” 2012. http://www.geonavsystems.com/ProMark 120 Brochure  2013.pdf.

St-Onge, B, C Vega, R A Fournier, and Y Hu. 2008. “Mapping Canopy Height Using a Combination of Digital Stereo-Photogrammetry and Lidar.” *International Journal of Remote Sensing* 29 (11): 3343–64. https://doi.org/10.1080/01431160701469040.

Stereńczak, Krzysztof, Mariusz Ciesielski, Radomir Bałazy, and Tomasz Zawiła-Niedźwiecki. 2016. “Comparison of Various Algorithms for DTM Interpolation from LIDAR Data in Dense Mountain Forests.” *European Journal of Remote Sensing* 49 (1): 599–621. https://doi.org/10.5721/EuJRS20164932.

Swatantran, Anu, Hao Tang, Terence Barrett, Phil Decola, and Ralph Dubayah. 2016. “Rapid, High-Resolution Forest Structure and Terrain Mapping over Large Areas Using Single Photon Lidar.” *Scientific Reports* 6 (1): 28277. https://doi.org/10.1038/srep28277.

Takahashi, Tomoaki, Kazukiyo Yamamoto, Yoshimichi Senda, and Masashi Tsuzuku. 2005. “Predicting Individual Stem Volumes of Sugi (Cryptomeria Japonica D. Don) Plantations in Mountainous Areas Using Small-Footprint Airborne LiDAR.” *Journal of Forest Research* 10 (4): 305–12. https://doi.org/10.1007/s10310-005-0150-2.

Tang, Lina, and Guofan Shao. 2015. “Drone Remote Sensing for Forestry Research and Practices.” *Journal of Forestry Research* 26 (4): 791–97. https://doi.org/10.1007/s11676-015-0088-y.

Thom, Dominik, and Rupert Seidl. 2016. “Natural Disturbance Impacts on Ecosystem Services and Biodiversity in Temperate and Boreal Forests.” *Biological Reviews of the Cambridge Philosophical Society* 91 (3): 760–81. https://doi.org/10.1111/brv.12193.

Tomaštík, Julián, Martin Mokroš, Šimon Saloň, František Chudý, Daniel Tunák, Julián Tomaštík, Martin Mokroš, Šimon Saloň, František Chudý, and Daniel Tunák. 2017. “Accuracy of Photogrammetric UAV-Based Point Clouds under Conditions of Partially-Open Forest Canopy.” *Forests* 8 (5): 151. https://doi.org/10.3390/f8050151.

Tompalski, Piotr, Nicholas C. Coops, Peter L. Marshall, Joanne C. White, Michael A. Wulder, and Todd Bailey. 2018. “Combining Multi-Date Airborne Laser Scanning and Digital Aerial Photogrammetric Data for Forest Growth and Yield Modelling.” *Remote Sensing* 10 (2): 347. https://doi.org/10.3390/rs10020347.

Tompalski, Piotr, Nicholas C. Coops, Joanne C. White, and Michael A. Wulder. 2015. "Enriching ALS-Derived Area-Based Estimates of Volume through Tree-Level Downscaling." *Forests* 6 (8): 2608–30. https://doi.org/10.3390/f6082608.

Tuominen, Sakari, Andras Balazs, Heikki Saari, Ilkka Pölönen, Janne Sarkeala, and Risto Viitala. 2015. "Unmanned Aerial System Imagery and Photogrammetric Canopy Height Data in Area-Based Estimation of Forest Variables." *Silva Fennica* 49 (5). https://doi.org/10.14214/sf.1348.

Ung, Chhun-Huor, Pierre Bernier, and Xiao-Jing Guo. 2008. "Canadian National Biomass Equations: New Parameter Estimates That Include British Columbia Data." *Canadian Journal of Forest Research* 38 (5): 1123–32. https://doi.org/10.1139/X07-224.

Vastaranta, Mikko, Ville Kankare, Markus Holopainen, Xiaowei Yu, Juha Hyyppä, and Hannu Hyyppä. 2012. "Combination of Individual Tree Detection and Area-Based Approach in Imputation of Forest Variables Using Airborne Laser Data." *ISPRS Journal of Photogrammetry and Remote Sensing* 67 (1): 73–79. https://doi.org/10.1016/j.isprsjprs.2011.10.006.

Vastaranta, Mikko, Tuula Kantola, Päivi Lyytikäinen-Saarenmaa, Markus Holopainen, Ville Kankare, Michael A. Wulder, Juha Hyyppä, and Hannu Hyyppä. 2013. "Area-Based Mapping of Defoliation of Scots Pine Stands Using Airborne Scanning LiDAR." *Remote Sensing* 5 (3): 1220–34. https://doi.org/10.3390/rs5031220.

Wallace, Luke, Chris Bellman, Bryan Hally, Jaime Hernandez, Simon Jones, and Samuel Hillman. 2019. "Assessing the Ability of Image Based Point Clouds Captured from a UAV

to Measure the Terrain in the Presence of Canopy Cover." *Forests* 10 (3): 284. https://doi.org/10.3390/f10030284.

Wallace, Luke, Arko Lucieer, Zbyněk Malenovský, Darren Turner, Petr Vopěnka, Luke Wallace, Arko Lucieer, Zbyněk Malenovský, Darren Turner, and Petr Vopěnka. 2016. "Assessment of Forest Structure Using Two UAV Techniques: A Comparison of Airborne Laser Scanning and Structure from Motion (SfM) Point Clouds." *Forests* 7 (12): 62. https://doi.org/10.3390/f7030062.

Wang, Yunsheng, Holger Weinacker, Barbara Koch, Yunsheng Wang, Holger Weinacker, and Barbara Koch. 2008. "A Lidar Point Cloud Based Procedure for Vertical Canopy Structure Analysis And 3D Single Tree Modelling in Forest." *Sensors* 8 (6): 3938–51. https://doi.org/10.3390/s8063938.

Westoby, M J, J Brasington, N F Glasser, M J Hambrey, and J M Reynolds. 2012. "'Structure-from-Motion' Photogrammetry: A Low-Cost, Effective Tool for Geoscience Applications." *Geomorphology* 179: 300–314. https://doi.org/10.1016/j.geomorph.2012.08.021.

White, Joanne C., Michael A. Wulder, Mikko Vastaranta, Nicholas C. Coops, Doug Pitt, and Murray Woods. 2013. "The Utility of Image-Based Point Clouds for Forest Inventory: A Comparison with Airborne Laser Scanning." *Forests*. Multidisciplinary Digital Publishing Institute. https://doi.org/10.3390/f4030518.

White, Joanne C, Michael A Wulder, Andrés Varhola, Mikko Vastaranta, Nicholas C Coops, Bruce D Cook, Doug Pitt, and Murray Woods. 2013. "A Best Practices Guide for Generating Forest Inventory Attributes from Airborne Laser Scanning Data Using an Area-

Based Approach." *Provincial Services Division*. Vol. 89. https://doi.org/10.5558/tfc2013-132.

Wimberly, Michael C., and Zhihua Liu. 2014. "Interactions of Climate, Fire, and Management in Future Forests of the Pacific Northwest." *Forest Ecology and Management* 327 (September): 270–79. https://doi.org/10.1016/j.foreco.2013.09.043.

Woodcock, W E. 1976. "Aerial Reconnaissance and Photogrammetry with Small Cameras." *Photogrammatric Engineering & Remote Sensing* 42 (4): 503–11. https://www.asprs.org/wp-content/uploads/pers/1976journal/apr/1976_apr_503-511.pdf.

Woods, Murray, Doug Pitt, Margaret Penner, Kevin Lim, Dave Nesbitt, and Paul Treitz. 2011. "Operational Implementation of LiDAR Inventories in Boreal Ontario Advanced Forest Resource Inventory Technologies." *The Forestry Chronicle* 87 (4): 512–28. http://pubs.cif-ifc.org/doi/pdf/10.5558/tfc2011-050.

Wulder, Michael A, Thomas Hilker, Christopher W Bater, Joanne C White, and Nicholas C Coops. 2014. "The Role of LiDAR in Sustainable Forest Management." *The Forestry Chronicle* 84 (6): 807–26. https://doi.org/10.5558/tfc84807-6.

Wulder, Michael A, Joanne C White, Geoffrey J Hay, and Guillermo Castilla. 2008. "Towards Automated Segmentation of Forest Inventory Polygons on High Spatial Resolution Satellite Imagery." *Forestry Chronicle* 84 (2): 221–30. https://doi.org/10.5558/tfc84221-2.

Yan, Li, Hua Liu, Junxiang Tan, Zan Li, Changjun Chen, Li Yan, Hua Liu, Junxiang Tan, Zan Li, and Changjun Chen. 2017. "A Multi-Constraint Combined Method for Ground Surface

Point Filtering from Mobile LiDAR Point Clouds.” *Remote Sensing* 9 (9): 958. https://doi.org/10.3390/rs9090958.

Yu, Xiaowei, Juha Hyyppä, Mikko Vastaranta, Markus Holopainen, and Risto Viitala. 2011. “Predicting Individual Tree Attributes from Airborne Laser Point Clouds Based on the Random Forests Technique.” *ISPRS Journal of Photogrammetry and Remote Sensing* 66 (1): 28–37. https://doi.org/10.1016/j.isprsjprs.2010.08.003.

Yunfei, Bao, Li Guoping, Cao Chunxiang, Li Xiaowen, Zhang Hao, He Qisheng, Bai Linyan, and Chang Chaoyi. 2002. “Classification of Lidar Point Cloud and Generation of Dtm.” *The International Archives of the Photogrammetry, Remote Sensing and Spatial Information Sciences*, 313–18. http://citeseerx.ist.psu.edu/viewdoc/download?doi=10.1.1.475.9678&rep=rep1&type=pdf.

Zhang, Jixian, and Xiangguo Lin. 2013. “Filtering Airborne LiDAR Data by Embedding Smoothness-Constrained Segmentation in Progressive TIN Densification.” *ISPRS Journal of Photogrammetry and Remote Sensing* 81: 44–59. https://doi.org/10.1016/j.isprsjprs.2013.04.001.

Zhang, Kai, Xu Zhi Li, and Jiu Xing Zhang. 2014. “A Robust Point-Matching Algorithm for Remote Sensing Image Registration.” *IEEE Geoscience and Remote Sensing Letters* 11 (2): 469–73. https://doi.org/10.1109/LGRS.2013.2267771.

Zhang, Keqi, Shu Ching Chen, Dean Whitman, Mei Ling Shyu, Jianhua Yan, and Chengcui Zhang. 2003. “A Progressive Morphological Filter for Removing Nonground Measurements from Airborne LIDAR Data.” *IEEE Transactions on Geoscience and Remote Sensing* 41 (4

PART I): 872–82. https://doi.org/10.1109/TGRS.2003.810682.

Zhang, Wuming, Jianbo Qi, Peng Wan, Hongtao Wang, Donghui Xie, Xiaoyan Wang, and Guangjian Yan. 2016. “An Easy-to-Use Airborne LiDAR Data Filtering Method Based on Cloth Simulation.” *Remote Sensing* 8 (6): 501. https://doi.org/10.3390/rs8060501.

Zhang, Z, M Gerke, G Vosselman, and M Y Yang. 2018. “FILTERING PHOTOGRAMMETRIC POINT CLOUDS USING STANDARD LIDAR FILTERS TOWARDS DTM GENERATION.” In *ISPRS Annals of the Photogrammetry, Remote Sensing and Spatial Information Sciences*, 4:319–26. https://doi.org/10.5194/isprs-annals-IV-2-319-2018.